Title

Galectin-mediated immune responses to infection with intracellular bacteria

Author

Morrison, Huntly Mariano

Publication Date

2022

Peer reviewed|Thesis/dissertation

Galectin-mediated immune responses to infection with intracellular bacteria

By

Huntly Mariano Morrison

A dissertation submitted in partial satisfaction of the

requirements for the degree of

Doctor of Philosophy

in

Molecular and Cell Biology

in the

Graduate Division

of the

University of California, Berkeley

Committee in charge:

Professor Jeffery Cox, Chair
Professor Sarah Stanley
Professor Russell Vance
Professor James Olzmann

Summer 2022

Abstract

Galectin-mediated immune responses to infection with intracellular bacteria

by

Huntly Mariano Morrison

Doctor of Philosophy in Molecular and Cell Biology

University of California, Berkeley

Professor Jeffery Cox, Chair

Macrophages employ an array of receptors to detect and eliminate intracellular pathogens that access the cytosol. Galectins represent one such class of receptors, and activate membrane repair or autophagy-mediated degradation of ruptured organelles. In macrophages, Gal-3, -8, and -9 promote innate immune signaling following recognition of luminal host glycoproteins in damaged pathogen-containing phagosomes, but their contributions to immunity during infection in vivo remain unclear. We found that Gal-9 interacts directly with the intracellular pathogens, *Mycobacterium tuberculosis* (*Mtb*) and *Salmonella typhimurium*. This interaction was dependent upon Gal-9 carbohydrate-binding and occurred both in vitro and in vivo. To determine the contribution of the galectin system to host resistance in vivo, we generated Gal-3, -8, -9 triple knockout mice (TKO) and challenged these mice with a panel of intracellular bacteria. We found that galectin deficiency leads to impairments in bacterial growth restriction and CD4 T cell activation during chronic *Mtb* infection. However, during acute infection with *Mtb, S. typhimurium,* or *L. monocytogenes*, TKO mice exhibited normal resistance. In addition, we found that galectin deficiency in macrophages leads to inefficient clearance of *Mtb* from the cytosol, despite TKO macrophages exhibiting normal bacterial growth restriction. Collectively, our findings indicate that the galectin system is dispensable for protection against acute bacterial infection but necessary for full resistance to chronic tuberculosis infection.

Table of Contents

Acknowledgments

I would like to first thank my thesis advisor, Jeff Cox, for welcoming me into the lab and thoughtfully guiding me through the ups and the downs of graduate school. Jeff, your passion for science is contagious and inspiring. You have always pushed and challenged me to think more deeply, creatively, and positively. You are a truly thoughtful mentor, and your continual support, patience, and encouragement throughout my graduate career have been instrumental in my success and perseverance. I am very grateful to have spent the past several years training with you. It has been an absolute joy to explore the mysteries of biology with you.

I would also like to thank Bennett Penn for providing me with invaluable support and advising, and for conducting the *Mtb* pull-down experiment that started this project. I have Bennett to thank for all the elegant data in figures 1 and S1. I am still so amazed and grateful that you were able to join me for long experiments in the BSL3. Your dedication, expertise, and enthusiasm made this collaboration successful and exciting.

My thesis committee members, Jeff Cox, Sarah Stanley, Russell Vance, and James Olzmann have always been very supportive through my entire graduate career. Our thesis committee meetings kept me on track and helped me prioritize future directions. Thank you for guiding me onto new projects and believing in me along the way.

The work in this dissertation would not have been possible without the contributions of several individuals and labs. Julia Craft contributed an immense amount of work—all of the *S. typhimurium* infections and shRNA knockdown experiments were conducted by her. Thank you to Rafael Rivera-Lugo for conducting all of the *L. monocytogenes* infections and sharing valuable insights. Claire Dodd helped immensely on this project by breeding mice and establishing the Gal-3, -8, -9 triple knockout mouse colony. Thank you to Jeff Johnson and Danielle Swaney for conducting the LC/MS. Thank you to Wandy Beatty for the very elegant electron microscopy. Thank you to Shally Margolis for conducting *L. pneumophila* infections. Thank you to Guillaume Golovkine and Teresa Repasy for assisting with the survival experiment, and Rita McCall for contributing hours of work in the BSL3. Many thanks to Allison Roberts and Dmitri Kotov for being so patient and helping me with flow cytometry experiments. Thank you to the Stanley and Vance labs for providing valuable feedback and ideas throughout my graduate career. Finally, I want to thank all the members of the Cox lab, past and present, for being so supportive, kind, and helpful. All of the trips to Jupiter, cake times, happy hours, and other good times we shared together in and outside lab will never be forgotten.

To all my friends, who have been and continue to be such an incredible and vital support system and source of joy and love, I can't thank you all enough. All of our meals together, excursions, hangouts, and dance parties make this ride through life truly exhilarating and wondrous.

To Rick and Olivia, the laughter, love, and music you bring into my life has always been so healing. I am so grateful for both of you. And to Rhea, you have taught me how to cultivate wellness, awareness, and empathy. You have and will always inspire me to become the best version of myself.

To my extended family and family friends, the Dorias, Hills, Bachars, Millers, Castillos, Vinluans, Chisholms, Nichols, Ricards, Bernases, and Quimados, thank you for always supporting me throughout this journey. I consider myself so lucky to be part of such a strong, loving, and supportive community, at home and abroad.

Lastly, I need to thank my family. To my brother-in-law, Kennedy, your pragmatic and get-it-done attitude has always reminded me to not overthink things, as I often do! Your thoughtfulness, wit, and positivity enrich our family. To my sister, Filomene, how lucky I am to have such a brilliant, inspiring, and caring sister. You have always been by my side, encouraging me, reassuring me, and lifting me up. The warmth and love you bring to my life and this world are boundless. And to my parents, Frank and Susan, how deeply grateful I am to have remained so close to both of you throughout this experience. Coming home after a long day and seeing your smiling faces has always restored my spirit. Your endless love and support have been my foundation.

Dedication

I dedicate this dissertation to my grandma, Sixta, who has nurtured our family with kindness, laughter, and love.

Chapter 1: Introduction

Tuberculosis: history and ongoing challenges

Tuberculosis (TB) is caused by the intracellular bacterium *Mycobacterium tuberculosis (Mtb),* which is spread between hosts in aerosolized droplets that are expelled when an infected individual breaths or coughs. Once the bacterium is inhaled into the lungs, the infection is established in sentinel immune cells called macrophages. Tuberculosis is possibly the oldest disease to have plagued humankind (Daniel et al., 2006). *Mtb* can be traced to an early progenitor species that likely originated in East Africa approximately 3 million years ago (Gutierrez et al., 2005). It is hypothesized that this ancestral strain likely infected hominids at the time, while archeological evidence of more recent tuberculosis has been discovered along early human migration routes out of Africa and into Europe, China, and pre-colonial America (Gutierrez et al., 2005). Thus, *Mtb* has lived and coevolved with humans for tens of thousands of years.

Today, TB remains one of the deadliest diseases worldwide. It is estimated that every year, *Mtb* infects tens of millions of people and kills almost 1.5 million people (WHO TB, 2020). Most of those infections are classified as latent TB. Patients with latent TB cannot spread TB to others and do not experience any of the clinical signs associated with active disease, such as chest pain, coughing up sputum or blood, fatigue, night sweats, fever, and weight loss (Lyon et al., 2017). While 90% of TB infections do not progress beyond latency, approximately 10% can develop into active disease. During active disease, bacteria contained in necrotic lesions in the infected lung begin to replicate and can overwhelm containment mechanisms established by the immune system. Unrestricted bacterial growth can lead to deleterious inflammatory responses, which in turn can cause extensive pulmonary tissue damage and death (Ravimohan et al., 2018). If left untreated, half of active TB patients will succumb to the disease (Young et al., 2009). Currently, treatment regimens for latent tuberculosis require 4-6 months of treatment with 2-4 frontline antibiotic drugs (Carr et al., 2022). However, drug resistance in *Mtb* is on the rise, and it is estimated that approximately 20% of TB cases globally are resistant to at least one of the four frontline antibiotics (Dheda et al., 2017). *Mtb* resistance to traditional antibiotic therapies necessitates deeper investigation of this deadly disease, as well as research of alternative non-antibiotic therapies. At the intersection of these approaches is host-directed therapy (HDT), which focuses on the development of immunomodulatory therapies that promote antibacterial immune functions (Tobin, 2015). HDT represents a promising new approach in the search for novel antitubercular drugs, but effective HDT design requires a comprehensive understanding of the host immune response to *Mtb* infection.

Macrophages: the focal point of the immune response to *Mtb*

Mtb is spread via aerosolized droplets, which are inhaled into the lungs where patrolling alveolar macrophages may encounter and engulf the bacteria (Torrelles and Schlesinger, 2017). To detect and suppress invading pathogens, macrophages have evolved numerous germline-encoded pathogen recognition receptors (PRRs), which activate potent antibacterial killing mechanisms following recognition of conserved pathogen-associated molecular patterns (PAMPs) (Medzhitov, 2001). Macrophages are

not limited to the direct detection of PAMPs and deploy additional surveillance mechanisms to detect cellular damage (Johannes et al., 2018), which is a common feature of infection with virulent bacteria. While macrophages have the capacity to sense and kill *Mtb* using these mechanisms, they fail to restrict bacterial growth without additional cell-modulating signals from the tissue environment and adaptive immune response (Russell et al., 2011). Therefore, elucidating the interactions between *Mtb* and the macrophage, and the impact of these interactions on the broader immune response, is crucial for understanding the immunological mechanisms underlying the containment of *Mtb.*

ESX-1-dependent activation of cytosolic PRRs

The hallmark of all virulent intracellular pathogens is their ability to access the host cytosol in order to manipulate the host and establish a replicative niche. However, these disruptive processes introduce unique opportunities for the host to detect cellular abnormalities, including membrane damage or newly exposed PAMPs. *Mtb* gains access to the cytosol using the type VII protein secretion system, ESX-1 (Abdallah et al., 2007). While ESX-1 is critical for *Mtb* virulence (Stanley et al., 2003, Hsu et al., 2003), it is also required for the activation of several macrophage detection mechanisms (Stanley et al., 2007, Wong and Jacobs, 2011, Wassermann et al., 2015). ESX-1-driven membrane damage uncovers PAMPs that are readily bound by cytosolic PRRs, such as cGAS and RIG-I, which bind bacterial DNA and RNA, respectively (Watson et al., 2015, Cheng and Schorey, 2018). Damaged *Mtb* phagosomes additionally become highly labeled with ubiquitin, suggesting membrane damage exposes substrates for host ubiquitin ligases (Wong and Jacobs, 2011, Watson et al., 2012), although the exact substrates are poorly defined. Finally, carbohydrates present on bacteria or host glycoproteins represent another class of ligands for cytosolic sensing pathways, as the cytosol is devoid of these molecules under normal conditions. While macrophages have been demonstrated to possess numerous surface and cytosolic receptors for carbohydrates, their contributions to immunity during infection in vivo are complicated by potential redundancies in receptor recognition and signaling.

Galectins: a cellular damage-response system

One class of carbohydrate receptors that are activated during intracellular bacterial infection are galectins, which are a family of fifteen soluble proteins defined by a conserved carbohydrate recognition domain (CRD) (Rabinovich et al., 2007). Galectins can initiate signaling by binding to glycosylated macromolecules or proteins using one or two CRDs (Johannes et al., 2018). While galectins have been reported to act extracellularly through an atypical secretion mechanism (Rabinovich 2007), several are described to function intracellularly in the response to membrane damage and infection. In macrophages, Gal-3, -8, and -9 have been demonstrated to be the primary responders to membrane damage (Johannes et al., 2018). Sterile damage of lysosomal membranes activates Gal-3, -8, and -9, which signal through distinct pathways to promote repair and clearance of damaged lysosomes (Maejima et al., 2013, Chauhan et al., 2016, Jia et al., 2020a, Jia et al., 2020b). During infection with intracellular bacteria, phagosomal membrane damage exposes luminal glycoproteins to cytosolic galectins (Paz et al., 2010, Thurston et al., 2012). Gal-3, -8, and -9 have been shown to recruit to

damaged phagosomes containing *Mtb, Salmonella enterica* serovar Typhimurium, *Shigella flexneri*, *Listeria monocytogenes*, *Legionella pneumophila,* and *Yersinia pseudotuberculosis* (Beatty et al., 2002, Wong and Jacobs, 2011, Bell et al., 2021, Thurston et al., 2012, Dupont et al., 2009, Paz et al., 2010, Feeley et al., 2017). Recruitment of these galectins to bacterial phagosomes has been shown to activate antibacterial selective autophagy induction (Thurston et al., 2012, Bell et al., 2021), transcriptional responses (Wu et al., 2021), and regulation of antibacterial guanylate-binding proteins (Feeley et al., 2017). In addition, we have previously shown that Gal-3, -8, and -9 are all ubiquitylated during *Mtb* infection (Budzik et al., 2020), although the significance of these modifications remains unclear. Despite rigorous characterization of Gal-3, -8, and -9 during infection of macrophages, the impact of galectin-mediated pathogen recognition on bacterial control and the broader immune response in vivo is only partially understood. During *Mtb* infection of mice, extracellular Gal-9 binding with the plasma membrane T cell receptor, Tim3, is proposed to promote IL-1β-dependent macrophage killing of *Mtb* (Jayaraman et al., 2010, Sada-Ovalle et al., 2012). This antibacterial role for Gal-9 in vivo is consistent with the finding that Gal-9$^{-/-}$ mice have increased *Mtb* burdens following aerosol infection (Wu et al., 2021). In addition, knockout of Gal-3 or Gal-8 in mice has been shown to increase susceptibility to *Mtb* infection (Chauhan et al., 2016, Jia et al., 2018), but a role for Gal-3 or Gal-8 in bacterial growth restriction in mice has yet to be defined.

Antibacterial selective autophagy

Selective autophagy is a conserved cytosolic pathway that targets and captures specific cargoes within double-membrane structures called autophagosomes, which then fuse with lysosomes to degrade the cargo and recycle the constituents (Mizushima, 2007). Among the diverse cargos selective autophagy has evolved to target are intracellular pathogens that access the cytosol (Levine et al., 2011). Targeting is achieved through deposition of ubiquitin on specific cargos by ubiquitin ligases, including Parkin and Smurf1, which ubiquitylate substrates with K63- and K48-linked polyubiquitin chains, respectively, in the case of *Mtb*-targeted selective autophagy (Manzanillo et al., 2013, Franco et al., 2016). Several ubiquitin-binding autophagy receptors then decode these ubiquitin signals into autophagy signaling cascades that nucleate autophagosome membranes around the cargo (Stolz et al., 2014). SQSTM, NDP52, TAX1BP1, NBR1, and OPTN are autophagy receptors that have been implicated in *Mtb*-targeted selective autophagy (Watson et al., 2012, Budzik et al., 2020, Bell et al., 2021). In addition to ubiquitin, Gal-8 has been shown to mediate the recruitment of NDP52 and TAX1BP1 during infection to suppress bacterial growth (Thurston et al., 2012, Bell et al., 2021). While we are beginning to understand the mechanisms underlying the activation of antibacterial selective autophagy, the relative contribution of these pathways to immunity in vivo remains poorly understood.

The immune response to *Mtb* infection

Mtb infection begins when alveolar macrophages phagocytose bacteria that are inhaled into the lungs. *Mtb* is highly resistant to clearance at this stage and inhibits, evades, and/or resists multiple macrophage killing mechanisms, allowing it to replicate significantly before the adaptive immune response is engaged (Mayer-Barber and

Barber, 2015). Dendritic cells bearing epitopes derived from *Mtb* antigens traffic from the infected lung to the draining lymph node where they present antigen to naïve T cells, thereby initiating the adaptive immune response (Cooper et al., 2009). Recognition of cognate antigen on MHC class II molecules activates CD4 T cells and promotes their maturation into specialized cells that secrete the cytokine IFN-γ, which is critical for host resistance to *Mtb* infection. Lung inflammation and chemokine gradients attract these activated CD4 T cells to the infected lung, where they promote host resistance by activating potent antibacterial responses in macrophages through IFN-γ secretion and other mechanisms (Mayer-Barber and Barber, 2015). These adaptive immune responses can promote the containment of bacteria and in some cases an equilibrium is established between the bacteria and the host, allowing the infection to enter the latent phase (Flynn and Chan., 2001). During this stage, impaired immunity can lead to reactivation and disease progression.

Innate immune recognition of the mycobacterial cell wall

The *Mtb* cell wall is a highly elaborate structure composed of fatty acids, polysaccharides, and glycolipids (Daffé, 2015). Despite this complexity, host receptors have evolved to bind specific cell wall ligands to activate pro-inflammatory signaling. Toll-like receptor 2 (TLR-2) is reported to recognize a large repertoire of mycobacterial cell wall lipoproteins and glycolipids (Ravesloot-Chavez et al., 2021), and promotes resistance to *Mtb* during chronic infection (Reiling et al., 2002). In addition to membrane-bound receptors, cytosolic receptors have been shown to sense cell wall components. Gal-9 was recently reported to bind *Mtb* in vitro via interactions with the mycobacterial polysaccharide, arabinogalactan (Wu et al., 2021). However, it remains unclear whether Gal-9-*Mtb* binding occurs in vivo and whether Gal-9 recognition of bacteria is strictly dependent on arabinogalactan-binding. Macrophages additionally employ several plasma membrane-bound C-type lectin receptors (CTLs) to recognize other *Mtb* cell wall polysaccharides. The glycolipid trehalose dimycolate (TDM) is recognized by Mincle and Marco, which activate MyD88-independent pro-inflammatory signaling, while mannose-capped lipoarabinomannan (ManLAM) is recognized by Dectin-2, mannose receptor and DC-SIGN (Ravesloot-Chavez et al., 2021). However, individual CLRs play limited roles in mice, possibly due to functional redundancies. Indeed, there is significant redundancy among macrophage innate sensing mechanisms (Nish and Medzhitov, 2011), and while many of these pathways have been rigorously characterized in isolation, the net effect of signal transduction through multiple receptors is poorly understood.

Investigation of the galectin system during intracellular bacterial infection

Here, we report our findings using mass spectrometry to identify proteins that bind to the surface of *Mtb*. We found that Gal-9 bound *Mtb* in a carbohydrate-binding-dependent manner, and that this interaction was specific to *Mtb* and *Salmonella enterica* serovar Typhimurium, but not *Listeria monocytogenes* or *Cryptococcus neoformans*. Using structured illumination microscopy, electron microscopy, and confocal microscopy, we found that Gal-9 maintained intimate interactions with *Mtb* throughout infection. To both address potential redundancies in galectin-mediated pathogen recognition and determine the importance of multiple key galectins in vivo, we

generated Gal-3, -8, -9 triple knockout mice (TKO) and challenged these mice with a panel of phylogenetically-distinct intracellular bacteria. Surprisingly, knockout of these three key galectins led to only minor defects in immunity. TKO macrophages showed defects in *Mtb*-targeted autophagy and accumulated *Mtb*-autophagy intermediates. However, despite these effects on autophagy, we found that Gal-3, -8 and -9 were dispensable for bacterial growth restriction in macrophages. In mice, we found that Gal-3, -8, and -9 are nonessential for host resistance to acute bacterial infection with *Mtb, L. monocytogenes, S. typhimurium* yet contribute to the control of chronic *Mtb* infection, possibly through the promotion of antigen-specific T cell responses. Our data thus provide evidence that Gal-3, -8, and -9 play limited roles during acute bacterial infection but promote host resistance to chronic tuberculosis infection.

Chapter 2: Galectin-mediated immune responses to infection with intracellular bacteria

Chapter 2.1: Results

Gal-9 binds to *Mtb* in a carbohydrate-binding-dependent manner

To identify host proteins that bind to the *Mtb* surface, we incubated human THP-1 macrophage lysates with formaldehyde-fixed *Mtb,* washed out non-binding proteins, and processed samples for liquid-chromatography mass spectrometry (LC/MS) (Fig. 1A). Using non-quantitative LC/MS, we detected approximately 670 unique peptides from 100-250 different proteins (Appendix, Table 2). We focused our attention on lipid- and carbohydrate-binding proteins, as these molecules are likely to recognize mycobacterial cell wall components during infection. Of notable interest from this dataset were LEG1 and LEG9 (hereafter referred to as Gal-1 and Gal-9), which are carbohydrate-binding lectins that have demonstrated roles in immunity (Rabinovich et al., 2007). Since previous reports have shown Gal-1 does not recruit to damaged phagosomes or promote bacterial growth restriction (Thurston et al., 2012, Bell et al., 2021), we did not include it in the present study. Gal-9 contains two distinct carbohydrate recognition domains (CRD) that are joined by a linker region (Fig. 1B). We detected five unique peptides that mapped to Gal-9 and accounted for 17.2% coverage of the polypeptide (Fig. 1B). The detected peptides mapped to all three human Gal-9 paralogs: Gal-9A, Gal-9B, and Gal-9C. Although this experiment does not allow us to determine which paralogs are capable of binding to *Mtb*, we independently tested the *Mtb*-Gal-9 interaction using lysates from RAW 264.7 mouse macrophages expressing 3xflag-tagged mouse Gal-9 and found robust binding of Gal-9-FLAG to *Mtb* (Fig. 1C). This interaction was dependent on Gal-9-carbohydrate binding on the bacterial surface, as addition of lactose to the in vitro binding reaction inhibited Gal-9 pull-down with *Mtb* (Fig. 1C). These results are consistent with a role for Gal-9 in the recognition of *Mtb* and the mycobacterial carbohydrate, arabinogalactan (Wu et al., 2021). To determine whether Gal-9 binds to other phylogenetically-distinct pathogens , we incubated Gal-9-FLAG lysates with Gram-positive *Listeria monocytogenes (L. mono.),* Gram-negative *Salmonella enterica* Serovar typhimurium (*S. typh)*, and the fungal pathogen *Cryptococcus neoformans (C. neo)* (Fig. 1C). We detected Gal-9-FLAG binding only with *S. typhimurium*, which supports a previously reported role for Gal-9 in the detection of *S. typh*imurium during infection of HeLa cells (Thurston et al., 2012).

Having established an interaction between Gal-9 and *Mtb* using a cell-free system, we next sought to determine whether Gal-9 localizes to *Mtb* during macrophage infection using structured illumination microscopy (SIM) of Gal-9-FLAG cells infected with mcherry-expressing *Mtb* (*Mtb*-mcherry) (Fig. 1D, 1E). Although this approach cannot distinguish between Gal-9 phagosome recruitment and direct *Mtb* binding, we observed clear localization of Gal-9-FLAG along the *Mtb* perimeter and confirmed this using fluorescence line scan quantification (Fig. 1G). To examine the association between Gal-9 and *Mtb* at higher resolution, *Mtb*-infected Gal-9-FLAG cells were processed for immunogold electron microscopy and probed with anti-FLAG antibody (Fig. S1). While the majority Gal-9-FLAG puncta localized to membrane structures

throughout the cell (Fig. S1A arrowheads, S1B), approximately 25% localized to phagosome membranes (Fig. S1A, black arrows, S1B), with a minority of puncta localizing to the edge of bacteria (Fig. S1A, white arrows, S1B). Taken together, these results suggest that Gal-9 can bind directly to *Mtb* via carbohydrate-binding, and that Gal-9 is recruited to both phagosomal and extra-phagosomal membranes during *Mtb* infection.

ESX-1 triggers recruitment of endogenous Gal-9 to *Mtb* in primary macrophages

We next sought to determine the role of ESX-1-driven membrane damage in the recruitment of endogenous Gal-9 using immunofluorescence microscopy. We infected WT BMDMs with WT GFP-expressing *Mtb* (*Mtb*-GFP) and fixed microscopy plates at 3, 5, 8, 12, and 24 hours-post infection. Using an automated analysis platform to quantify Gal-9 recruitment to *Mtb* from >4000 bacteria, we found *Mtb*-Gal-9 colocalization was evident as early as 3 hours post-infection, and reached a maximum of 15% at 8 hours post-infection before returning to 10-12% for the remainder of the time course (Fig. 2A, 2B). We observed minimal colocalization between Gal-9 and the ESX-1 secretion mutant, Δ*EccC*, indicating a requirement for ESX-1-driven membrane damage in Gal-9 recruitment. We also measured endogenous Gal-3 recruitment to *Mtb* as a positive control for galectin recruitment, as this galectin has been shown previously to recruit to *Mtb* (Chauhan et al., 2016, Bell et al., 2021). Consistent with a role for ESX-1 in galectin activation, we found that Gal-3 colocalized with approximately 8-11% of WT *Mtb* but showed no recruitment to Δ*EccC Mtb* (Fig. 2C, 2D). Thus, endogenous Gal-9 and Gal-3 are recruited to *Mtb* in an ESX-1-dependent manner early after infection and maintain steady localization with a minority of bacteria throughout infection.

Generation and validation of a Gal-3, -8, and -9 triple knockout (TKO) mouse

While the roles of galectins during macrophage infection are well documented, their contributions to immunity in vivo are poorly understood. Our discovery of Gal-9 as an *Mtb*-binding host protein motivated us to consider the potential contributions of other closely related galectins that could act separately or together with Gal-9 in the response to infection. Of the fifteen identified murine galectins, Gal-3, -8, and -9 have been demonstrated to sense damage phagosomes and recruit to intracellular bacteria (Thurston et al., 2012, Bell et al., 2021). Considering these shared characteristics, we reasoned Gal-3, -8, and -9 might serve redundant functions in the response to infection, and that compensatory effects might mask phenotypes of single gene knockouts. Therefore, we used CRISPR/Cas9 to generate Gal-3, -8, and -9 triple knockout mice (designated TKO) (Fig. S2). We generated two TKO mouse strains, S1 and S2, both of which harbor mutations in exon 1 of Gal-3, -8, and -9 that result in premature STOP codons. Strain S1 was used for all experiments except *S. typhimurium* experiments, which used strain S2. We found that TKO mice exhibited normal development and growth (Fig. S2B). In addition, we performed western blots on isolated BMDMs using antibodies that recognize Gal-3, -8, and -9 and confirmed that these mutations lead to dramatic decreases in protein expression (Fig. S2A). We also validated knockout of Gal-3 and Gal-9 in strain S1 using immunofluorescence of *Mtb*-infected BMDMs (Fig. S2C, S2D), but could not validate Gal-8 knockout with this approach since the anti-Gal-8 antibodies we tested did not perform well in immunofluorescence experiments.

Galectins have documented roles in the response to lysosomal damage, which entail activation of lysophagy and ESCRT-mediated repair (Chauhan et al., 2016, Jia et al., 2020a, Jia et al., 2020b). To phenotypically validate our TKO cells, we treated WT and TKO BMDMs with lysosome membrane damaging agent Leu-Leu-OMe (LLOMe) or PBS control and stained with Lysotracker Green to assess lysosome abundance and quality (Fig. S2E). We observed increased loss of lysotracker signal in TKO BMDMs relative to WT, indicating an impairment in lysosomal repair in galectin-deficient cells. Thus, we have established a system to evaluate the function of the galectin damage-response system in vivo.

Deficiency in Gal-3, -8, and -9 leads to impaired *Mtb* lysosomal trafficking and accumulation of autophagic targeting intermediates

Considering galectins have well characterized roles in autophagy activation (Thurston et al., Chauhan et al., 2016, Bell et al., 2021), we first sought to determine whether Gal-3, -8, and -9 play a role in targeting *Mtb* to autophagy in primary macrophages. Cytosolic access by *Mtb* activates ubiquitin-mediated selective autophagy, which is characterized by deposition of ubiquitin and ubiquitin-binding autophagy receptors, such as p62, around *Mtb* (Watson et al., 2012, Manzanillo et al., 2013). To determine whether Gal-3, -8, and -9 activate ubiquitin-mediated selective autophagy, we quantified polyubiquitin, polyubiquitin linkage subtypes, and p62 recruitment to *Mtb*-GFP in WT and TKO BMDMs. At 8 hours post-infection, we found a 40-70% increase in *Mtb* colocalization with all autophagy markers in TKO macrophages (Fig. 3A-D), indicating Gal-3, -8, and -9 are dispensable for ubiquitin and p62 recruitment to *Mtb*, and act downstream of these proteins by directing ubiquitin- and p62-associated *Mtb* to the lysosome for degradation. The accumulation of ubiquitin-labeled bacteria in TKO macrophages was dependent on ESX-1-mediated phagosome permeabilization (Fig. 3C, 3D), and reached a maximum of ~20% at 8 hours post-infection that persisted until 24 hours post-infection (Fig. 3E, 3F), indicating a sustained block in the clearance of cytosol-exposed *Mtb*. We hypothesized this accumulation phenotype could indicate poor engagement of autophagosome-nucleating autophagy receptors (Stolz et al., 2014), similar to how *Tax1bp1*$^{-/-}$ BMDMs accumulate autophagy intermediates (Budzik et al., 2020). Indeed, in cell lines Gal-8 is reported to recruit TAX1BP1 and NDP52 to restrict *Mtb* and *S. typhimurium*, respectively (Bell et al., 2021, Thurston et al., 2012). Whether Gal-3 and Gal-9 recruit autophagy receptors is unknown, but an interaction between Gal-9 and OPTN was recently demonstrated (Bell et al., 2021). We measured *Mtb*-GFP colocalization with TAX1BP1, OPTN, and p62 (included as a positive control for recruitment), and observed no differences between genotypes, but found a reduction in TAX1BP1 and OPTN colocalization relative to p62 in TKO macrophages (Fig S3). This result is challenging to interpret because it is unclear whether this reduction is due to defective autophagy receptor recruitment, or differences in galectin-driven clearance of TAX1BP1- and OPTN-associated *Mtb* compared to p62-associated *Mtb*. Nevertheless, these data support the notion that ESX-1-driven phagosome perforation activates galectin-dependent clearance of ubiquitin- and p62-labeled *Mtb*.

To more directly test whether Gal-3, -8, and -9 mediate clearance of *Mtb*, we measured *Mtb* delivery to the lysosome, the final step of *Mtb*-targeted selective

autophagy. After staining *Mtb*-GFP-infected cells with Lysotracker Red-DND99, we found a 20% decrease in *Mtb*-Lysotracker colocalization in TKO macrophages relative to WT (Fig. 3G, 3H). This decrease was likely not due to defects in lysosomal homeostasis or repair in TKO cells (as seen during LLOMe treatment in Fig. S2E), as both resting and infected WT or TKO macrophages showed similar numbers of Lysotracker puncta (Fig. 3I). Intracellular pathogens are directed to the lysosome via the endosomal pathway or the cytosolic autophagy pathway. Because *Mtb*-lysotracker colocalization cannot distinguish between these two pathways, we measured responses to Δ*EccC Mtb*, which cannot access the cytosol and remains in endosomes. In contrast to WT *Mtb*-lysotracker colocalization, galectin deficiency had no impact on Δ*EccC Mtb*-lysotracker colocalization (Fig. 3J, 3K), suggesting Gal-3, -8, and -9 are nonessential for *Mtb* endosomal trafficking, but partially required for delivery of *Mtb* to the lysosome via autophagy. Taken together, these data indicate that while galectins are dispensable for the initiation of ubiquitin-mediated selective autophagy, they are necessary for efficient clearance of cytosol exposed *Mtb*.

Gal-3, -8, and -9 are nonessential for control of intracellular bacteria in primary macrophages

Because we observed a slight clearance defect in *Mtb*-infected TKO macrophages, we tested whether this defect would impact *Mtb* growth, as defects in autophagy can lead to loss of restriction (Watson et al., 2012, Manzanillo et al., 2013). Previous reports utilizing knockdown or knockout cell lines have demonstrated a role for Gal-8 in the suppression of *Mtb* and *S. Typhimurium* growth via antibacterial selective-autophagy induction (Thurston et al., 2012, Bell et al., 2021). However, whether Gal-3, -8 and -9 cooperate to restrict bacterial growth in primary macrophages remains unexplored. By measuring bacterial growth of a bioluminescent *Mtb* reporter strain at a multiplicity of infection (MOI) of 1 or 5 (Fig. 4A, B), or enumerating colony-forming units (CFUs) on days 0 and 4 post-infection (Fig. 4C), we found that *Mtb* growth was unaltered in TKO macrophages (Fig. 4A-C). Thus, despite a role for Gal-3, -8, and -9 in *Mtb*-targeted autophagy (Fig. 3), these galectins are dispensable for restriction of *Mtb* growth, possibly suggesting TKO macrophages can mount compensatory defenses or maintain sufficient autophagic responses, likely through activation of alternate autophagy pathways (Watson et al., 2012, Manzanillo et al., 2013, Franco et al., 2016).

To more broadly examine the function of Gal-3, -8, and -9 in the defense against diverse pathogens, we tested TKO macrophages against a panel of phylogenetically-distinct intracellular bacteria. TKO macrophages exhibited normal restriction of bacterial growth against all pathogens tested (Fig. 4D-F). Furthermore, we found that Gal-3, -8, and -9 were not required for control of either WT or Δ*flaA L. pneumophila* (Fig. 4E), indicating that these galectins are dispensable for inflammasome-dependent and -independent immunity (Ren et al., 2006). We also found that *L. monocytogenes* grew unhindered in both WT and TKO macrophages (Fig. 4F). *L. monocytogenes* replicates efficiently in macrophages due in part to virulence factor-mediated inhibition of autophagy, which comprises ActA-mediated actin polymerization and PlcA- and PlcB-mediated cleavage of LC3-II from autophagosome membranes (Mitchell et al., 2015, Mitchell et al., 2018). To test a role for Gal-3, -8, and -9 in *L. monocytogenes*-targeted autophagy, we evaluated an autophagy-sensitive strain of *L. monocytogenes* (Δ*actA*

PlcA^{H86A} PlcB^{H69G}, designated “triple mutant”) (Mitchell et al., 2018). TKO macrophages showed robust restriction of the autophagy-sensitive triple mutant, indicating no requirement for Gal-3, -8, and -9 in *L. monocytogenes*-targeted autophagy. Thus, Gal-3, -8, and -9 are dispensable for bacterial growth restriction in primary macrophages.

Although we did not observe any bacterial growth phenotypes in mouse macrophages deficient for Gal-3, -8, and -9, we reasoned galectins might have distinct effects on cell-autonomous immunity in mouse and human cells, and therefore evaluated galectin function in human THP-1 macrophages. We observed no differences in *Mtb* growth in two different Gal-9 shRNA knockdown cell lines compared to control shRNA cells (Fig. 4G), indicating Gal-9 is nonessential for control of *Mtb* infection in THP-1 macrophages.

Galectins contribute to the control of *Mtb* during the chronic phase of infection

To assess the role of Gal-3, -8, and -9 during *Mtb* infection in vivo, TKO and WT mice were infected with a low dose of *Mtb* via the aerosol infection route (Fig. 5). During the acute phase of infection, no differences in bacterial burden were observed in TKO lungs or spleens compared with WT (Fig. 5A, 5B). These data are consistent with the understanding that *Mtb* is largely resistant to innate effector functions during the acute phase (Mayer-Barber and Barber, 2015). However, by 63 days post-infection, there was 2.5-fold higher bacterial burden in TKO lungs (Fig. 5A). We also observed a higher bacterial burden in TKO spleens at this time point, although this effect fell below a $p = 0.05$ threshold for statistical significance (Fig. 5B). The chronic phase bacterial burden phenotype in TKO mice aligned with a slight increase in susceptibility (Fig. 5C), indicating that these galectins are important for full resistance to infection during the chronic phase of infection. We also challenged these mice with a high dose of *Mtb* and observed a similar trend towards increased bacterial burdens in TKO mice (Fig. S5). Taken together, these data support a partial role for the galectins in controlling bacterial burden primarily during the chronic phase of infection.

Galectins are not required for control of *L. monocytogenes* or *S. typhimurium* in vivo

To assess the role of galectins during infection with diverse intracellular bacteria in vivo, we challenged TKO mice and WT mice with *L. monocytogenes* or *S. typhimurium.* In a *L. monocytogenes* intravenous acute infection model, we detected similar bacterial burdens in spleen and liver from WT and TKO mice at 48 hours post-infection (Fig. S6A, S6B). Likewise, bacterial burdens were unaltered in TKO mice that were infected with *S. typhimurium* via intraperitoneal injection (Fig. S6C, S6D). This result is surprising, considering the extensive characterization of Gal-8-driven control of *S. typhimurium* in cells (Thurston et al., 2012, Ravenhill et al., 2018). Thus, Gal-3, -8, and -9 are not required for antibacterial immunity during *L. monocytogenes* and *S. typhimurium* systemic infection in vivo.

Galectin deficiency leads to defective antigen-specific T cell responses in the spleen

Because Gal-3, -8, and -9 were found to be nonessential for cell-autonomous immunity, yet TKO mice had higher bacterial burdens during the chronic phase of *Mtb*

infection, we hypothesized that galectins could play a role in shaping the adaptive immune response. An important component of the adaptive immune response to *Mtb* infection is IFN-γ production by activated *Mtb*-specific CD4 T cells (Mayer-Barber and Barber, 2015). To test whether galectins promote CD4 T cell responses in vivo, we performed IFN-γ enzyme-linked immunospot (ELISpot) on cells isolated from mice infected with *Mtb* via the aerosol route, and quantified responses to immunodominant I-A^b presented epitopes from *Mtb* antigens ESAT-6, and Ag85B (Fig. 6). In TKO spleens harvested at 3 or 4 weeks post-infection, we unexpectedly detected a significant decrease in IFN-γ-secreting CD4 T cells specific for Ag85B. In contrast, we observed no differences for ESAT-6-specific CD4 T cells (Fig. 6A), which are chronically activated throughout *Mtb* infection due to sustained antigen exposure (Moguche et al., 2015, Moguche et al., 2017). We also measured T cell responses in the lung at this time point but found no differences between WT and TKO mice for either antigen (Fig. 6B), possibly reflecting the robust enrichment of highly activated T cells in this organ. At 9 weeks post-infection we were unable to detect any significant Ag85B-specific T cell response (Fig. 6C), consistent with the contraction of this T cell subset due to diminished antigen exposure during chronic infection (Moguche et al., 2017). Lastly, we measured splenic T cell responses in a high dose infection and, in contrast to our low dose infection results, observed no differences in Ag85B-specific T cell responses (Fig. 6D), suggesting increased antigen exposure at high doses of *Mtb* can promote robust T cell activation in the absence of Gal-3, -8, and -9. These findings suggest that Gal-3, -8, and -9 are necessary for full activation of select antigen-specific CD4 T cells in the spleen but are dispensable for T cell activation in tissues replete with antigen. In addition, these results reveal an unexpected role for the galectin system in T cell activation that contrasts with Gal-9/Tim-3-mediated suppression of T cell function (Zhu et al., 2005).

Chapter 2.2: Discussion

Macrophage infection studies have demonstrated important roles for individual galectins in the detection of and defense against intracellular pathogens. However, evidence that galectins are required for bacterial control and host resistance in the mouse model is limited. Here, we establish a system to evaluate the function of membrane damage sensing in the immune response to intracellular bacteria. Due to the extensive characterization of the many antibacterial functions of galectins, we hypothesized that disabling the galectin system in vivo might lead to defective innate immune recognition of bacteria and loss in bacterial growth restriction. To our surprise, we found that antibacterial immunity was largely intact in these galectin-deficient mice. First, we found that Gal-9 can bind to *Mtb* and *S. typhimurium* in a carbohydrate binding-dependent manner. Second, we found that TKO macrophages had slight defects in *Mtb*-targeted autophagy, despite showing normal restriction of bacterial growth. Finally, we found that mice deficient for Gal-3, -8, and -9 maintained normal bacterial growth restriction during acute infection with *S. typhimurium* and *L. monocytogenes* but exhibited slight defects in bacterial containment and T cell activation during chronic *Mtb* infection. Thus, although Gal-3, -8, and -9 are nonessential for bacterial control during acute infection, they make contributions to host defense against chronic tuberculosis infection.

The cell wall is a critical determinant of mycobacterial pathogenicity, and recognition of its constituents by innate immune receptors shapes the host immune response (Ravesloot-Chavez et al., 2021). The mycobacterial cell wall comprises an inner layer of peptidoglycan and arabinogalactan (AG) to which an outer layer of long-chain mycolic acids is covalently attached (Daffé, 2015). In addition, the surface of *Mtb* has been demonstrated to comprise a thick non-covalently linked polysaccharide "capsule," which is likely prone to release or shedding under different conditions in vitro or in vivo (Sani et al., 2010, Daffé, 2015). While many cell wall constituents are known modulators of host immune pathways (Pitarque et al., 2008, Russell, 2011), their accessibility to innate immune receptors during infection is poorly understood. Moreover, the nature of these interactions is further complicated by the dynamic exchange of cell wall constituents between phagosomal bacteria and their hosts, which is thought to involve active trafficking of glycolipids or passive shedding of the mycobacterial capsule (Beatty et al., 2000). Our data revealed that the carbohydrate-binding protein, Gal-9, can bind to *Mtb* in vitro. Importantly, this interaction was inhibited by adding lactose to the binding reaction, which suggests Gal-9 carbohydrate-binding is critical for Gal-9 association with *Mtb*. Using immuno-EM, we observed localization of Gal-9 to the edge of bacteria, suggesting this interaction occurred in vivo. These findings are consistent with a recent report that demonstrated Gal-9 could bind *Mtb* and chemically-synthesized AG in vitro (Wu et al., 2021). As AG is likely not surface-exposed under native conditions (Daffé, 2015), release of the outer layer and capsule in vivo, or with the use of detergents in growth medium, might expose AG to Gal-9, like how TLR-2 might gain access to the glycolipid TDM, which has not been detected in the outermost layer of *Mtb* (Ortalo-Magné et al., 1996). Additionally, release of AG or other Gal-9-binding glycolipids could localize Gal-9 to extra-phagosomal compartments (Beatty et al., 2000), as suggested by our immuno-EM data. However, it is likely that

Gal-9 additionally associates with host glycoproteins in these instances, as sterile damage to endosomes has been shown to induce robust Gal-9 puncta formation (Thurston et al., 2012). Our observation that Gal-9 could also bind *S. typhimurium* suggests Gal-9 recognition of bacterial constituents is not limited to AG. Indeed, galectins have been shown to bind and recognize other intracellular pathogens and their polysaccharide constituents (Pelletier et al., 2003, Rabinovich et al., 2007), further supporting a role for these proteins in the direct recognition of pathogens. Finally, Gal-9-pathogen interactions have been proposed to modulate macrophage function (Rabinovich et al., 2007, Wu et al., 2021). During infection, Gal-9 localization to the bacterial surface might enhance autophagic targeting by nucleating autophagy factors, such as OPTN (Bell et al., 2021), directly onto bacteria, as opposed to recruiting them to damaged membranes in the vicinity of cytosolic bacteria.

Autophagy is a critical innate immune pathway that promotes clearance of intracellular pathogens from the cytosol. Our data show that deficiency in Gal-3, -8, and -9 in primary macrophages in vitro leads to inefficient lysosomal trafficking of cytosolic *Mtb* and an accumulation of ubiquitin- and p62-associated bacteria, suggesting that galectins promote clearance of these *Mtb*-autophagy intermediates. However, the exact mechanism of this galectin-driven autophagy pathway, and whether one or multiple galectins are required, remains unclear. Galectin-dependent clearance of *Mtb* is proposed to occur through Gal-3-mediated recruitment of the ubiquitin ligase, Trim16, which promotes autophagy via ubiquitin deposition around *Mtb*, and Gal-8-mediated recruitment of the autophagy receptor, TAX1BP1 (Chauhan et al., 2016, Bell et al., 2021). Although we found robust ubiquitin recruitment in TKO macrophages, indicating no Gal-3/Trim16 effect in our system, we observed a 25% decrease in TAX1BP1 and OPTN recruitment relative to another autophagy receptor, p62, leaving open the possibility that TAX1BP1 and OPTN do not accumulate or recruit to *Mtb* as well as p62 in TKO macrophages. Further investigation into the precise mechanisms at hand should consider the contributions of other critical autophagy proteins, such as the kinase TBK1, which phosphorylates OPTN, p62, and TAX1BP1 to promote their activation (Wild et al., 2011, Richter et al., 2016, Matsumoto et al., 2015, Fu et al., 2018). In addition, the robust ubiquitin recruitment to *Mtb* in TKO macrophages suggests that the galectin and ubiquitin pathways operate separately in the context of autophagy, and that ubiquitin-mediated selective autophagy is largely intact in TKO macrophages. Indeed, macrophages employ several proteins that can target *Mtb* to the ubiquitin-mediated selective autophagy pathway, such as Parkin, Smurf1, and cGAS/STING (Manzanillo et al., 2013, Franco et al., 2016, Watson et al., 2012). In addition, it was recently proposed that a ubiquitin-binding *Mtb* surface protein (Rv1468c) could promote ubiquitin recruitment and p62-dependent autophagic targeting of *Mtb* (Chai et al., 2019), further implying that numerous autophagy activation mechanisms exist in macrophages to ensure clearance of *Mtb* from the cytosol. Considering several routes to autophagy are likely possible during infection, future investigation of Parkin- or STING-deficient macrophages, which show dramatic defects in ubiquitin-mediated selective autophagy, may provide a suitable genetic background to investigate the ubiquitin-independent galectin contribution to autophagy.

Our observation that galectin-deficiency leads to defects in both autophagy and antigen-specific CD4 T cell responses raises the possibility that these phenotypes could

be linked. Indeed, the role of autophagy in immunity is known to extend beyond cell-intrinsic pathogen restriction and is additionally reported to involve regulation of MHC class II antigen presentation of both self and foreign cytosolic antigens (Levine and Deretic, 2007, Lee et al., 2010), thereby linking autophagy to the adaptive immune response. Mechanistically, autophagy mediates the capture and degradation of cytosolic pathogens and antigens, after which the peptide constituents are trafficked to MHC-class-II-containing late endosomes, and then loaded onto MHC class II complexes for presentation to CD4 T cells (Levine and Deretic, 2007, Paludan et al., 2005, Schmidt et al., 2007). In mouse infections with OVA-expressing *L. monocytogenes*, autophagy in dendritic cells has been shown to promote OVA antigen-specific CD4 T cell activation, indicating a role for autophagy in MHC class II presentation of microbial antigens to CD4 T cells in vivo (Lee et al., 2010). Furthermore, inhibition of host autophagy by the secreted *Mtb* effector, Rv2741, has been shown to impair Ag85B-specific, but not ESAT-6-specific, CD4 T cell activation in vivo (Saini et al., 2016), possibly suggesting that some microbial antigens, but not others, rely on autophagy for antigen presentation. Interestingly, the CD4 T cell activation defect we observed in TKO mice was similarly specific to Ag85B, while ESAT-6 CD4 T cell responses were unchanged. How some antigens, but not others, might access MHC class II compartments via autophagy is an interesting question. Because ESAT-6 is highly expressed throughout *Mtb* infection (Moguche et al., 2015), it is possible that the abundance of this protein relative to Ag85B, which exhibits downregulation 3 weeks post-infection (Rogerson et al., 2006), negates a requirement for autophagy in antigen presentation. Alternatively, Ag85B might preferentially access the autophagy pathway through association with *Mtb* via interactions with mycolic acid substrates in the cell wall (Kremer et al., 2002), whereas ESAT-6 is highly secreted into the cytosol or extracellular milieu, possibly enabling it to access other cellular compartments not targeted by autophagy (Sreejit et al., 2014), or to access the antigen presentation pathway through phagocytosis and endolysosomal trafficking. Antigen presentation assays using APC and antigen-specific CD4 T cell co-culture systems will prove useful in determining whether the galectin system indeed acts as a link between innate and adaptive immunity.

Our observation that galectin-deficiency leads to CD4 T cell activation defects in the spleen but not the lung indicates galectin-dependent T cell activation is organ-specific and likely depends on the immune cell composition of the infected organ or tissue. In the *Mtb*-infected lung, extensive inflammation and chemokine gradients drive strong enrichment of highly activated antigen-specific CD4 T cells into the lung (Mihret et al., 2012, Sakai et al., 2014). In contrast, the spleen exhibits mild and contained inflammation, and maintains a diverse population of both naïve and activated T cells (Cooper et al., 2009). Thus, naïve T cells in the spleen may rely on additional antigen presentation mechanisms in cognate APCs, such as galectin-mediated antigen presentation via autophagy, for efficient priming and activation.

In this study, we found that TKO mice exhibit a loss in bacterial growth restriction during chronic *Mtb* infection, while bacterial control was unaltered during acute infection with *S. typhimurium*, *L. monocytogenes,* and *Mtb*. TKO mice likely control *S. typhimurium* infection via other potent innate immune mechanisms that have been shown to mediate restriction in vivo, such as inflammasome assembly and Caspase-1 activation, TLR-11 signaling, and LC3-associated phagocytosis (Broz et al., 2012,

Mathur et al., 2012, Masud et al., 2019). In addition, while TKO mice exhibit normal resistance to intraperitoneal *S. typhimurium* infection and intravenous *L. monocytogenes* infection, it is possible oral infection, which has been shown to elicit protective antibacterial autophagy in the gut epithelium (Conway et al., 2013), may uncover other roles for galectins in vivo. Moreover, the effects of certain innate immune mechanisms are only evident during infection of the gut epithelium, as exemplified by NOD2-mediated restriction of *L. monocytogenes* growth during oral but not intravenous infection (Kobayashi et al., 2005). Previous investigations have identified few innate immune genes that, alone, can significantly restrict bacterial growth after intravenous injection with a lethal dose of *L. monocytogenes.* This is due in part to rapid bacterial growth in the absence of IFN-γ-induction and protective CD8 T cell responses (D'Orazio, 2019). Nevertheless, TKO mice likely restrict bacterial growth via Myd88- and TNF-mediated pro-inflammatory signaling (Witte et al., 2012, D'Orazio, 2019). In addition, any galectin-driven autophagy pathway is likely inhibited through the combined actions of the secreted virulence factors, ActA, PlcA, and PlcB, which mediate autophagy evasion via actin-based motility and LC3-II cleavage from autophagosome membranes (Mitchell et al., 2018).

During the acute phase of *Mtb* infection, macrophages are established as the primary site of infection and the innate immune response is activated, while the chronic phase comprises coordinated responses between both the innate and adaptive immune response that aim to contain the infection (Mayer Barber and Barber, 2015). *Mtb* is highly resistant to innate immune functions, as demonstrated by the surprisingly short list of innate immune genes that have been shown to promote restriction of bacterial growth at this stage. However, during chronic infection, galectin deficiency and potential defects in antibacterial selective autophagy, antigen presentation, and CD4 T cell activation, may lead to cumulative effects on bacterial containment. Similarly, *Mtb*-infected *Smurf1-/-* mice have higher *Mtb* burdens exclusively during the chronic phase (Franco et al., 2016), further supporting a role for certain autophagy-activating genes in the containment of *Mtb* during chronic infection.

In conclusion, our data suggest that the galectin system plays a limited role in the innate immune response to acute bacterial infection, and functions primarily to promote optimal antibacterial immunity during chronic infection via regulation of both innate and adaptive immune responses. These findings have implications for understanding the roles and limitations of damage and pathogen sensors in chronic disease.

Chapter 2.3: Figures

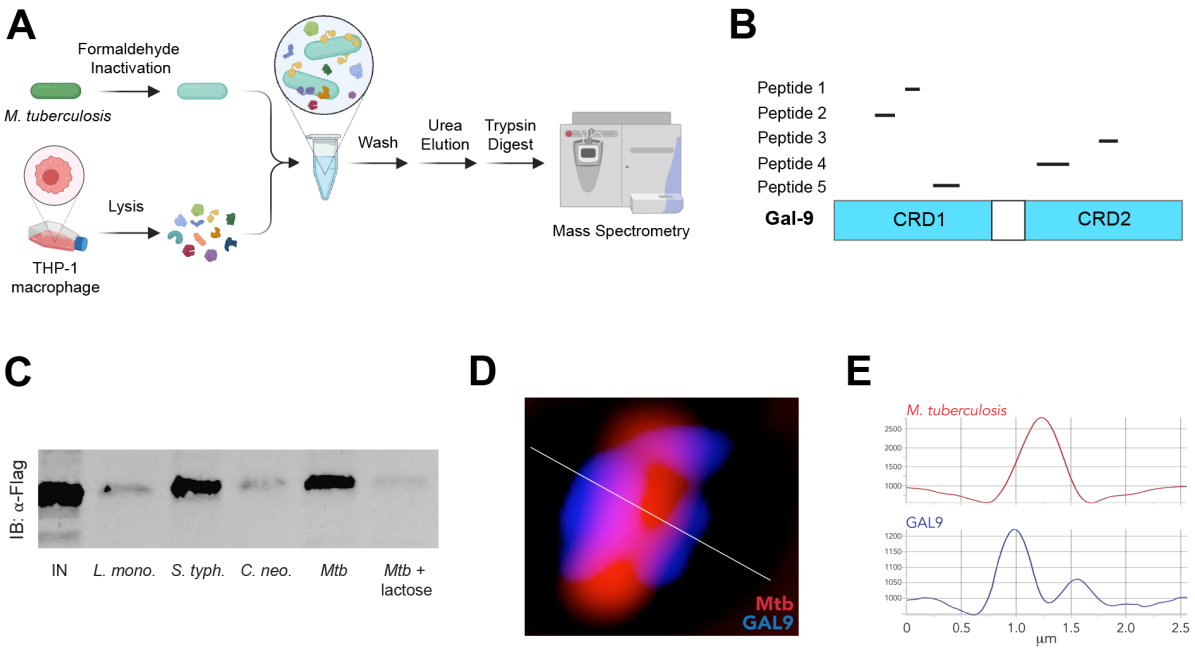

Figure 1. Gal-9 binds to *Mtb* and *S. typhimurium.*
(**A**) Experimental design for *Mtb* pull-down mass spectrometry (MS) identification of *Mtb*-binding proteins. (**B**) Domain organization of Gal-9 displaying unique peptides identified by MS in (A). CRD, carbohydrate recognition domain. (**C**) Immunoblot of in vitro binding reactions between indicated pathogens and Gal-9-FLAG lysate, immunostained for FLAG. IB, immunoblot; IN, input; *L. mono*, *Listeria monocytogenes*; *S. typh*, *Salmonella typhimurium*; *C. neo*, *Cryptococcus neoformans*; *Mtb*, *Mycobacterium tuberculosis*. (**D**) Structured illumination microscopy (SIM) of RAW 264.7 cells stably expressing Gal-9-FLAG (blue) infected with WT *Mtb*-mCherry (red) (MOI = 1) 6 hours post-infection. (**E**) Mean fluorescence intensity (MFI) line scan along white line in (D).

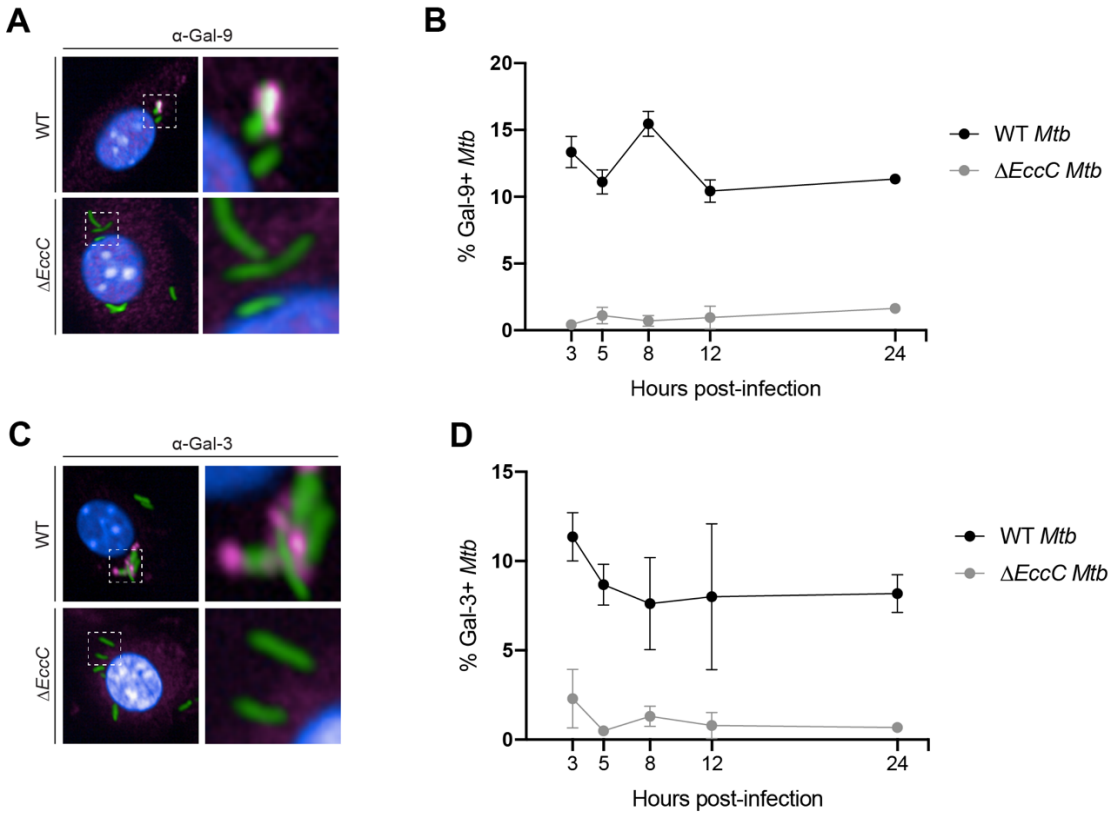

Figure 2. ESX-1 triggers recruitment of endogenous Gal-9 to *Mtb* in primary macrophages.
(**A**) Immunofluorescence of WT BMDMs infected with WT or Δ*EccC Mtb*-GFP (green) (MOI = 2) 8 hours post-infection and immunostained for Gal-9 (magenta). (**B**) Quantification of WT or Δ*EccC Mtb* colocalization with Gal-9 at indicated time points. Representative images at 8 hours post-infection shown in (A). (**C**) Same as in (A) but immunostained for Gal-3. (**D**) Same as in (B) but WT or Δ*EccC Mtb* colocalization with Gal-3. Figures represent data from two independent experiments (3, 5, 8, and 12 hours post-infection time points in B and C), or one experiment (24 hour post-infection time points in B and C).

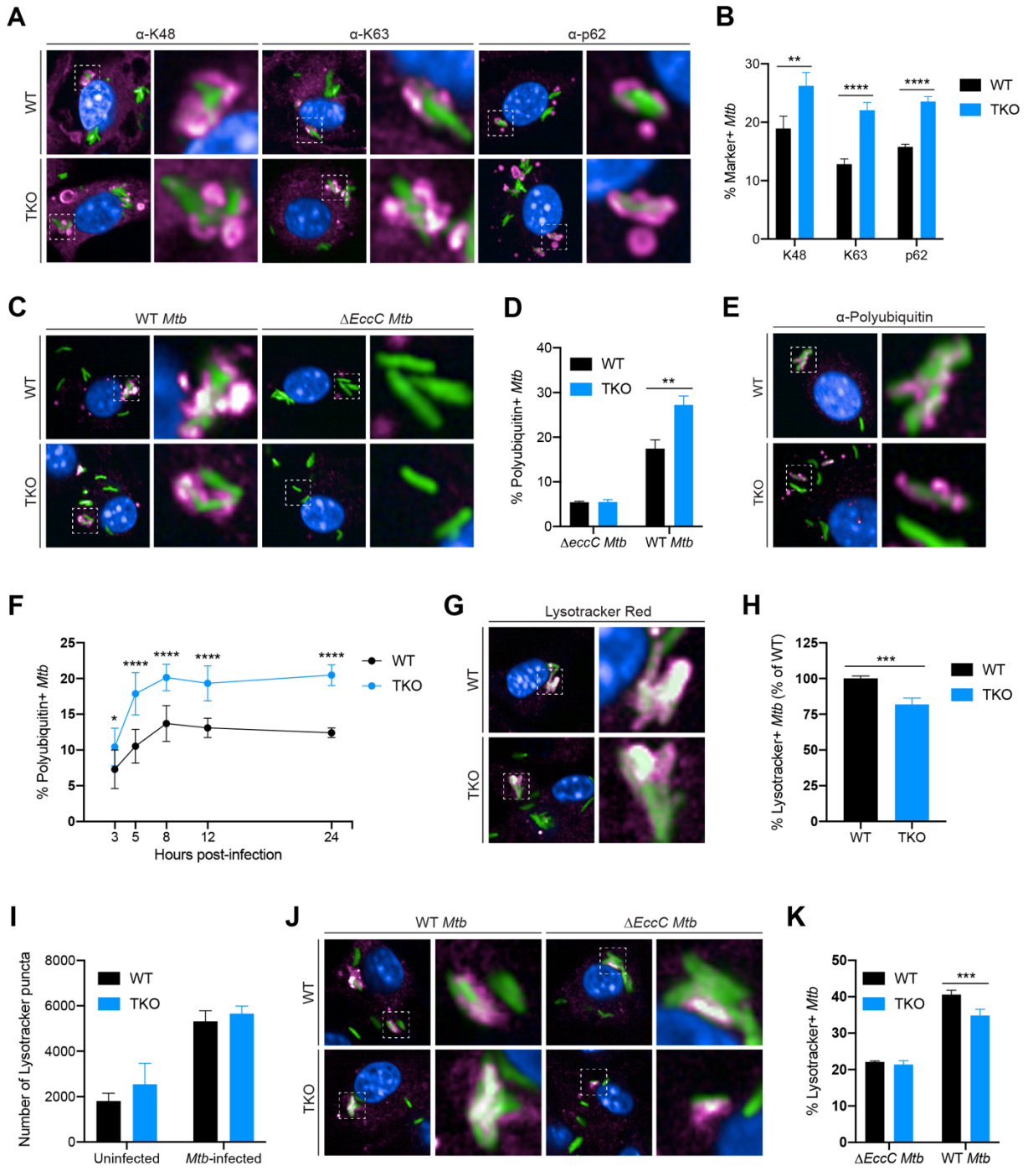
A
α-K48
α-K63
α-p62
WT
TKO
B
% Marker+ Mtb
WT
TKO
K48
K63
p62
C
WT Mtb
ΔEccC Mtb
D
% Polyubiquitin+ Mtb
ΔeccC Mtb
WT Mtb
E
α-Polyubiquitin
F
% Polyubiquitin+ Mtb
Hours post-infection
G
Lysotracker Red
H
% Lysotracker+ Mtb (% of WT)
I
Number of Lysotracker puncta
Uninfected
Mtb-infected
J
K
% Lysotracker+ Mtb

Figure 3. TKO macrophages exhibit impaired *Mtb* lysosomal trafficking and accumulate autophagic targeting intermediates.
(**A**) Immunofluorescence of WT or TKO BMDMs infected with *Mtb*-GFP (green) (MOI = 2) 8 hours post-infection and immunostained for K48, K63, or p62 (magenta). (**B**) Quantification of (A) for *Mtb*-GFP colocalization with indicated markers. (**C**) Same as in (A) but infected with WT or ∆*EccC Mtb*-GFP and immunostained for polyubiquitin. (**D**) Quantification of (C) for WT or ∆*EccC Mtb*-GFP colocalization with polyubiquitin. (**E**) Same as in (A) but immunostained for polyubiquitin. (**F**) Quantification of WT *Mtb*-GFP colocalization with polyubiquitin in WT or TKO BMDMs at indicated time points. Representative images at 5 hours post-infection shown in (E). (**G**) Same as in (A) but stained with Lysotracker Red. (**H**) Quantification of (G) for WT *Mtb*-GFP colocalization with Lysotracker Red signal. (**I**) Quantification of Lysotracker Red puncta 8 hours post-infection in mock- or WT *Mtb*-GFP-infected (MOI = 2) WT or TKO BMDMs. (**J**) Same as in (C) but stained with Lysotracker Red. (**K**) Quantification of (J) for WT or ∆*EccC Mtb* colocalization with Lysotracker Red signal. Figures represent data from three independent experiments (G, H) or are representative of two independent experiments (A-F, I-K). Error bars are SD from four technical replicates, *p<0.05., **p<0.01, ***p<0.001, ****p<0.0001 by unpaired t-test.

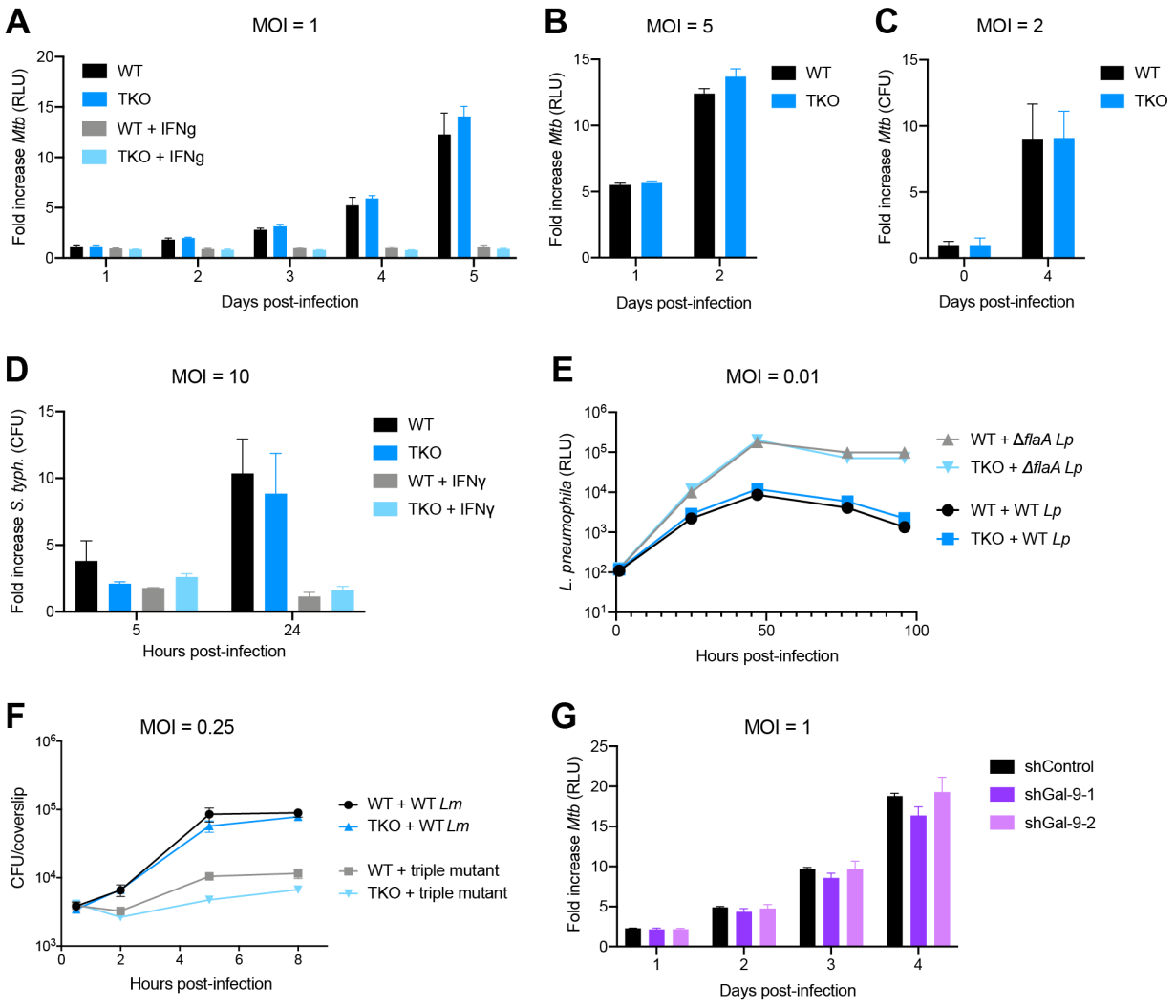

Figure 4. Gal-3, -8, and -9 are nonessential for bacterial growth restriction in macrophages.
(**A** and **B**) Relative light units (RLU) fold change of WT or TKO BMDMs infected with *Mtb*-lux (MOI = 1, A; MOI = 5, B) at indicated time points. (**C**) Colony-forming unit (CFU) fold change of WT or TKO BMDMs infected with WT *Mtb* (MOI = 2) at indicated time points. (**D**) Same as in (C) but infected with WT *S. typhimurium* (MOI = 10). (**E**) RLU of WT or TKO BMDMs infected with WT or Δ*flaA L. pneumophila*-lux (MOI = 0.01) at indicated time points. (**F**) CFU per coverslip of WT or TKO BMDMs infected with WT or Δ*actA* PlcA^{H86A} PlcB^{H69G} (triple mutant) *L. monocytogenes* (MOI = 0.25) at indicated time points. (**G**) RLU fold change of control or Gal-9 knockdown shRNA THP-1 cells infected with *Mtb*-lux (MOI = 1) at indicated time points. Figures represent one (B, E), or two (F) experiments, or are representative of two (C, D), or three (A, G) independent experiments. Error bars are SD from three (D, F, G), four (A-C), or five (E) technical replicates.

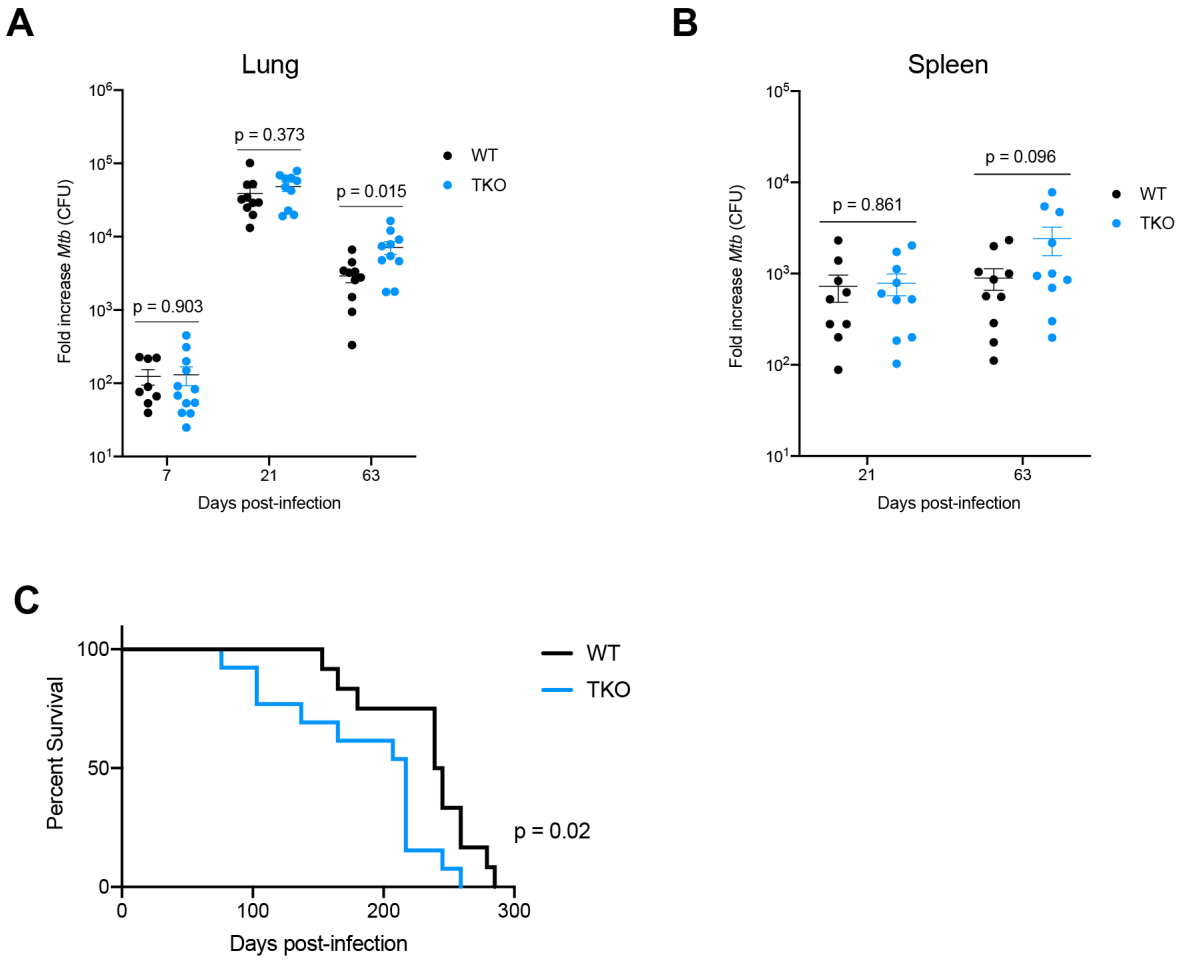

Figure 5. TKO mice exhibit impaired resistance during chronic *Mtb* infection
(**A**) WT and TKO mice were aerosol infected with 20-100 CFUs of *Mtb* Erdman and bacterial loads in lungs were enumerated by plating for CFU at indicated time points. To account for differences in day 0 CFU between the two pooled independent experiments, CFU fold change relative to day 0 is displayed. *n* = 10-12 mice per genotype (**B**) Same as in (A) but bacterial loads in spleens. (**C**) Survival of aerosol infected mice. *n* = 12-13 mice per genotype. Figures represent one experiment (C) or represent data from two independent experiments (A, C). Error bars are SEM (A, B) and p-values were determined by unpaired t-test (A, B), or Mantel-Cox log (C).

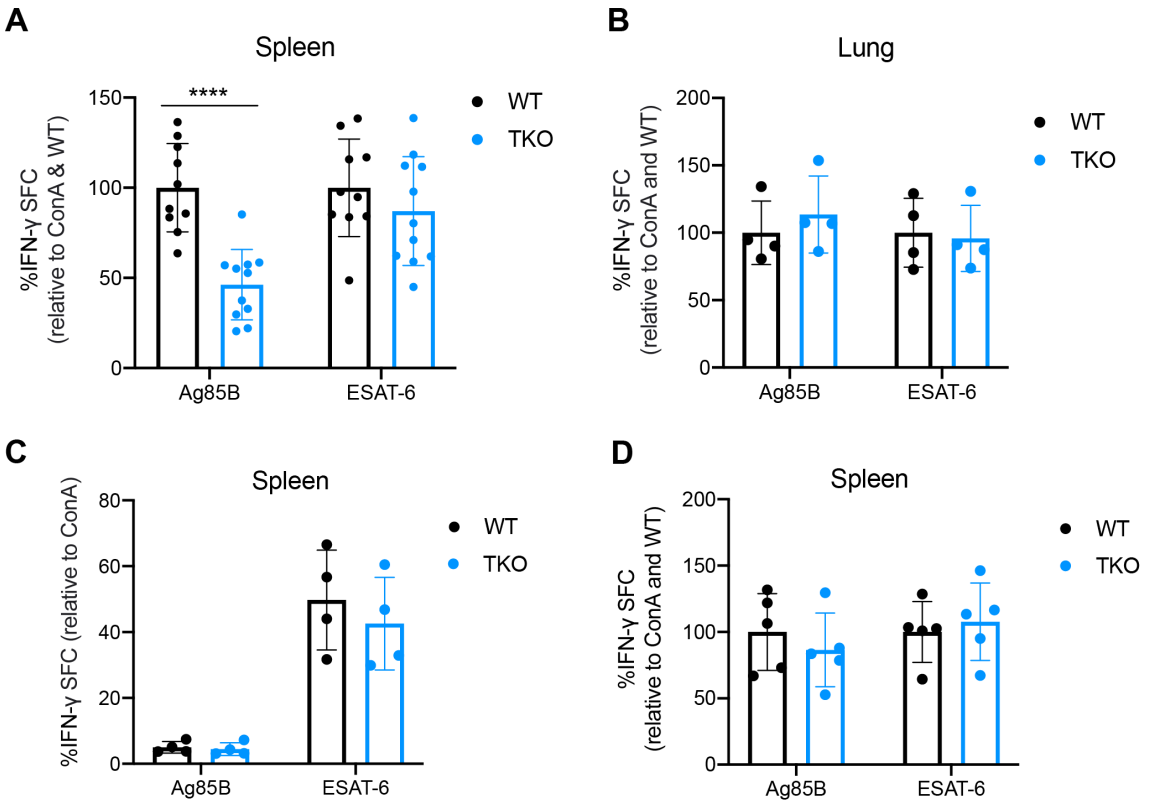

Figure 6. Galectins promote splenic Ag85B-specific T cell responses.
(**A**) WT and TKO mice were aerosol infected with 100-200 CFUs of *Mtb* Erdman and ELISpot was performed at 3-4 weeks post-infection on spleen single-cell suspension to detect IFN-γ spot-forming cells (SFC) responding to re-stimulation in vitro with *Mtb* peptides corresponding to I-A^b presented epitopes of indicated *Mtb* antigens. Data shown is IFN-γ SFC count relative to Concanavalin A (ConA) stimulated wells and WT. *n* = 10-11 mice per genotype. (**B**) Same as in (A) but ELISpot was performed on lung single-cell suspension. *n* = 4 mice per genotype. (**C**) Same as in (A) but ELISpot was performed at 9 weeks post-infection. Data shown is IFN-γ SFC count relative to Concanavalin A (ConA) stimulated wells. *n* = 4 mice per genotype. (**D**) Same as in (A) but mice were aerosol infected with 800 CFUs. *n* = 5 mice per genotype. Figures represent data from one (B-D) or three (A) independent experiments. Error bars are SD, ****p<0.0001 by unpaired t-test.

A

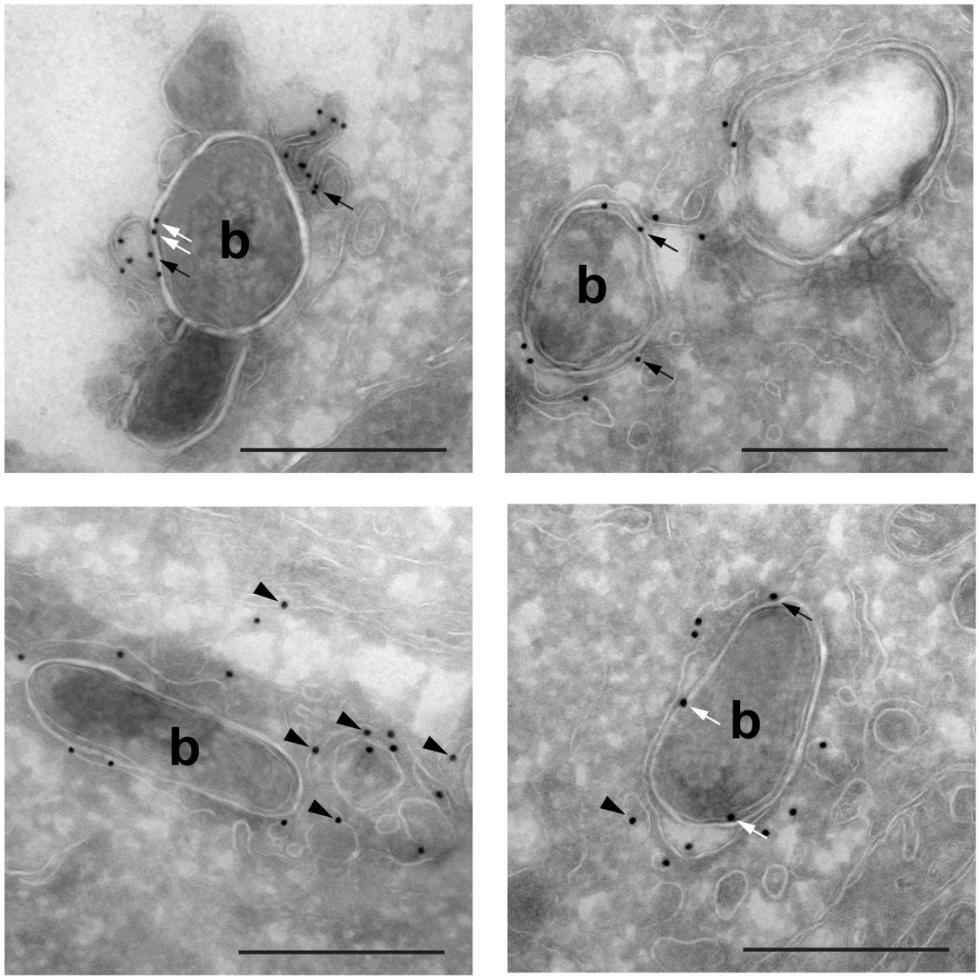

B

Membrane	Unknown	Phagosome	*Mtb*
61.05%	14.83%	19.48%	4.65%

Figure S1. Localization of Gal-9 during *Mtb* infection.
(**A**) Cryosections of RAW 264.7 cells stably expressing Gal-9-FLAG infected with WT *Mtb* (MOI = 1) 6 hours post-infection. Gal-9 localization to extra-phagosomal membranes (arrowheads), phagosomal membranes (black arrows), and *Mtb* (white arrows). Four representative images are shown from a dataset of 26 total images. b, bacteria. Scale bar = 0.5 μm. (**B**) Quantification of Gal-9-FLAG localization to indicated structures. Values are a percent of total Gal-9-FLAG puncta.

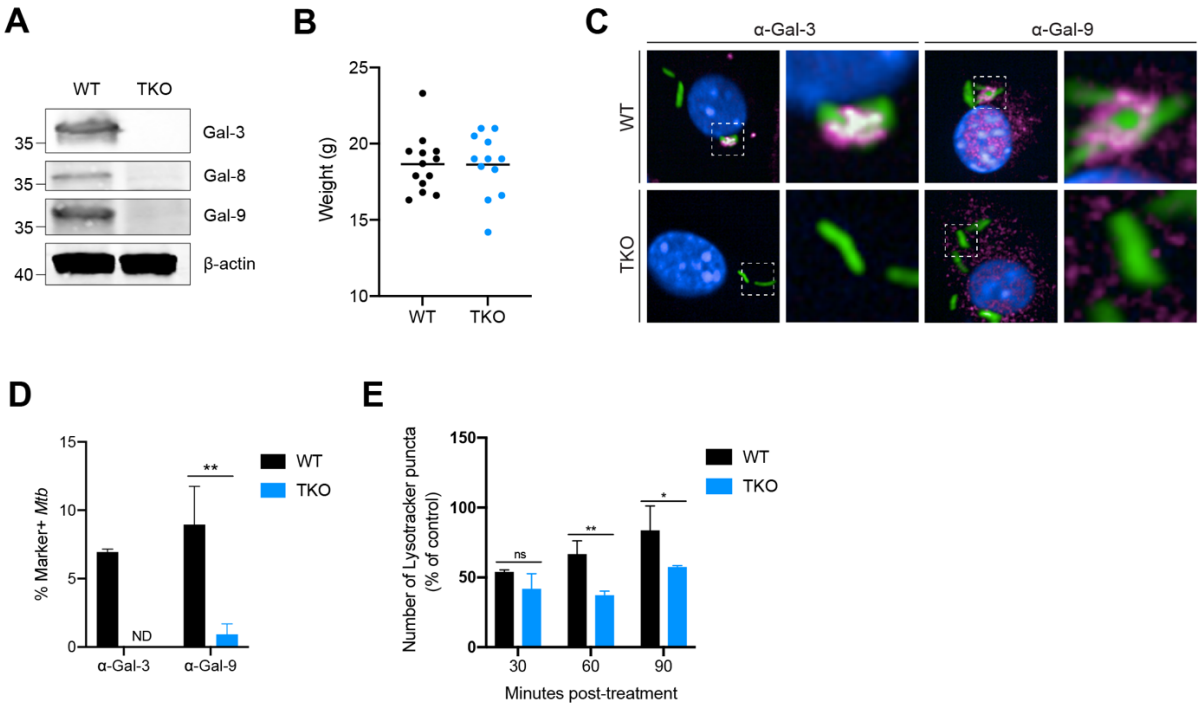

Figure S2. Generation and validation of Gal-3, -8, -9 triple knockout mice (TKO). (**A**) Immunoblots of bone marrow-derived macrophage (BMDM) lysates from WT, and TKO strain S1, immunostained for indicated proteins. (**B**) Weight (grams) of 8-week old WT and TKO female mice. (**C**) Immunofluorescence of WT or TKO strain S1 BMDMs infected with *Mtb*-GFP (green) (MOI = 2) 8 hours post-infection and immunostained for Gal-3 or Gal-9 (magenta). (**D**) Quantification of (C) for *Mtb*-GFP colocalization with Gal-3 or Gal-9; ND, no data. (**E**) Quantification of Lysotracker Green puncta in PBS control- or 1 mM LLOMe-treated WT or TKO strain S1 BMDMs at indicated time points. Figures represent one experiment (B), or are representative of two (A, C-E) independent experiments. Error bars are SD from four technical replicates, *p<0.05., **p<0.01 by unpaired t-test.

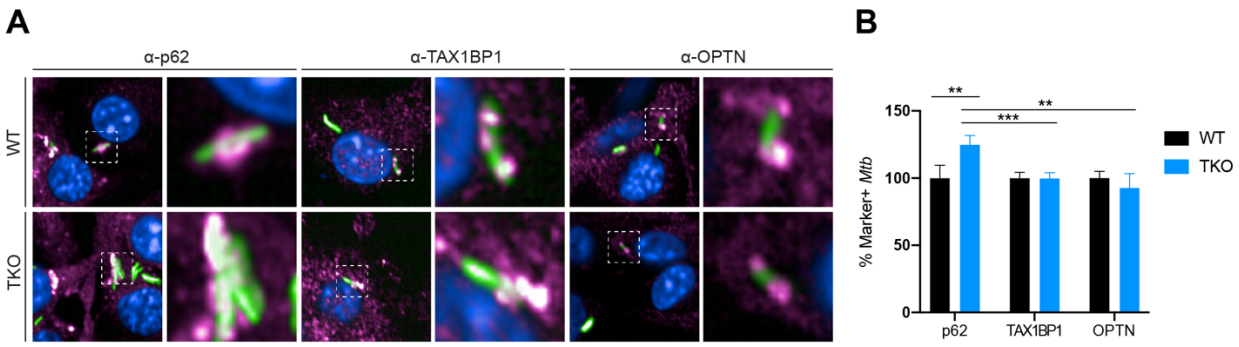

Figure S3. Autophagy receptor recruitment in TKO macrophages.
(**A**) Immunofluorescence of WT or TKO BMDMs infected with *Mtb*-GFP (green) (MOI = 2) 8 hours post-infection and immunostained for p62, TAX1BP1, or OPTN (magenta). (**B**) Quantification of (A) for *Mtb*-GFP colocalization with indicated markers. Figures are representative of two independent experiments. Error bars are SD from four technical replicates, **p<0.01, ***p<0.001 by unpaired t-test.

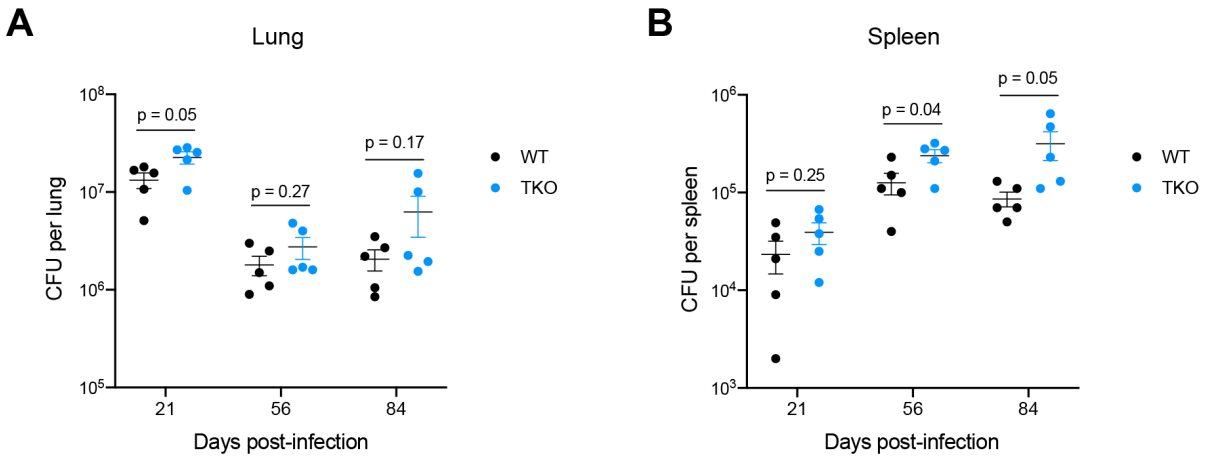

Figure S4. Gal-3, -8, and -9 are partially required for control of *Mtb* in a high dose aerosol infection.
(**A**) WT and TKO mice were aerosol infected with 450 CFUs of *Mtb* Erdman and bacterial loads in lungs were enumerated by plating for CFU at indicated time points. *n* = 5 mice per genotype (**B**) Same as in (A) but bacterial loads in spleens. Figures represent one experiment. Error bars are SEM and p-values were determined by unpaired t-test.

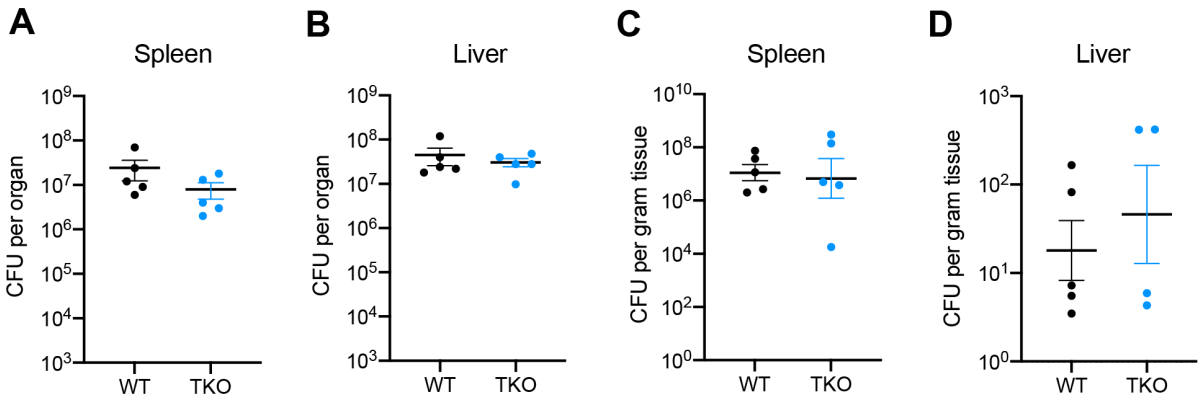

Figure S5. Galectin-deficient mice exhibit normal bacterial control during infection with *L. monocytogenes* or *S. typhimurium*.
(**A**) WT and TKO mice were intravenously infected with 1 x 10^5 CFUs of *L. monocytogenes* and bacterial loads in spleens were enumerated by plating for CFU at 48 hours post-infection. *n* = 5 mice per genotype. (**B**) Same as in (A) but bacterial loads in livers. (**C**) WT and TKO mice were infected via the intraperitoneal route with 1000 CFUs of *S. typhimurium* and bacterial loads in spleens were enumerated by plating for CFU at 24 hours post-infection. *n* = 5 mice per genotype. (**D**) Same as in (C) but bacterial loads in livers. *n* = 4-5 mice per genotype. Figures represent data from one experiment (A, B), or are representative of three independent experiments (C, D). Error bars are SEM.

Chapter 3: Conclusion and Future Directions

Conclusions

Galectins are best known for their role in the detection of damaged membranes and organelles. During infection, recruitment of galectins to damaged bacterial phagosomes can lead to autophagy activation, transcriptional responses, and regulation of antibacterial proteins (Thurston et al., 2012, Wu et al., 2021, Feeley et al., 2017, Johannes et al., 2018). While individual galectins have been thoroughly characterized in isolation, the net effect of signaling through multiple damage-activated galectins has never been explored in vivo.

Here, we have established a system to evaluate galectin function in the immune response to diverse intracellular bacteria. Acknowledging the numerous antibacterial functions that have been reported for galectins, we hypothesized that galectin-deficiency in vivo might lead to both poor innate immune recognition and suppression of bacteria. Surprisingly, we found that TKO macrophages and mice exhibited normal resistance to multiple intracellular pathogens. Although TKO macrophages showed slight defects in autophagic clearance of *Mtb* from the cytosol, as shown by an accumulation of *Mtb* autophagy intermediates and a decrease in *Mtb*-lysosome colocalization, these macrophages were capable of efficiently restricting growth of *Mtb*, *S. typhimurium, L. monocytogenes,* and *L. pneumophila*. Because *L. pneumophila* is a potent inducer of inflammasome-mediated restriction via flagellin (Ren et al., 2006), we also tested Δ*flaA* mutants to investigate an inflammasome-independent role for the galectin system and observed no differences between WT and TKO macrophages. In addition, we examined an autophagy sensitive *L. monocytogenes* mutant to test whether Gal-3, -8, and -9 promote *L. monocytogenes*-targeted autophagy and did not observe any loss of restriction (Mitchell et al, 2018). These findings indicate that the galectin system promotes efficient clearance of some intracellular pathogens, but not others. Despite these effects on autophagy, this work shows that the key damage activated galectins, Gal-3, -8, and -9, are not required for bacterial growth restriction in primary macrophages.

Although we did not observe any defects in TKO mice during acute infection with *L. monocytogenes, S. typhimurium,* or *Mtb*, we found that galectin deficiency led to an impairment in bacterial containment during chronic *Mtb* infection. In a low dose aerosol infection, we observed a 2.5-fold increase in lung bacterial burden in TKO mice compared to WT during the chronic phase, while bacterial burdens were unaltered in TKO mice at one and three weeks post-infection. We additionally examined bacterial restriction in a high dose infection model and observed a slight trend towards increased bacterial burden in TKO mice. Consistent with a role for the galectin system in promoting bacterial containment during the chronic phase, we found that TKO mice succumbed to chronic tuberculosis slightly faster than WT mice. While the precise mechanism of galectin-mediated bacterial restriction during chronic infection remains unknown, we did find that splenic CD4 T cells from infected TKO mice exhibited defects in IFN-γ production after in vitro restimulation of Ag85B peptide, but not ESAT-6 peptide. However, this effect was specific to the spleen, and no differences were observed in the

lung. These findings implicate a role for the galectin system in the promotion of efficient T cell activation, possibly exclusively in tissues that do not already select for highly activated T cells through alternate mechanisms (Cooper et al., 2009, Mihret et al., 2012). These data also indicate that galectins might promote antigen processing and presentation of select antigens, but the mechanisms underlying this specificity require further investigation.

Finally, we demonstrated that Gal-9 bound both *Mtb* and *S. typhimurium* in vitro. Importantly, we found that the Gal-9 recognition of *Mtb* was dependent on carbohydrate-binding, which is consistent with recent reports that have shown Gal-9 can bind mycobacterial AG (Wu et al., 2021). Using immuno-EM, we demonstrated that this interaction occurred in vivo, as Gal-9-FLAG puncta were observed on the edges of bacteria. We additionally observed localization of Gal-9 to many extra-phagosomal compartments, suggesting that Gal-9 is likely interacting with a variety of ligands throughout the cell during infection. These findings expand on the role of Gal-9 as a damage sensor and suggest this galectin can additionally act as a direct sensor of cytosolic pathogens.

Future Directions

Our observation that galectin deficiency leads to defects in antibacterial autophagy and Ag85B-specific but not ESAT-6 specific CD4 T cell activation led us to hypothesize that galectins might promote autophagic capture and antigen presentation of certain cytosolic antigens. However, why some antigens, but not others, might rely on autophagy for antigen presentation is an interesting question. Future studies, using in vitro APC-T cell co-culture antigen presentation systems that enable localization of a model antigen, such as OVA, to specific APC cellular compartments and measurement of cognate antigen-specific T cells, may facilitate deeper mechanistic investigation into the nature of antigen accessibility to autophagy-driven antigen presentation (Lee et al., 2010). Additionally, coculture of *Mtb*-infected WT or TKO BMDCs with Ag85B- or ESAT-6-specific T cell hybridomas will prove useful in testing whether galectins promote antigen-specific CD4 T cell responses via autophagy in vitro (Saini et al., 2016). To test this model in vivo, several approaches could be explored. Infusion of *Mtb*-infected WT or TKO BMDCs into naïve ESAT-6- or Ag85B-specific TCR transgenic mice and measurement of the resulting T cell response can permit measurement of a large pool of T cells via in vitro restimulation followed by ELISpot or flow cytometry. Alternatively, infusion of *Mtb*-infected WT or TKO mice with Ag85B peptide, to promote expansion of Ag85B-specific CD4 T cells (Moguche et al., 2017), followed by *Mtb* aerosol infection, could facilitate analysis of galectin-dependent T cell functionality in the context of an *Mtb*-infected mouse. Similarly, Ag85B-specific CD4 T cells could be isolated from TCR transgenic mice and adoptively transferred into WT or TKO mice prior to *Mtb* aerosol infection. Finally, analysis of antigen-specific CD4 T cell responses in *Mtb*-infected autophagy-mutant mice, such as *Atg16L*$^{fl/fl}$ *LysMcre*$^{+/+}$ or *Atg7*$^{fl/fl}$ *LysMcre*$^{+/+}$ (Kimmey et al., 2015), will permit more direct testing of whether autophagy within the myeloid cell lineage, which includes APCs, is necessary for CD4 T cell activation.

We found that TKO mice exhibited impaired CD4 T cell activation in the spleen but not the lung. This led us to hypothesize that naïve T cells in the spleen may rely on additional antigen presentation mechanisms in APCs, such as galectin-mediated antigen presentation via autophagy, in order to fully activate. Thus, investigation of tissues with high proportions of naïve CD4 T cells may reveal stronger galectin-dependent effects. The draining lymph node is the first site of naïve CD4 T cell activation (Cooper et al., 2009), where migrating dendritic cells from the lung present *Mtb* peptides to CD4 T cells and secrete IL-12 (Mihret et al., 2012), thereby promoting expansion and activation of cognate CD4 T cells. Because the draining lymph node is critical for early antigen presentation, future analysis of T cell activation in this organ may prove useful in defining a specific role for galectins in the priming and activation of naïve CD4 T cells early after infection.

In this study, we did not observe a loss in bacterial restriction in TKO mice during acute infection with *S. typhimurium* and *L. monocytogenes*. However, this data may not fully reflect the role of the galectin system in the immune response to these intracellular pathogens. Considering that both bacteria are enteric pathogens, and that autophagy has been demonstrated to restrict pathogen translocation through the gut epithelium (Conway et al., 2013), oral infection models may prove useful in evaluating galectin function at the natural site of infection. In addition, the acute infection models that were used in this study do not elicit adaptive immune responses. Our observation that TKO mice exhibit bacterial restriction and T cell activation defects exclusively during chronic infection suggests that galectins may function in cases where both the innate and adaptive immune response are involved. Thus, implementation of the *L. monocytogenes* immunization and rechallenge model (Zenewicz and Shen, 2007), which elicits protective humoral recall responses, may provide a suitable system to explore additional roles for galectins at the intersection of the innate and adaptive immune responses. However, there could be limitations with this approach, since this model elicits primarily a memory CD8 T cell response, while CD4 T cells have been shown to play a minor role in bacterial clearance (D'Orazio et al., 2019).

Finally, while we did not observe dramatic defects in bacterial restriction in TKO mice, these data may not reflect the role of galectins in the immune response to viruses. Galectins, in particular Gal-3, -8, and -9, have been demonstrated to mediate both protective and detrimental immune responses during viral infection (Wang et al., 2020). Both Gal-3 and Gal-8 have been shown to recruit to cytosolic adenovirus, and Gal-8 has been shown to promote p62- and NDP52-mediated autophagic clearance of an autophagy sensitive adenovirus mutant (Montespan et al., 2017). Gal-8 has additionally been shown to suppress picornavirus through autophagy activation (Staring et al., 2017). Moreover, Gal-9-TIM3 signaling is reported to modulate T cell function during HSV-1 infection (Wang et al., 2020). Utilization of in vivo infection models may reveal additional functions for the galectin system in the immune response to viral infection.

Chapter 4: Methods

Ethics Statement

Mouse use and procedures were approved by the Office of Laboratory and Animal Care at the University of California, Berkeley (protocol AUP-2015-11-8096), in adherence with federal guidelines from the *Guide for the Care and Use of Laboratory Animals* of the National Institutes of Health.

Bacterial and fungal cultures

Mtb*. Mtb* Erdman strain was used for all experiments. Low passage frozen stocks of *Mtb* were grown to log phase in 7H9 (BD) liquid media supplemented with 10% Middlebrook OADC (Sigma), 0.05% Tween-80 and 0.5% glycerol in roller bottles at 37°C. *M. tuberculosis*-lux expressing luciferase from the *luxCDABE* operon has been described previously and was cultured as described above (Rosenberg et al., 2015, Roberts et al., 2019). WT or Δ*EccC M. tuberculosis* expressing eGFP under control of the MOP promoter was a gift from Dr. Sarah Stanley's laboratory (Sogi et al., 2017), and cultured as described above. Log phase bacteria were washed twice with PBS, and sonicated three times at 90% amplitude for 30 seconds each and diluted into BMDM media (DMEM with 10% FBS, 2mM L-glutamine, 10% MCSF, 11mg/mL sodium pyruvate) prior to infection.

S. typhimurium. For pathogen pull-down experiments, *S. typhimurium* strain SL1344 was cultured overnight in Luria-Bertani (LB) broth shaking at 37°C. It was back-diluted 1:100 1 day prior to infection and allowed to recover to mid-log prior to infection. For *S. typhimurium* BMDM infections, strain IR715 phoN::KanR was cultured as described above.

L. monocytogenes. All *L. monocytogenes* strains used in this study were derived from strain 10403S (streptomycin-resistant). Δ*actA* $PlcA^{H86A}$ $PlcB^{H69G}$ (triple mutant) has been previously described (Mitchell et al., 2018). For macrophage infections, *L. monocytogenes* was grown to stationary phase overnight, slanted at 30°C in filter-sterilized BHI media with 200 µg/ml streptomycin then diluted into PBS for OD600 measurement and inoculum preparation.

L. pneumophila. All *L. pneumophila* strains used are JR32 and express the *Photorhabdus luminescens luxCDABE* operon. *LuxCDABE*-expressing WT or isogenic mutant for *flaA* have been previously described (Goncalves and Margolis et al., 2019). Bacteria were cultured in Charcoal-Yeast Extract Agar (CYE, 10 g/L 4-morpholinepropanesulfonic acid [MOPS], 10 g/L Yeast extract, 15 g/L technical agar, 2 g/L activated charcoal, supplemented with 0.4 g/L L-cysteine and 0.135 g/L $Fe(NO_3)_3$) at 35-37°C for 4 days from frozen stocks. Single colonies were grown on fresh plates for another 2 days. For macrophage infections, bacteria were grown on solid plates and resuspended in autoclaved water and diluted in RPMI.

C. neoformans. Serotype A strain H99 was grown in yeast culture conditions on YPAD medium [1% yeast extract, 2% Bacto-peptone, 2% glucose, 0.015% L-tryptophan, 0.004% adenine] at 30-degrees. Cells were harvested mid-log phase for in vitro binding studies.

Mice

All mice used were specific pathogen free, maintained in 12 hour light-dark cycle, and given standard chow diet ad libitum. 8-12 week old male and female mice were used. WT C57BL/6J mice were obtained from Jackson Laboratories (JAX). CRISPR/Cas9 targeting was performed by electroporation of Gal-3, Gal-8, and Gal-9-targeting Cas9-sgRNA RNP complexes into fertilized zygotes from C57BL/6J female mice (JAX, stock no. 000664) (Wang et al., 2013). TKO mice were generated by targeting exon 1 of each galectin using two guides per exon; sgRNA sequences: 5'-GGCTGGTTCCCCCATGCACC-3' and 5'-CTCCAGGGGCAGTTGGGCCG-3' (Gal-3), 5'-CAGCTAGACCTTTTGAACCG-3' and 5'-CACCATGAACACGATCTCAA-3' (Gal-8), and 5'-TACCCTCCTTCCTCAAACCG-3' and 5'-GAACGGACAGTGGGGTCCTG-3' (Gal-9). Founder mice were genotyped as described below, and founders carrying mutations were bred to WT C57BL/6J mice to separate modified haplotypes. Homozygous lines were generated by interbreeding heterozygotes carrying matched haplotypes.

Cell culture, LLOMe treatment, THP-1 shRNA generation

Primary murine bone marrow-derived macrophages (BMDMs) were isolated and cultured as previously described (Roberts et al., 2019). For all infections, BMDMs were thawed three days prior to replating for infections. For LLOMe treatment, BMDMs were incubated with Lysotracker Red DND-99 (Thermo Fisher Scientific) for 3 hours prior to incubation with LLOMe (Cayman Chemical) at 1 mM. Cells were imaged live on an Opera Phenix microscope and images were acquired at the indicated time points. For THP-1 experiments, THP-1 cells were cultured in RPMI 1640 medium supplemented with 1mM sodium pyruvate, 10mM HEPES, 4.5 g/L glucose, 0.05mM 2-mercaptoethanol, 2mM L-glutamine, 5% fetal calf serum, and 5% bovine growth serum. Cells were maintained at a concentration between 2e5 cells/mL and 1e6 cells/mL. shRNAs were designed to target human Galectin-9 mRNA and cloned into the pLKO.1 vector (Addgene #10878). The sense shRNA sequences are CCTGGTGCAGAGCTCAGATTT (Gal-9-1) and GCTCTGTGCAGCTGTCCTA (Gal-9-2). Lentiviral particles were produced in Lenti-X cells (Clontech) per manufacturer's instructions. Early passage THP1 cells were transduced with lentiviral particles containing the shRNA expression vector. The cells were selected in 0.5ug/mL puromycin to obtain a polyclonal population. Knockdown efficiency was assessed via qPCR using the following primers: 5'-CCGAAAAATGCCCTTCGTCC-3' (forward), 5'-ACCTTGAGGCAGTGAGCTTC-3' (reverse) and determined to be 95% and 91% knockdown for Gal-9-1 and Gal-9-2, respectively.

Pathogen pull-down for mass spectrometry and immunoblotting

For *Mtb* pull-down and mass spectrometry, Mtb was fixed in 4% PFA, washed three times with PBS, and pelleted. 50uL of *Mtb* pellet was incubated for 3 hours with 1mL of 10mg/mL THP-1 lysate, washed four times with PBS, and eluted in 8M urea with or without Rapigest (Waters) before LC-MS sample preparation. For *Mtb*, *L. monocytogenes, S. typhimurium*, and *C. neoformans* pull-down for Gal-9-FLAG immunoblotting, pathogens were fixed, washed, and pelleted as described above. 1mL

of 10mg/mL RAW 264.7 Gal-9-FLAG lysate was incubated, washed, and eluted as described above prior to immunoblotting.

Mass spectrometry and data acquisition
Peptides were resuspended in 0.1% formic acid and 3% directly injected on a 75 µm ID column (New Objective) packed with 25 cm of Reprosil C18 3 µm, 120 Å particles (Dr. Maisch). Peptides were eluted in positive ion mode into an Orbitrap Elite mass spectrometer (Thermo Fisher Scientific) via a Nanospray Flex Ion Source (Thermo Fisher Scientific). Elution of peptides was achieved by an acetonitrile gradient delivered at a flow rate of 400 nL/min by an Easy1000 nLC system (Thermo Fisher Scientific). All mobile phases contained 0.1% formic acid as buffer A. The total gradient time was 70 min, during which mobile phase buffer B (0.1% formic acid in 90% acetonitrile) was ramped from 5% to 30% B over 55 min, followed by a ramp to 100% buffer B over a subsequent 5 min, and held at 100% for 10 min to wash the column. MS data was collected over the first 60min of the gradient. The ion transfer tube was set to 180°C and the spray voltage was 1500V. MS1 scan was collected in the ion trap in centroid mode with 120K resolution over a scan range of 200-2000 m/z, an S-Lens RF of 68%, a 50ms maximum injection time, and a AGC target of 3e4. Species with a charge state z=1 or unassigned charge states were excluded from selection for MS/MS. Resonance excitation MS/MS was performed on the 20 most abundance precursors with a minimum signal intensity of 200, an isolation width of 2 m/z, a 0.25 activation Q, a 10ms activation time, a 100ms maximum injection time, and an AGC target of 1e3. Dynamic exclusion was employed to exclude a list of 50 previously selected precursors within 180s and using a +/- 1.5 Da window.

Structured illumination microscopy
Coverslips were processed as described in the immunofluorescence methods section and imaged on a Nikon N-SIM 4-color super resolution microscope.

Electron-microscopy
RAW 264.7 cells expressing mouse Gal9-3xFLAG were infected with *Mtb* at an MOI =1 for 6 hours. Cells were then detached using 1mM EDTA in PBS, and fixed for 10 minutes at room temperature using freshly prepared periodate-lysine-paraformaldehyde stain (0.2M lysine-HCl pH 7.4, 4% paraformaldehyde, 0.1M sodium m-periodate). Following fixation, cells were pelleted and resuspended in PBS without washing and stored at 4-deg until EM embedding was performed. Samples were then embedded in 10% gelatin and infiltrated overnight with 2.3M sucrose/20% polyvinyl pyrrolidone in PIPES/$MgCl_2$ at 4°C. Samples were trimmed, frozen in liquid nitrogen, and sectioned with a Leica Ultracut UCT7 cryo-ultramicrotome (Leica Microsystems). Ultrathin sections of 50nm were blocked with 5% FBS/5% NGS for 30 min and subsequently incubated with mouse anti-FLAG (clone M2, Sigma) for 1 hour at room temperature. Following washes in block buffer, sections were incubated with goat anti-mouse IgG + IgM 18nm colloidal gold conjugated secondary antibody (Jackson ImmunoResearch Laboratories) for 1 hour. Sections were stained with 0.3% uranyl acetate/2% methyl cellulose and viewed on a JEOL 1200 EX transmission electron microscope (JEOL USA) equipped with an AMT 8 megapixel digital camera and AMT Image Capture Engine V602

software (Advanced Microscopy Techniques). All labeling experiments were conducted in parallel with controls omitting the primary antibody.

Immunoblotting

WT or TKO BMDMs were seeded in 15 cm tissue culture plates at a density of 1 x 10^6 cells per plate and allowed to equilibrate for three days. Cells were lysed using RIPA buffer (Pierce) supplemented with Complete Mini EDTA-free Protease Inhibitor (Roche). Lysate protein concentration was determined using BCA protein assay kit (Pierce). Proteins were separated with denaturing PAGE 4-20% Mini-PROTEAN TGX Precast Protein gel (Bio-Rad) and transferred to Trans-Blot Turbo Mini Nitrocellulose (Bio-Rad) using Trans-Blot Turbo Transfer System (Bio-Rad). Membranes were blocked with Li-Cor Odyssey blocking buffer for one hour at room temperature with agitation. Primary antibodies were added and incubated overnight at 4°C with agitation. Primary antibodies used were: anti-Gal-3 (Santa Cruz Biotechnology B2C10, primary 1:1000, secondary 1:5000), anti-Gal-8 (Abcam ab69631, primary 1:500, secondary 1:5000), anti-Gal-9 (Abcam ab69630, primary 1:500, secondary 1:5000), anti-β-actin (primary 1:1000, secondary 1:5000), anti-FLAG (Sigma clone M2, primary 1:1000, secondary 1:5000). Secondary antibodies used were Li-Cor IRDye 680RD or 800CW goat anti-mouse IgG or anti-rabbit IgG and used at dilutions indicated above. PBS 0.1% Tween 20 was used for washing for all immunoblots, except anti-Gal-8 and anti-Gal-9 immunoblots, which used PBS no tween for washes.

Immunofluorescence

Following fixation, washing, and storage in PBS at 4°C, cells were blocked and permeabilized in PBS with 5% FBS or 2% BSA and 0.1% Triton X-100 for 30 minutes at room temperature. Cells were then stained in blocking buffer overnight at 4°C with the following primary antibodies at the indicated dilutions: anti-FLAG (Sigma clone M2, primary 1:1000, secondary 1:2000), anti-Gal-9 (Abcam ab275877, primary 1:100, secondary 1:500), anti-Gal-3 (Santa Cruz Biotechnology B2C10, primary 1:50, secondary 1:500), anti-polyubiquitin (Millipore Sigma ST1200, primary 1:400, secondary 1:2000), anti-ubiquitin K63-specific (Millipore Sigma 05-1308, primary 1:200, secondary 1:2000), anti-ubiquitin K48-specific (Millipore Sigma 05-1307, primary 1:200, secondary 1:2000), anti-p62 (Abcam ab109012, primary 1:400, secondary 1:4000), anti-Tax1bp1 (Bethyl Laboratories A303-791A, primary 1:200, secondary 1:1000), and anti-Optineurin (Bethyl Laboratories A301-829A, primary 1:200, secondary 1:1000). Cells were washed three times with PBS for 5 minutes each. DAPI and secondary antibody staining was performed at room temperature for 30 minutes using anti-mouse or anti-rabbit Alexa Fluor 647 (Invitrogen) at the above indicated dilutions. Cells were washed three times with PBS for 5 minutes then imaged on an Opera Phenix High-Content Screening System confocal microscope. Plates were imaged at 40X magnification for colocalization analysis, or 63X magnification for representative images. Automated colocalization analysis was performed using PerkinElmer Harmony software package. An analysis script was created to measure colocalization of *Mtb* and indicated markers from >4000 bacteria.

Macrophage infections

Mtb. To limit cell density-dependent effects in all Mtb BMDM macrophage infections, WT BMDMs were plated in 96-well plates at a specified target cell density, while TKO BMDMs were plated on a cell density gradient in order to ensure equivalent plating numbers of each genotype. During analysis, wells of different genotypes were only compared if cell counts were matched within <5% of each other. After plating, cells were allowed to adhere and equilibrate for 2 days prior to infection. For Mtb-lux infections, WT cells were plated at 4 x 10^4 cells per well (target density) while TKO cells were plated at 10% below and 10% above the target density in 10% increments. On day 0 of infection, one 96-well plate containing the same arrangement of cell dilutions of WT and TKO BMDMs plated in parallel was fixed in PBS with 4% PFA, DAPI stained, and nuclei were counted at 5X magnification on an Opera Phenix microscope, thus allowing determination of cell density-matched wells. BMDMs were infected at a multiplicity of infection (MOI) of 1 or 5 in macrophage media by 10 min spinfection at 300 rcf. Luminescence of Mtb-lux-infected BMDMs was measured as previously described (Penn et al., 2018). For WT or ΔEccC Mtb-GFP infections for microscopy, BMDMs were plated at 2 x 10^5 cells per well in 24-well glass-bottom Cellvis plates. For 96-well plate infections for microscopy, WT BMDMs were plated at 2.5 x 10^4 cells per well (target density) while TKO macrophages were plated on a cell density gradient that ranged from 30% below to 40% above the target density in 10% increments in 96-well PerkinElmer Cell Carrier Ultra plates. All infections for microscopy used an MOI of 2. At indicated time points, microscopy plates were washed in warm PBS, fixed in PBS with 4% PFA, removed from the BSL3, washed three times with PBS, and stored in PBS at 4°C before immunostaining. For lysotracker experiments, cells were stained with 50nM Lysotracker Red DND-99 in macrophage media for 3 hours prior to fixation and imaged on an Opera Phenix microscope immediately after washing out the fixative. For *Mtb* CFU experiments, BMDMs were plated in 24-well plates at 2 x 10^5 cells per well, infected using an MOI of 2, and Mtb CFU enumeration was performed as previously described (Sogi et al., 2017). For THP-1 infections, THP-1 cells were differentiated for 3 days in DMEM with 2mM L-glutamine, 1mM sodium pyruvate, and 10% heat-inactivated fetal calf serum with 10 ng/mL PMA and 0.1 ng/mL Vitamin D. On day 1 of differentiation, THP-1 cells were plated at 4 x 10^4 cells per well in a 96-well plate. The media was exchanged with fresh differentiation media with PMA and Vitamin D daily. On the day of infection, 10 mL of the *Mtb* culture was washed twice in PBS with 10% heat-inactivated horse serum. After the washes, the *Mtb* was resuspended in 5 mL of PBS with 10% heat-inactivated horse serum and sonicated twice at 50% amplitude for 15 seconds to generate a single-cell suspension. *Mtb* was diluted into DMEM with 10% heat-inactivated horse serum, and this inoculum was added to THP-1 cells at an MOI of 1. THP-1 cells were spinfected for 5 min. Cells were incubated at 37 C for 30 minutes. THP-1 cells were washed 3 times with PBS (+ca/mg) with 1% heat-inactivated horse serum. Differentiation media lacking phenol red with PMA and Vitamin D was replaced after the washes, and the effective *Mtb* inoculum was determined by measuring the luminescence of infected cells in a plate reader. The fold-growth was calculated by dividing the luminescence read each day by the effective inoculum. Half of the media

was discarded and replaced with fresh differentiation media with PMA and Vitamin D on days 1, 3, and 5 post-infection.

S. typhimurium. 1 x 10^5 BMDMs were plated on 24-well plates 24 hours prior to infection. For IFN-γ treatment, cells were incubated with 0.01 ug/mL IFN-γ the night before infection. Bacteria grown to mid-log phase were pelleted and resuspended in BMDM media. Suspension was incubated at 37°C for 30 minutes for opsonization. Bacteria were then pelleted and resuspended to 1 x 10^9 CFU/mL prior to spinfection with BMDMs for 5 minutes at 250 x g followed by 37°C incubation for 30 minutes for phagocytosis. Cells were washed with PBS and incubated with BMDM media with 100ug/mL gentamicin at 37°C incubation for 30 minutes, then washed with PBS and incubated with BMDM media with 5ug/mL gentamicin. For CFU enumeration, cells were washed with PBS and lysed in 500uL water for 10 minutes prior to lysate serial dilution and plating on LB agar plates.

L. monocytogenes. A total of 3 x 10^6 BMDMs were plated on 14 coverslips in 60 mm non-TC treated dishes and infected the next day at an MOI of 0.25. *L. monocytogenes* CFU enumeration was performed as previously described (Portnoy et al., 1988, Reniere et al., 2016).

***L. pneumophila*.** Bacterial replication was measured using a luminescence-based replication assay as previously described (Coers et al., 2007). Briefly, 10^5 WT or TKO BMDMs were plated on 96-well plates and incubated overnight. Medium was replaced with bacterial suspension in RPMI with 10% FBS at an MOI of 0.01. At indicated time points, luminescence emission was measured at 470 nm with a Spectra-L plate reader (Molecular Devices).

Mtb aerosol infection

To prepare infection inoculum*, Mtb* Erdman strain frozen stock was diluted in sterile water and sonicated at 90% amplitude three times for 30 seconds. 8- to 12-week old male and female mice were infected with approximately 20-100 CFUs (low dose) or >400 CFUs (high dose) of prepared inoculum using a Glas-Col inhalation exposure system. At indicated time points, lungs and spleens were harvested, homogenized, and plated on 7H10 plates with Polymyxin B (200,000 U/L), Carbenicillin (50 mg/L), Trimethoprim lactate (20 mg/L) and Amphotericin B (5 mg/L). Plates were incubated at 37°C for 25-28 days before counting colonies. For survival experiment, 10 to 12 mice per genotype were infected with *M. tuberculosis*. Mouse weight was measured weekly, and mice were sacrificed after losing 15% of maximum body weight.

S. typhimurium intraperitoneal infection

S. typhimurium strain IR715 was cultured in LB broth overnight at 37°C with shaking. Mice received 100 µl of sterile PBS or 1000 CFUs diluted in 100 µl PBS by intraperitoneal injection. Mouse weights were monitored daily during infection. Systemic bacterial levels were characterized at day 1, 2, or 3 post-infection by determining tissue loads of bacteria. Liver and spleen were collected in PBS, weighed, and homogenized. Homogenates were serially diluted and plated on LB agar plates. CFU per gram tissue was calculated after overnight growth at 37°C.

L. monocytogenes intravenous infection

L. monocytogenes was grown at 37°C with shaking at 200 rpm to mid-log phase. Bacteria were washed in PBS and resuspended at 5 x 10^5 colony-forming units (CFU) per 200 µl of sterile PBS. Mice were then injected with 1 x 10^5 CFU via the tail vein. 48 hours post-infection, livers and spleens were collected, homogenized, and plated on LB streptomycin 200 µg/ml to determine the number of CFU per organ.

Interferon-γ enzyme-linked immunospot (ELISpot)

Splenocytes were harvested and pressed through a 70 µm cell strainer to generate a single cell suspension. Lung cells were harvested and digested in RPMI with Liberase TM (70 µg/ml) and DNase I (30 µg/ml) in gentleMACS C-tubes then placed at 37°C for 30 minutes, followed by gentleMACS tissue homogenization for single cell suspension. Cells were pelleted and RBCs were lysed using ACK lysing buffer. Cells were washed, pelleted, resuspended in X-VIVO TM 15 (Lonza), and counted on a hemocytometer or using fluorescent count beads on an SH800 Sony Sorter. Cells were plated, stimulated overnight with indicated peptides (2 µg/ml), developed, and analyzed as previously described (Van dis et al., 2018). Cells were additionally stimulated with Concanavalin A (ConA, 2.5 µg/ml) as a positive control. IFN-γ spot-forming cell (SFC) counts from peptide-stimulated wells were normalized to SFC counts from ConA-stimulated wells to control for variability in cell density between samples.

References

1. Abdallah AM, Gey van Pittius NC, Champion PA, Cox J, Luirink J, Vandenbroucke-Grauls CM, Appelmelk BJ, Bitter W. Type VII secretion--mycobacteria show the way. Nat Rev Microbiol. 2007 Nov;5(11):883-91.
2. Beatty WL, Rhoades ER, Hsu DK, Liu FT, Russell DG. Association of a macrophage galactoside-binding protein with Mycobacterium-containing phagosomes. Cell Microbiol. 2002;4(3):167-76.
3. Beatty WL, Rhoades ER, Ullrich HJ, Chatterjee D, Heuser JE, Russell DG. Trafficking and release of mycobacterial lipids from infected macrophages. Traffic. 2000;1(3):235-47.
4. Bell SL, Lopez KL, Cox JS, Patrick KL, Watson RO. Galectin-8 Senses Phagosomal Damage and Recruits Selective Autophagy Adapter TAX1BP1 To Control Mycobacterium tuberculosis Infection in Macrophages. mBio. 2021;12(4):e0187120.
5. Broz P, Ohlson MB, Monack DM. Innate immune response to Salmonella typhimurium, a model enteric pathogen. Gut Microbes. 2012;3(2):62-70.
6. Budzik JM, Swaney DL, Jimenez-Morales D, Johnson JR, Garelis NE, Repasy T, Roberts AW, Popov LM, Parry TJ, Pratt D, Ideker T, Krogan NJ, Cox JS. Dynamic post-translational modification profiling of Mycobacterium tuberculosis-infected primary macrophages. Elife. 2020;9:e51461.
7. Carr W, Kurbatova E, Starks A, Goswami N, Allen L, Winston C. Interim Guidance: 4-Month Rifapentine-Moxifloxacin Regimen for the Treatment of Drug-Susceptible Pulmonary Tuberculosis - United States, 2022. MMWR Morb Mortal Wkly Rep. 2022;71(8):285-289.
8. Chai Q, Wang X, Qiang L, Zhang Y, Ge P, Lu Z, Zhong Y, Li B, Wang J, Zhang L, Zhou D, Li W, Dong W, Pang Y, Gao GF, Liu CH. A Mycobacterium tuberculosis surface protein recruits ubiquitin to trigger host xenophagy. Nat Commun. 2019;10(1):1973.
9. Chauhan S, Kumar S, Jain A, Ponpuak M, Mudd MH, Kimura T, Choi SW, Peters R, Mandell M, Bruun JA, Johansen T, Deretic V. TRIMs and Galectins Globally Cooperate and TRIM16 and Galectin-3 Co-direct Autophagy in Endomembrane Damage Homeostasis. Dev Cell. 2016;39(1):13-27.
10. Cheng Y, Schorey JS. Mycobacterium tuberculosis-induced IFN-β production requires cytosolic DNA and RNA sensing pathways. J Exp Med. 2018;215(11):2919-2935.
11. Coers J, Vance RE, Fontana MF, Dietrich WF. Restriction of Legionella pneumophila growth in macrophages requires the concerted action of cytokine and Naip5/Ipaf signalling pathways. Cell Microbiol. 2007;9(10):2344-57.
12. Conway KL, Kuballa P, Song JH, Patel KK, Castoreno AB, Yilmaz OH, Jijon HB, Zhang M, Aldrich LN, Villablanca EJ, Peloquin JM, Goel G, Lee IA, Mizoguchi E, Shi HN, Bhan AK, Shaw SY, Schreiber SL, Virgin HW, Shamji AF, Stappenbeck TS, Reinecker HC, Xavier RJ. Atg16l1 is required for autophagy in intestinal epithelial cells and protection of mice from Salmonella infection. Gastroenterology. 2013;145(6):1347-57.

13. Cooper AM. Cell-mediated immune responses in tuberculosis. Annu Rev Immunol. 2009;27:393-422.
14. Daffé M. The cell envelope of tubercle bacilli. Tuberculosis (Edinb). 2015;95 Suppl 1:S155-8.
15. Daniel TM. The history of tuberculosis. Respir Med. 2006;100(11):1862-70.
16. Dheda K, Gumbo T, Maartens G, Dooley KE, McNerney R, Murray M, Furin J, Nardell EA, London L, Lessem E, Theron G, van Helden P, Niemann S, Merker M, Dowdy D, Van Rie A, Siu GK, Pasipanodya JG, Rodrigues C, Clark TG, Sirgel FA, Esmail A, Lin HH, Atre SR, Schaaf HS, Chang KC, Lange C, Nahid P, Udwadia ZF, Horsburgh CR Jr, Churchyard GJ, Menzies D, Hesseling AC, Nuermberger E, McIlleron H, Fennelly KP, Goemaere E, Jaramillo E, Low M, Jara CM, Padayatchi N, Warren RM. The epidemiology, pathogenesis, transmission, diagnosis, and management of multidrug-resistant, extensively drug-resistant, and incurable tuberculosis. Lancet Respir Med. 2017;S2213-2600(17)30079-6.
17. D'Orazio SEF. Innate and Adaptive Immune Responses during Listeria monocytogenes Infection. Microbiol Spectr. 2019;7(3).
18. Dupont N, Lacas-Gervais S, Bertout J, Paz I, Freche B, Van Nhieu GT, van der Goot FG, Sansonetti PJ, Lafont F. Shigella phagocytic vacuolar membrane remnants participate in the cellular response to pathogen invasion and are regulated by autophagy. Cell Host Microbe. 2009 Aug 20;6(2):137-49.
19. Feeley EM, Pilla-Moffett DM, Zwack EE, Piro AS, Finethy R, Kolb JP, Martinez J, Brodsky IE, Coers J. Galectin-3 directs antimicrobial guanylate binding proteins to vacuoles furnished with bacterial secretion systems. Proc Natl Acad Sci U S A. 2017;114(9):E1698-E1706.
20. Flynn JL, Chan J. Tuberculosis: latency and reactivation. Infect Immun. 2001;69(7):4195-201.
21. Franco LH, Nair VR, Scharn CR, Xavier RJ, Torrealba JR, Shiloh MU, Levine B. The Ubiquitin Ligase Smurf1 Functions in Selective Autophagy of Mycobacterium tuberculosis and Anti-tuberculous Host Defense. Cell Host Microbe. 2017;21(1):59-72.
22. Fu T, Liu J, Wang Y, Xie X, Hu S, Pan L. Mechanistic insights into the interactions of NAP1 with the SKICH domains of NDP52 and TAX1BP1. Proc Natl Acad Sci U S A. 2018;115(50):E11651-E11660.
23. Gehring AJ, Dobos KM, Belisle JT, Harding CV, Boom WH. Mycobacterium tuberculosis LprG (Rv1411c): a novel TLR-2 ligand that inhibits human macrophage class II MHC antigen processing. J Immunol. 2004;173(4):2660-8.
24. Gutierrez MC, Brisse S, Brosch R, Fabre M, Omaïs B, Marmiesse M, Supply P, Vincent V. Ancient origin and gene mosaicism of the progenitor of Mycobacterium tuberculosis. PLoS Pathog. 2005;1(1):e5.
25. Hsu T, Hingley-Wilson SM, Chen B, Chen M, Dai AZ, Morin PM, Marks CB, Padiyar J, Goulding C, Gingery M, Eisenberg D, Russell RG, Derrick SC, Collins FM, Morris SL, King CH, Jacobs WR Jr. The primary mechanism of attenuation of bacillus Calmette-Guerin is a loss of secreted lytic function required for invasion of lung interstitial tissue. Proc Natl Acad Sci U S A. 2003 Oct 14;100(21):12420-5.

26. Jayaraman P, Sada-Ovalle I, Beladi S, Anderson AC, Dardalhon V, Hotta C, Kuchroo VK, Behar SM. Tim3 binding to galectin-9 stimulates antimicrobial immunity. J Exp Med. 2010;207(11):2343-54.
27. Jia J, Abudu YP, Claude-Taupin A, Gu Y, Kumar S, Choi SW, Peters R, Mudd MH, Allers L, Salemi M, Phinney B, Johansen T, Deretic V. Galectins Control mTOR in Response to Endomembrane Damage. Mol Cell. 2018;70(1):120-135.e8.
28. Jia J, Bissa B, Brecht L, Allers L, Choi SW, Gu Y, Zbinden M, Burge MR, Timmins G, Hallows K, Behrends C, Deretic V. AMPK, a Regulator of Metabolism and Autophagy, Is Activated by Lysosomal Damage via a Novel Galectin-Directed Ubiquitin Signal Transduction System. Mol Cell. 2020;77(5):951-969.e9.
29. Jia J, Claude-Taupin A, Gu Y, Choi SW, Peters R, Bissa B, Mudd MH, Allers L, Pallikkuth S, Lidke KA, Salemi M, Phinney B, Mari M, Reggiori F, Deretic V. Galectin-3 Coordinates a Cellular System for Lysosomal Repair and Removal. Dev Cell. 2020;52(1):69-87.e8.
30. Johannes L, Jacob R, Leffler H. Galectins at a glance. J Cell Sci. 2018;131(9):jcs208884.
31. Kimmey JM, Huynh JP, Weiss LA, Park S, Kambal A, Debnath J, Virgin HW, Stallings CL. Unique role for ATG5 in neutrophil-mediated immunopathology during M. tuberculosis infection. Nature. 2015;528(7583):565-9.
32. Kobayashi KS, Chamaillard M, Ogura Y, Henegariu O, Inohara N, Nuñez G, Flavell RA. Nod2-dependent regulation of innate and adaptive immunity in the intestinal tract. Science. 2005;307(5710):731-4.
33. Kremer L, Maughan WN, Wilson RA, Dover LG, Besra GS. The M. tuberculosis antigen 85 complex and mycolyltransferase activity. Lett Appl Microbiol. 2002;34(4):233-7.
34. Lee HK, Mattei LM, Steinberg BE, Alberts P, Lee YH, Chervonsky A, Mizushima N, Grinstein S, Iwasaki A. In vivo requirement for Atg5 in antigen presentation by dendritic cells. Immunity. 2010;32(2):227-39.
35. Levine B, Deretic V. Unveiling the roles of autophagy in innate and adaptive immunity. Nat Rev Immunol. 2007;7(10):767-77.
36. Levine B, Mizushima N, Virgin HW. Autophagy in immunity and inflammation. Nature. 2011;469(7330):323-35.
37. Lyon SM, Rossman MD. Pulmonary Tuberculosis. Microbiol Spectr. 2017;5(1).
38. Maejima I, Takahashi A, Omori H, Kimura T, Takabatake Y, Saitoh T, Yamamoto A, Hamasaki M, Noda T, Isaka Y, Yoshimori T. Autophagy sequesters damaged lysosomes to control lysosomal biogenesis and kidney injury. EMBO J. 2013;32(17):2336-47.
39. Manzanillo PS, Ayres JS, Watson RO, Collins AC, Souza G, Rae CS, Schneider DS, Nakamura K, Shiloh MU, Cox JS. The ubiquitin ligase parkin mediates resistance to intracellular pathogens. Nature. 2013;501(7468):512-6.
40. Masud S, Prajsnar TK, Torraca V, Lamers GEM, Benning M, Van Der Vaart M, Meijer AH. Macrophages target Salmonella by Lc3-associated phagocytosis in a systemic infection model. Autophagy. 2019;15(5):796-812.
41. Mathur R, Oh H, Zhang D, Park SG, Seo J, Koblansky A, Hayden MS, Ghosh S. A mouse model of Salmonella typhi infection. Cell. 2012;151(3):590-602.

42. Matsumoto G, Shimogori T, Hattori N, Nukina N. TBK1 controls autophagosomal engulfment of polyubiquitinated mitochondria through p62/SQSTM1 phosphorylation. Hum Mol Genet. 2015;24(15):4429-42.
43. Mayer-Barber KD, Barber DL. Innate and Adaptive Cellular Immune Responses to Mycobacterium tuberculosis Infection. Cold Spring Harb Perspect Med. 2015;5(12):a018424.
44. Medzhitov R. Toll-like receptors and innate immunity. Nat Rev Immunol. 2001;1(2):135-45.
45. Mihret A. The role of dendritic cells in Mycobacterium tuberculosis infection. Virulence. 2012;3(7):654-9.
46. Mitchell G, Cheng MI, Chen C, Nguyen BN, Whiteley AT, Kianian S, Cox JS, Green DR, McDonald KL, Portnoy DA. Listeria monocytogenes triggers noncanonical autophagy upon phagocytosis, but avoids subsequent growth-restricting xenophagy. Proc Natl Acad Sci U S A. 2018;115(2):E210-E217.
47. Mitchell G, Ge L, Huang Q, Chen C, Kianian S, Roberts MF, Schekman R, Portnoy DA. Avoidance of autophagy mediated by PlcA or ActA is required for Listeria monocytogenes growth in macrophages. Infect Immun. 2015;83(5):2175-84.
48. Mizushima N. Autophagy: process and function. Genes Dev. 2007;21(22):2861-73.
49. Moguche AO, Musvosvi M, Penn-Nicholson A, Plumlee CR, Mearns H, Geldenhuys H, Smit E, Abrahams D, Rozot V, Dintwe O, Hoff ST, Kromann I, Ruhwald M, Bang P, Larson RP, Shafiani S, Ma S, Sherman DR, Sette A, Lindestam Arlehamn CS, McKinney DM, Maecker H, Hanekom WA, Hatherill M, Andersen P, Scriba TJ, Urdahl KB. Antigen Availability Shapes T Cell Differentiation and Function during Tuberculosis. Cell Host Microbe. 2017;21(6):695-706.e5.
50. Moguche AO, Shafiani S, Clemons C, Larson RP, Dinh C, Higdon LE, Cambier CJ, Sissons JR, Gallegos AM, Fink PJ, Urdahl KB. ICOS and Bcl6-dependent pathways maintain a CD4 T cell population with memory-like properties during tuberculosis. J Exp Med. 2015;212(5):715-28.
51. Montespan C, Marvin SA, Austin S, Burrage AM, Roger B, Rayne F, Faure M, Campell EM, Schneider C, Reimer R, Grünewald K, Wiethoff CM, Wodrich H. Multi-layered control of Galectin-8 mediated autophagy during adenovirus cell entry through a conserved PPxY motif in the viral capsid. PLoS Pathog. 2017;13(2):e1006217.
52. Nish S, Medzhitov R. Host defense pathways: role of redundancy and compensation in infectious disease phenotypes. Immunity. 2011;34(5):629-36.
53. Noss EH, Pai RK, Sellati TJ, Radolf JD, Belisle J, Golenbock DT, Boom WH, Harding CV. Toll-like receptor 2-dependent inhibition of macrophage class II MHC expression and antigen processing by 19-kDa lipoprotein of Mycobacterium tuberculosis. J Immunol. 2001;167(2):910-8.
54. Ortalo-Magné A, Lemassu A, Lanéelle MA, Bardou F, Silve G, Gounon P, Marchal G, Daffé M. Identification of the surface-exposed lipids on the cell envelopes of Mycobacterium tuberculosis and other mycobacterial species. J Bacteriol. 1996;178(2):456-61.
55. Paludan C, Schmid D, Landthaler M, Vockerodt M, Kube D, Tuschl T, Münz C. Endogenous MHC class II processing of a viral nuclear antigen after autophagy. Science. 2005;307(5709):593-6.

56. Paz I, Sachse M, Dupont N, Mounier J, Cederfur C, Enninga J, Leffler H, Poirier F, Prevost MC, Lafont F, Sansonetti P. Galectin-3, a marker for vacuole lysis by invasive pathogens. Cell Microbiol. 2010;12(4):530-44.
57. Pelletier I, Hashidate T, Urashima T, Nishi N, Nakamura T, Futai M, Arata Y, Kasai K-, Hirashima M, Hirabayashi J, Sato S. Specific recognition of Leishmania major poly-beta-galactosyl epitopes by galectin-9: possible implication of galectin-9 in interaction between L. major and host cells. J Biol Chem. 2003;278(25):22223-30.
58. Penn BH, Netter Z, Johnson JR, Von Dollen J, Jang GM, Johnson T, Ohol YM, Maher C, Bell SL, Geiger K, Golovkine G, Du X, Choi A, Parry T, Mohapatra BC, Storck MD, Band H, Chen C, Jäger S, Shales M, Portnoy DA, Hernandez R, Coscoy L, Cox JS, Krogan NJ. An Mtb-Human Protein-Protein Interaction Map Identifies a Switch between Host Antiviral and Antibacterial Responses. Mol Cell. 2018;71(4):637-648.e5.
59. Pitarque S, Larrouy-Maumus G, Payré B, Jackson M, Puzo G, Nigou J. The immunomodulatory lipoglycans, lipoarabinomannan and lipomannan, are exposed at the mycobacterial cell surface. Tuberculosis (Edinb). 2008;88(6):560-5.
60. Portnoy DA, Jacks PS, Hinrichs DJ. Role of hemolysin for the intracellular growth of Listeria monocytogenes. J Exp Med. 1988;167(4):1459-71.
61. Rabinovich GA, Liu FT, Hirashima M, Anderson A. An emerging role for galectins in tuning the immune response: lessons from experimental models of inflammatory disease, autoimmunity and cancer. Scand J Immunol. 2007;66(2-3):143-58.
62. Ravenhill BJ, Boyle KB, von Muhlinen N, Ellison CJ, Masson GR, Otten EG, Foeglein A, Williams R, Randow F. The Cargo Receptor NDP52 Initiates Selective Autophagy by Recruiting the ULK Complex to Cytosol-Invading Bacteria. Mol Cell. 2019;74(2):320-329.e6.
63. Ravesloot-Chávez MM, Van Dis E, Stanley SA. The Innate Immune Response to Mycobacterium tuberculosis Infection. Annu Rev Immunol. 2021;39:611-637.
64. Ravimohan S, Kornfeld H, Weissman D, Bisson GP. Tuberculosis and lung damage: from epidemiology to pathophysiology. Eur Respir Rev. 2018;27(147):170077.
65. Reiling N, Hölscher C, Fehrenbach A, Kröger S, Kirschning CJ, Goyert S, Ehlers S. Cutting edge: Toll-like receptor (TLR)2- and TLR4-mediated pathogen recognition in resistance to airborne infection with Mycobacterium tuberculosis. J Immunol. 2002;169(7):3480-4.
66. Ren T, Zamboni DS, Roy CR, Dietrich WF, Vance RE. Flagellin-deficient Legionella mutants evade caspase-1- and Naip5-mediated macrophage immunity. PLoS Pathog. 2006;2(3):e18.
67. Reniere ML, Whiteley AT, Portnoy DA. An In Vivo Selection Identifies Listeria monocytogenes Genes Required to Sense the Intracellular Environment and Activate Virulence Factor Expression. PLoS Pathog. 2016;12(7):e1005741.
68. Richter B, Sliter DA, Herhaus L, Stolz A, Wang C, Beli P, Zaffagnini G, Wild P, Martens S, Wagner SA, Youle RJ, Dikic I. Phosphorylation of OPTN by TBK1 enhances its binding to Ub chains and promotes selective autophagy of damaged mitochondria. Proc Natl Acad Sci U S A. 2016;113(15):4039-44.
69. Roberts AW, Popov LM, Mitchell G, Ching KL, Licht DJ, Golovkine G, Barton GM, Cox JS. Cas9^{+} conditionally-immortalized macrophages as a tool for bacterial pathogenesis and beyond. Elife. 2019;8:e45957.

70. Rogerson BJ, Jung YJ, LaCourse R, Ryan L, Enright N, North RJ. Expression levels of Mycobacterium tuberculosis antigen-encoding genes versus production levels of antigen-specific T cells during stationary level lung infection in mice. Immunology. 2006;118(2):195-201.
71. Rosenberg OS, Dovala D, Li X, Connolly L, Bendebury A, Finer-Moore J, Holton J, Cheng Y, Stroud RM, Cox JS. Substrates Control Multimerization and Activation of the Multi-Domain ATPase Motor of Type VII Secretion. Cell. 2015;161(3):501-512.
72. Russell DG. Mycobacterium tuberculosis and the intimate discourse of a chronic infection. Immunol Rev. 2011;240(1):252-68.
73. Sada-Ovalle I, Chávez-Galán L, Torre-Bouscoulet L, Nava-Gamiño L, Barrera L, Jayaraman P, Torres-Rojas M, Salazar-Lezama MA, Behar SM. The Tim3-galectin 9 pathway induces antibacterial activity in human macrophages infected with Mycobacterium tuberculosis. J Immunol. 2012;189(12):5896-902.
74. Saini NK, Baena A, Ng TW, Venkataswamy MM, Kennedy SC, Kunnath-Velayudhan S, Carreño LJ, Xu J, Chan J, Larsen MH, Jacobs WR Jr, Porcelli SA. Suppression of autophagy and antigen presentation by Mycobacterium tuberculosis PE_PGRS47. Nat Microbiol. 2016;1(9):16133.
75. Sakai S, Kauffman KD, Schenkel JM, McBerry CC, Mayer-Barber KD, Masopust D, Barber DL. Cutting edge: control of Mycobacterium tuberculosis infection by a subset of lung parenchyma-homing CD4 T cells. J Immunol. 2014;192(7):2965-9.
76. Sani M, Houben EN, Geurtsen J, Pierson J, de Punder K, van Zon M, Wever B, Piersma SR, Jiménez CR, Daffé M, Appelmelk BJ, Bitter W, van der Wel N, Peters PJ. Direct visualization by cryo-EM of the mycobacterial capsular layer: a labile structure containing ESX-1-secreted proteins. PLoS Pathog. 2010;6(3):e1000794.
77. Schmid D, Pypaert M, Münz C. Antigen-loading compartments for major histocompatibility complex class II molecules continuously receive input from autophagosomes. Immunity. 2007;26(1):79-92.
78. Sogi KM, Lien KA, Johnson JR, Krogan NJ, Stanley SA. The Tyrosine Kinase Inhibitor Gefitinib Restricts Mycobacterium tuberculosis Growth through Increased Lysosomal Biogenesis and Modulation of Cytokine Signaling. ACS Infect Dis. 2017;3(8):564-574.
79. Sreejit G, Ahmed A, Parveen N, Jha V, Valluri VL, Ghosh S, Mukhopadhyay S. The ESAT-6 protein of Mycobacterium tuberculosis interacts with beta-2-microglobulin (β2M) affecting antigen presentation function of macrophage. PLoS Pathog. 2014;10(10):e1004446.
80. Stanley SA, Johndrow JE, Manzanillo P, Cox JS. The Type I IFN response to infection with Mycobacterium tuberculosis requires ESX-1-mediated secretion and contributes to pathogenesis. J Immunol. 2007;178(5):3143-52.
81. Stanley SA, Raghavan S, Hwang WW, Cox JS. Acute infection and macrophage subversion by Mycobacterium tuberculosis require a specialized secretion system. Proc Natl Acad Sci U S A. 2003;100(22):13001-6.
82. Stolz A, Ernst A, Dikic I. Cargo recognition and trafficking in selective autophagy. Nat Cell Biol. 2014;16(6):495-501.
83. Thurston TL, Wandel MP, von Muhlinen N, Foeglein A, Randow F. Galectin 8 targets damaged vesicles for autophagy to defend cells against bacterial invasion. Nature. 2012;482(7385):414-8.

84. Tobin DM. Host-Directed Therapies for Tuberculosis. Cold Spring Harb Perspect Med. 2015;5(10):a021196.
85. Torrelles JB, Schlesinger LS. Integrating Lung Physiology, Immunology, and Tuberculosis. Trends Microbiol. 2017;(8):688-697.
86. Wang WH, Lin CY, Chang MR, Urbina AN, Assavalapsakul W, Thitithanyanont A, Chen YH, Liu FT, Wang SF. The role of galectins in virus infection - A systemic literature review. J Microbiol Immunol Infect. 2020;53(6):925-935.
87. Wang C, Mei L. In utero electroporation in mice. Methods Mol Biol. 2013;1018:151-63.
88. Wassermann R, Gulen MF, Sala C, Perin SG, Lou Y, Rybniker J, Schmid-Burgk JL, Schmidt T, Hornung V, Cole ST, Ablasser A. Mycobacterium tuberculosis Differentially Activates Watson RO, Bell SL, MacDuff DA, Kimmey JM, Diner EJ, Olivas J, Vance RE, Stallings CL, Virgin HW, Cox JS. The Cytosolic Sensor cGAS Detects Mycobacterium tuberculosis DNA to Induce Type I Interferons and Activate Autophagy. Cell Host Microbe. 2015;17(6):811-819.
89. Watson RO, Bell SL, MacDuff DA, Kimmey JM, Diner EJ, Olivas J, Vance RE, Stallings CL, Virgin HW, Cox JS. The Cytosolic Sensor cGAS Detects Mycobacterium tuberculosis DNA to Induce Type I Interferons and Activate Autophagy. Cell Host Microbe. 2015;17(6):811-819.
90. Watson RO, Manzanillo PS, Cox JS. Extracellular M. tuberculosis DNA targets bacteria for autophagy by activating the host DNA-sensing pathway. Cell. 2012;150(4):803-15.
91. Wild P, Farhan H, McEwan DG, Wagner S, Rogov VV, Brady NR, Richter B, Korac J, Waidmann O, Choudhary C, Dötsch V, Bumann D, Dikic I. Phosphorylation of the autophagy receptor optineurin restricts Salmonella growth. Science. 2011;333(6039):228-33.
92. Witte CE, Archer KA, Rae CS, Sauer JD, Woodward JJ, Portnoy DA. Innate immune pathways triggered by Listeria monocytogenes and their role in the induction of cell-mediated immunity. Adv Immunol. 2012;113:135-56.
93. Wong KW, Jacobs WR Jr. Critical role for NLRP3 in necrotic death triggered by Mycobacterium tuberculosis. Cell Microbiol. 2011;13(9):1371-84.
94. World Health Organization. 2020. Global Tuberculosis Report 2020.
95. Wu X, Wu Y, Zheng R, Tang F, Qin L, Lai D, Zhang L, Chen L, Yan B, Yang H, Wang Y, Li F, Zhang J, Wang F, Wang L, Cao Y, Ma M, Liu Z, Chen J, Huang X, Wang J, Jin R, Wang P, Sun Q, Sha W, Lyu L, Moura-Alves P, Dorhoi A, Pei G, Zhang P, Chen J, Gao S, Randow F, Zeng G, Chen C, Ye XS, Kaufmann SHE, Liu H, Ge B. Sensing of mycobacterial arabinogalactan by galectin-9 exacerbates mycobacterial infection. EMBO Rep. 2021;22(7):e51678.
96. Young DB, Gideon HP, Wilkinson RJ. Eliminating latent tuberculosis. Trends Microbiol. 2009;17(5):183-8.
97. Zenewicz LA, Shen H. Innate and adaptive immune responses to Listeria monocytogenes: a short overview. Microbes Infect. 2007;9(10):1208-15.
98. Zhu C, Anderson AC, Schubart A, Xiong H, Imitola J, Khoury SJ, Zheng XX, Strom TB, Kuchroo VK. The Tim-3 ligand galectin-9 negatively regulates T helper type 1 immunity. Nat Immunol. 2005;6(12):1245-52.

Appendix

Table 1: *Mtb* pull-down mass spectrometry dataset key

Sample ID	Buffer	Condition
TBIP-387	6M Urea + Tris pH 7.4 + 150mM NaCl	WT *Mtb*
TBIP-388	6M Urea + Tris pH 7.4 + 150mM NaCl	Mas *Mtb* + THP1
TBIP-389	6M Urea + Tris pH 7.4 + 150mM NaCl	WT *Mtb* + THP1
TBIP-390	6M Urea + Tris pH 7.4 + 150mM NaCl + 0.1% Rapigest	WT *Mtb*
TBIP-391	6M Urea + Tris pH 7.4 + 150mM NaCl + 0.1% Rapigest	Mas *Mtb* + THP1
TBIP-392	6M Urea + Tris pH 7.4 + 150mM NaCl + 0.1% Rapigest	WT *Mtb* + THP1

Table 2: *Mtb* pull-down mass spectrometry results

Sample ID	Rank	Uniq Pep	Acc #	Num Uniq	% Cov	Best Disc Score	Best Expect Val	MW	Protein Name
TBIP-387	[2]		P04264	32	51.7	4.83	6.10E-09	66039.2	K2C1_HUMAN Keratin, type II cytoskeletal 1
TBIP-387	[2-1]	18	P35908	20	37.1	4.62	2.30E-08	65433.4	K22E_HUMAN Keratin, type II cytoskeletal 2 epidermal
TBIP-387	[2-2, 10-1]	3	P04259	5	10.3	3.38	4.30E-05	60067.4	K2C6B_HUMAN Keratin, type II cytoskeletal 6B
TBIP-387	[3]		P35527	21	46.4	6.13	1.20E-11	62064.8	K1C9_HUMAN Keratin, type I cytoskeletal 9
TBIP-387	[3-1]	18	P02533	19	38.8	4.29	1.10E-07	51561.9	K1C14_HUMAN Keratin, type I cytoskeletal 14
TBIP-387	[3-2]	15	P13645	16	26.7	4.56	3.50E-08	58827.5	K1C10_HUMAN Keratin, type I cytoskeletal 10
TBIP-387	[3-3]	12	P08779	13	26.4	2.78	2.70E-06	51268.3	K1C16_HUMAN Keratin, type I cytoskeletal 16
TBIP-387	[3-4]	7	Q04695	8	14.6	1.9	1.20E-04	48106.1	K1C17_HUMAN Keratin, type I cytoskeletal 17
TBIP-387	[10]		P13647	11	19.2	3.61	1.00E-05	62378.9	K2C5_HUMAN Keratin, type II cytoskeletal 5
TBIP-387	[2-2, 10-1]	3	P04259	5	10.3	3.38	4.30E-05	60067.4	K2C6B_HUMAN Keratin, type II cytoskeletal 6B
TBIP-387	[10-2]	3	P02538	5	10.3	3.19	1.40E-04	60045.4	K2C6A_HUMAN Keratin, type II cytoskeletal 6A
TBIP-387	[10-3]	3	P48668	5	10.3	3.19	1.40E-04	60025.4	K2C6C_HUMAN Keratin, type II cytoskeletal 6C
TBIP-388	[2]		P60709	25	70.9	6.58	8.20E-11	41737.1	ACTB_HUMAN Actin, cytoplasmic 1
TBIP-388	[2-1]	1	P63261	26	70.9	5.26	2.80E-09	41793.2	ACTG_HUMAN Actin, cytoplasmic 2
TBIP-388	[2-2]	4	P68032	15	41.9	3.73	3.40E-07	42019.4	ACTC_HUMAN Actin, alpha cardiac muscle 1
TBIP-388	[2-3]	4	P68133	15	41.9	3.73	3.40E-07	42051.4	ACTS_HUMAN Actin, alpha skeletal muscle
TBIP-388	[2-4]	4	P62736	14	39	3.73	3.40E-07	42009.4	ACTA_HUMAN Actin, aortic smooth muscle
TBIP-388	[2-5]	4	P63267	14	39.1	3.73	3.40E-07	41877.3	ACTH_HUMAN Actin, gamma-enteric smooth muscle
TBIP-388	[2-9]	2	Q562R1	6	21.3	3.32	3.40E-07	42003.6	ACTBL_HUMAN Beta-actin-like protein 2
TBIP-388	[2-11]	0	Q9BYX7	5	10.9	3.01	2.70E-06	42016.6	ACTBM_HUMAN Putative beta-actin-like protein 3
TBIP-388	[3]		Q15643	29	24.3	5.13	4.20E-09	227588.2	TRIPB_HUMAN Thyroid receptor-interacting protein 11

TBIP-388	[4]		P49748	28	52.8	3.83	1.70E-06	70390.7	ACADV_HUMAN Very long-chain specific acyl-CoA dehydrogenase, mitochondrial
TBIP-388	[5]		P11021	22	40.2	5.24	9.60E-09	72333.5	GRP78_HUMAN 78 kDa glucose-regulated protein
TBIP-388	[5-1]	18	P11142	19	35.6	3.56	1.80E-06	70898.7	HSP7C_HUMAN Heat shock cognate 71 kDa protein
TBIP-388	[5-2]	7	P54652	8	13.8	3.1	1.80E-06	70021.5	HSP72_HUMAN Heat shock-related 70 kDa protein 2
TBIP-388	[6]		P35579	26	19.5	4.83	8.00E-09	226534.2	MYH9_HUMAN Myosin-9
TBIP-388	[7]		P02545	23	39.6	4.18	6.00E-07	74140.1	LMNA_HUMAN Prelamin-A/C
TBIP-388	[8]		P23246	22	44.1	4.54	3.40E-08	76150	SFPQ_HUMAN Splicing factor, proline- and glutamine-rich
TBIP-388	[8-1]	17	Q15233	18	53.7	4.17	2.30E-07	54232	NONO_HUMAN Non-POU domain-containing octamer-binding protein
TBIP-388	[9]		Q01518	19	44.4	4.86	5.30E-08	51901.9	CAP1_HUMAN Adenylyl cyclase-associated protein 1
TBIP-388	[10]		Q08379	22	32.9	3.28	2.00E-05	113087.2	GOGA2_HUMAN Golgin subfamily A member 2
TBIP-388	[11]		Q00610	26	22.9	2.94	2.40E-05	191616.3	CLH1_HUMAN Clathrin heavy chain 1
TBIP-388	[12]		P25705	14	33.5	5.04	1.30E-07	59751.1	ATPA_HUMAN ATP synthase subunit alpha, mitochondrial
TBIP-388	[13]		P10809	17	37.2	3.37	2.10E-05	61055.2	CH60_HUMAN 60 kDa heat shock protein, mitochondrial
TBIP-388	[14]		P07237	16	37.6	4.16	5.70E-07	57116.8	PDIA1_HUMAN Protein disulfide-isomerase
TBIP-388	[15]		P06576	13	40.6	4.27	1.60E-06	56560.4	ATPB_HUMAN ATP synthase subunit beta, mitochondrial
TBIP-388	[16]		P11940	16	29.4	4.01	1.30E-07	70671.5	PABP1_HUMAN Polyadenylate-binding protein 1
TBIP-388	[16-1]	6	Q13310	14	31.2	4.01	1.30E-07	70783.5	PABP4_HUMAN Polyadenylate-binding protein 4
TBIP-388	[16-2]	0	Q9H361	6	11.6	2.98	1.50E-06	70031.5	PABP3_HUMAN Polyadenylate-binding protein 3
TBIP-388	[17]		P08670	17	48.1	3.77	3.90E-07	53652.1	VIME_HUMAN Vimentin
TBIP-388	[18]		P30101	15	35.2	3.56	6.20E-06	56782.9	PDIA3_HUMAN Protein disulfide-isomerase A3
TBIP-388	[19]		P40227	15	40.7	3.6	7.60E-06	58024.7	TCPZ_HUMAN T-complex protein 1 subunit zeta
TBIP-388	[20]		P52272	18	31	3.11	1.60E-06	77516.4	HNRPM_HUMAN Heterogeneous nuclear ribonucleoprotein M
TBIP-388	[21]		P27694	13	32.3	3.81	1.30E-06	68138.8	RFA1_HUMAN Replication protein A 70 kDa DNA-binding subunit
TBIP-388	[22]		P82094	14	16.7	3.33	1.10E-05	122842.7	TMF1_HUMAN TATA element modulatory factor
TBIP-388	[23]		Q9NW68	14	49.3	3.4	3.60E-06	47163.6	BSDC1_HUMAN BSD domain-containing protein 1
TBIP-388	[24]		P60660	12	71.5	4.22	3.90E-08	16930.2	MYL6_HUMAN Myosin light polypeptide 6
TBIP-388	[24-1]	0	P14649	2	11.5	3.78	3.30E-07	22764.2	MYL6B_HUMAN Myosin light chain 6B
TBIP-388	[25]		P15144	11	13	4.39	3.40E-07	109540.5	AMPN_HUMAN Aminopeptidase N
TBIP-388	[26]		P09382	10	94.8	4.85	5.70E-08	14715.8	LEG1_HUMAN Galectin-1
TBIP-388	[27]		P14618	14	44.8	3.78	2.90E-07	57937.4	KPYM_HUMAN Pyruvate kinase isozymes M1/M2
TBIP-388	[29]		O75410	13	26.3	4.05	1.10E-07	87795	TACC1_HUMAN Transforming acidic coiled-coil-containing protein 1
TBIP-388	[30]		P06733	9	33.2	5.45	3.40E-09	47169.4	ENOA_HUMAN Alpha-enolase
TBIP-388	[30-1]	4	P13929	6	24	5.45	3.40E-09	46932.2	ENOB_HUMAN Beta-enolase
TBIP-388	[31]		P62873	11	59.1	3.68	1.60E-06	37377.3	GBB1_HUMAN Guanine nucleotide-binding protein G(I)/G(S)/G(T) subunit beta-1
TBIP-388	[31-1]	6	P62879	10	52.1	2.94	1.90E-06	37331.4	GBB2_HUMAN Guanine nucleotide-binding protein G(I)/G(S)/G(T) subunit beta-2
TBIP-388	[31-2]	2	Q9HAV0	6	26.2	2.22	1.80E-05	37567.5	GBB4_HUMAN Guanine nucleotide-binding protein subunit beta-4
TBIP-388	[33]		P50897	13	57.2	3.77	1.60E-07	34193.8	PPT1_HUMAN Palmitoyl-protein thioesterase 1
TBIP-388	[34]		O14950	8	51.7	5.77	7.80E-10	19779.3	ML12B_HUMAN Myosin regulatory light chain 12B
TBIP-388	[34-1]	0	P19105	8	52	5.77	7.80E-10	19794.3	ML12A_HUMAN Myosin regulatory light chain 12A
TBIP-388	[34-2]	0	P24844	4	27.9	5.77	7.80E-10	19827.4	MYL9_HUMAN Myosin regulatory light polypeptide 9
TBIP-388	[35]		P05107	16	26.7	2.82	1.10E-05	84782.7	ITB2_HUMAN Integrin beta-2
TBIP-388	[36]		P20700	14	32.1	3.08	8.80E-06	66408.9	LMNB1_HUMAN Lamin-B1
TBIP-388	[37]		Q9H0U4	9	55.7	5.63	1.10E-10	22171.4	RAB1B_HUMAN Ras-related protein Rab-1B
TBIP-388	[37-1]	2	P62820	7	49.8	5.63	1.10E-10	22678	RAB1A_HUMAN Ras-related protein Rab-1A
TBIP-388	[37-2]	-1	Q92928	6	33.3	4.23	1.20E-07	22017.2	RAB1C_HUMAN Putative Ras-related protein Rab-1C

TBIP-388	[37-3]	1	P61026	3	16.5	2.84	2.40E-05	22541.1	RAB10_HUMAN Ras-related protein Rab-10
TBIP-388	[37-4]	3	P61106	4	37.7	2.27	2.30E-04	23897.2	RAB14_HUMAN Ras-related protein Rab-14
TBIP-388	[37-5]	0	P59190	2	10.4	2.09	9.60E-05	24390.8	RAB15_HUMAN Ras-related protein Rab-15
TBIP-388	[37-6]	0	P61006	2	10.6	2.09	9.60E-05	23668.4	RAB8A_HUMAN Ras-related protein Rab-8A
TBIP-388	[37-7]	0	Q15286	2	10.9	2.09	9.60E-05	23025.4	RAB35_HUMAN Ras-related protein Rab-35
TBIP-388	[37-8]	0	Q92930	2	10.6	2.09	9.60E-05	23584.3	RAB8B_HUMAN Ras-related protein Rab-8B
TBIP-388	[37-9]	1	P20340	2	11.5	1.94	2.30E-04	23593	RAB6A_HUMAN Ras-related protein Rab-6A
TBIP-388	[38]		Q96PK6	10	19.6	4.13	6.90E-07	69492.2	RBM14_HUMAN RNA-binding protein 14
TBIP-388	[40]		P40939	12	23.7	3.5	7.60E-07	83000.4	ECHA_HUMAN Trifunctional enzyme subunit alpha, mitochondrial
TBIP-388	[42]		P31943	10	32.7	4.19	3.90E-07	49229.9	HNRH1_HUMAN Heterogeneous nuclear ribonucleoprotein H
TBIP-388	[42-1]	0	P55795	4	12.5	4.19	3.90E-07	49264	HNRH2_HUMAN Heterogeneous nuclear ribonucleoprotein H2
TBIP-388	[42-2]	1	P52597	3	10.6	1.7	1.70E-04	45672.3	HNRPF_HUMAN Heterogeneous nuclear ribonucleoprotein F
TBIP-388	[44]		Q9UMX0	10	31.7	3.13	5.00E-06	62519.5	UBQL1_HUMAN Ubiquilin-1
TBIP-388	[44-1]	3	Q9UHD9	6	13.3	3.93	4.00E-08	65696.7	UBQL2_HUMAN Ubiquilin-2
TBIP-388	[45]		P27797	10	42.7	4.46	8.10E-09	48141.9	CALR_HUMAN Calreticulin
TBIP-388	[46]		P67809	7	56.2	4.73	5.60E-07	35924.5	YBOX1_HUMAN Nuclease-sensitive element-binding protein 1
TBIP-388	[47]		P14314	11	28.6	4.22	1.30E-08	59425.9	GLU2B_HUMAN Glucosidase 2 subunit beta
TBIP-388	[48]		Q02818	11	27.1	3.41	4.00E-06	53879.7	NUCB1_HUMAN Nucleobindin-1
TBIP-388	[49]		Q7Z417	10	21.4	3.23	1.30E-05	76121.7	NUFP2_HUMAN Nuclear fragile X mental retardation-interacting protein 2
TBIP-388	[50]		O14773	6	23.4	5.44	3.00E-09	61248.4	TPP1_HUMAN Tripeptidyl-peptidase 1
TBIP-388	[51]		P19338	13	25.1	2.94	6.90E-06	76615	NUCL_HUMAN Nucleolin
TBIP-388	[52]		Q9Y371	13	39.2	2.51	5.00E-05	40796.7	SHLB1_HUMAN Endophilin-B1
TBIP-388	[53]		Q92841	8	13.4	4.48	1.80E-07	72372.1	DDX17_HUMAN Probable ATP-dependent RNA helicase DDX17
TBIP-388	[53-1]	2	P17844	6	15.1	1.27	4.70E-04	69148.7	DDX5_HUMAN Probable ATP-dependent RNA helicase DDX5
TBIP-388	[54]		P14625	14	23.9	2.48	1.80E-05	92469.6	ENPL_HUMAN Endoplasmin
TBIP-388	[55]		P68104	11	35.5	2.84	5.90E-06	50141.3	EF1A1_HUMAN Elongation factor 1-alpha 1
TBIP-388	[55-1]	0	Q5VTE0	11	35.5	2.84	5.90E-06	50185.5	EF1A3_HUMAN Putative elongation factor 1-alpha-like 3
TBIP-388	[55-2]	0	Q05639	6	14	2.28	4.00E-05	50470.6	EF1A2_HUMAN Elongation factor 1-alpha 2
TBIP-388	[56]		P62158	6	53.7	4.76	2.20E-07	16837.7	CALM_HUMAN Calmodulin
TBIP-388	[57]		P47756	10	45.1	3.01	1.10E-05	31350.8	CAPZB_HUMAN F-actin-capping protein subunit beta
TBIP-388	[58]		O43399	8	54.4	3.41	2.40E-06	22237.9	TPD54_HUMAN Tumor protein D54
TBIP-388	[60]		Q8N6T3	9	41.9	3.56	9.50E-07	44668.3	ARFG1_HUMAN ADP-ribosylation factor GTPase-activating protein 1
TBIP-388	[63]		P68366	8	29.2	3.13	1.10E-05	49924.9	TBA4A_HUMAN Tubulin alpha-4A chain
TBIP-388	[63-1]	0	P68363	7	25.7	3.13	1.10E-05	50152.1	TBA1B_HUMAN Tubulin alpha-1B chain
TBIP-388	[63-2]	0	Q9NY65	4	15.6	3.13	1.10E-05	50094	TBA8_HUMAN Tubulin alpha-8 chain
TBIP-388	[63-3]	0	Q9BQE3	4	13.8	3.13	1.10E-05	49895.8	TBA1C_HUMAN Tubulin alpha-1C chain
TBIP-388	[63-4]	0	Q71U36	5	19.7	2.22	6.60E-05	50136.1	TBA1A_HUMAN Tubulin alpha-1A chain
TBIP-388	[63-5]	0	Q13748	4	17.8	2.22	6.60E-05	49960	TBA3C_HUMAN Tubulin alpha-3C/D chain
TBIP-388	[63-6]	0	Q6PEY2	4	17.8	2.22	6.60E-05	49859	TBA3E_HUMAN Tubulin alpha-3E chain
TBIP-388	[65]		P52907	9	59.1	3.01	2.80E-06	32923	CAZA1_HUMAN F-actin-capping protein subunit alpha-1
TBIP-388	[65-1]	3	P47755	4	24.1	1.8	3.60E-04	32949.4	CAZA2_HUMAN F-actin-capping protein subunit alpha-2
TBIP-388	[66]		P49585	6	22.6	4.75	1.60E-08	41731.4	PCY1A_HUMAN Choline-phosphate cytidylyltransferase A
TBIP-388	[67]		Q0VD83	8	12.3	2.9	1.70E-05	114820.9	APOBR_HUMAN Apolipoprotein B receptor
TBIP-388	[68]		Q13049	7	13.2	4.09	7.30E-08	71989.2	TRI32_HUMAN E3 ubiquitin-protein ligase TRIM32
TBIP-388	[74]		Q9UN86	7	24.3	3	2.20E-05	54121.6	G3BP2_HUMAN Ras GTPase-activating protein-binding protein 2

TBIP-388	[76]		P40926	7	29.9	2.9	1.10E-05	35503.6	MDHM_HUMAN Malate dehydrogenase, mitochondrial
TBIP-388	[78]		P15927	5	37.8	3.66	5.10E-06	29247.1	RFA2_HUMAN Replication protein A 32 kDa subunit
TBIP-388	[79]		P22626	7	34.8	2.76	1.60E-05	37430	ROA2_HUMAN Heterogeneous nuclear ribonucleoproteins A2/B1
TBIP-388	[81]		P37802	7	46.2	3.11	9.00E-07	22391.7	TAGL2_HUMAN Transgelin-2
TBIP-388	[82]		Q9BUP3	6	22.7	3.74	5.20E-07	27049.2	HTAI2_HUMAN Oxidoreductase HTATIP2
TBIP-388	[85]		P38159	8	22.3	2.66	8.90E-06	42332.2	RBMX_HUMAN RNA-binding motif protein, X chromosome
TBIP-388	[85-1]	0	Q96E39	4	14.1	2.66	8.90E-06	42141.9	RMXL1_HUMAN RNA binding motif protein, X-linked-like-1
TBIP-388	[87]		O43765	6	23.3	2.97	1.80E-06	34063.4	SGTA_HUMAN Small glutamine-rich tetratricopeptide repeat-containing protein alpha
TBIP-388	[88]		P06396	7	15.1	2.19	4.00E-04	85698.2	GELS_HUMAN Gelsolin
TBIP-388	[90]		Q9BS26	5	17.5	3.18	9.70E-06	46971.6	ERP44_HUMAN Endoplasmic reticulum resident protein 44
TBIP-388	[91]		P12814	7	10.1	3.06	1.30E-06	103058.4	ACTN1_HUMAN Alpha-actinin-1
TBIP-388	[91-1]	2	O43707	8	11.2	1.9	3.60E-04	104854.9	ACTN4_HUMAN Alpha-actinin-4
TBIP-388	[93]		P23528	5	50	3.36	7.40E-07	18502.7	COF1_HUMAN Cofilin-1
TBIP-388	[93-1]	0	Q9Y281	2	16.9	3.04	7.40E-07	18736.8	COF2_HUMAN Cofilin-2
TBIP-388	[96]		P06748	5	32.7	3.52	5.10E-07	32575.3	NPM_HUMAN Nucleophosmin
TBIP-388	[97]		P51149	5	32.9	3.28	6.00E-06	23490	RAB7A_HUMAN Ras-related protein Rab-7a
TBIP-388	[98]		O43615	5	13.3	2.76	1.10E-04	51356.2	TIM44_HUMAN Mitochondrial import inner membrane translocase subunit TIM44
TBIP-388	[101]		P02768	5	10.5	2.89	4.70E-05	69367.4	ALBU_HUMAN Serum albumin
TBIP-388	[103]		P39023	8	21.8	2.37	2.00E-05	46109.3	RL3_HUMAN 60S ribosomal protein L3
TBIP-388	[104]		P05387	3	55.7	4.47	1.10E-07	11665	RLA2_HUMAN 60S acidic ribosomal protein P2
TBIP-388	[105]		P04406	4	20.9	3.38	2.30E-05	36053.5	G3P_HUMAN Glyceraldehyde-3-phosphate dehydrogenase
TBIP-388	[107]		P62937	4	42.4	3.3	1.60E-06	18012.7	PPIA_HUMAN Peptidyl-prolyl cis-trans isomerase A
TBIP-388	[108]		P31949	4	43.8	3.9	1.80E-07	11740.6	S10AB_HUMAN Protein S100-A11
TBIP-388	[109]		P84090	3	32.7	4.7	5.20E-09	12259.1	ERH_HUMAN Enhancer of rudimentary homolog
TBIP-388	[110]		P25398	2	31.1	6.71	1.10E-09	14515.1	RS12_HUMAN 40S ribosomal protein S12
TBIP-388	[111]		O00182	5	17.2	3.06	6.40E-07	39518.5	LEG9_HUMAN Galectin-9
TBIP-388	[111-1]	1	Q3B8N2	5	17.1	2.93	6.40E-07	39660.7	LEG9B_HUMAN Galectin-9B
TBIP-388	[111-2]	1	Q6DKI2	5	17.1	2.93	6.40E-07	39607.8	LEG9C_HUMAN Galectin-9C
TBIP-388	[112]		Q14444	6	11.7	2.13	5.80E-05	78366.9	CAPR1_HUMAN Caprin-1
TBIP-388	[114]		P31146	5	17.8	2.61	1.00E-05	51026.7	COR1A_HUMAN Coronin-1A
TBIP-388	[115]		Q9NYL9	5	19	3.04	4.00E-06	39595.1	TMOD3_HUMAN Tropomodulin-3
TBIP-388	[116]		P00918	3	14.6	4.43	4.30E-07	29246.3	CAH2_HUMAN Carbonic anhydrase 2
TBIP-388	[117]		P04075	4	19.5	2.89	8.60E-06	39420.4	ALDOA_HUMAN Fructose-bisphosphate aldolase A
TBIP-388	[118]		P09651	3	15.3	4.03	1.10E-07	38746.9	ROA1_HUMAN Heterogeneous nuclear ribonucleoprotein A1
TBIP-388	[120]		P06732	5	23.4	2.47	1.60E-05	43101.5	KCRM_HUMAN Creatine kinase M-type
TBIP-388	[123]		P62805	6	54.4	1.9	3.20E-04	11367.4	H4_HUMAN Histone H4
TBIP-388	[124]		P07737	4	48.6	2.95	4.40E-06	15054.4	PROF1_HUMAN Profilin-1
TBIP-388	[126]		P38646	6	10.8	1.92	1.40E-04	73681.1	GRP75_HUMAN Stress-70 protein, mitochondrial
TBIP-388	[128]		P10412	5	20.5	2.11	1.20E-04	21865.4	H14_HUMAN Histone H1.4
TBIP-388	[128-1]	1	P16403	5	21.1	2.11	1.20E-04	21364.9	H12_HUMAN Histone H1.2
TBIP-388	[128-2]	0	P16402	4	12.7	2.11	1.20E-04	22350.1	H13_HUMAN Histone H1.3
TBIP-388	[129]		P55072	6	11.7	1.95	1.40E-04	89322.6	TERA_HUMAN Transitional endoplasmic reticulum ATPase
TBIP-388	[130]		P62829	4	34.3	2.45	8.20E-05	14865.6	RL23_HUMAN 60S ribosomal protein L23
TBIP-388	[132]		P35613	4	14.8	2.36	3.20E-04	42200.7	BASI_HUMAN Basigin
TBIP-388	[133]		P62263	4	31.1	2.41	5.70E-05	16272.9	RS14_HUMAN 40S ribosomal protein S14

TBIP-388	[134]		P62491	5	26.9	2.39	1.40E-05	24393.7	RB11A_HUMAN Ras-related protein Rab-11A
TBIP-388	[134-1]	0	Q15907	5	26.6	2.39	1.40E-05	24488.7	RB11B_HUMAN Ras-related protein Rab-11B
TBIP-388	[136]		P08754	4	14.1	2.89	1.10E-05	40532.6	GNAI3_HUMAN Guanine nucleotide-binding protein G(k) subunit alpha
TBIP-388	[139]		P61224	3	13.6	3.32	4.90E-06	20825	RAP1B_HUMAN Ras-related protein Rap-1b
TBIP-388	[139-1]	0	P62834	3	13.6	3.32	4.90E-06	20987.4	RAP1A_HUMAN Ras-related protein Rap-1A
TBIP-388	[140]		P62913	3	20.2	3.22	2.30E-06	20252.6	RL11_HUMAN 60S ribosomal protein L11
TBIP-388	[141]		Q8NBZ7	5	23.6	2.03	4.90E-04	47577.2	UXS1_HUMAN UDP-glucuronic acid decarboxylase 1
TBIP-388	[142]		P07910	4	15.7	2.67	6.80E-05	33670.3	HNRPC_HUMAN Heterogeneous nuclear ribonucleoproteins C1/C2
TBIP-388	[143]		Q9H8Y8	4	12.8	2.56	2.10E-05	47145.7	GORS2_HUMAN Golgi reassembly-stacking protein 2
TBIP-388	[144]		P61978	5	15.1	2.27	3.90E-05	50976.7	HNRPK_HUMAN Heterogeneous nuclear ribonucleoprotein K
TBIP-388	[145]		O75531	3	42.7	3.17	1.10E-05	10058.7	BAF_HUMAN Barrier-to-autointegration factor
TBIP-388	[146]		P06753	3	13	3.44	3.40E-06	32819.1	TPM3_HUMAN Tropomyosin alpha-3 chain
TBIP-388	[148]		P80723	5	44.9	1.91	1.30E-04	22693.6	BASP1_HUMAN Brain acid soluble protein 1
TBIP-388	[149]		Q15942	6	18.5	1.78	5.50E-04	61277.9	ZYX_HUMAN Zyxin
TBIP-388	[150]		P0C0S8	3	30	3.53	2.50E-06	14091.6	H2A1_HUMAN Histone H2A type 1
TBIP-388	[150-1]	0	P20671	3	30	3.53	2.50E-06	14107.6	H2A1D_HUMAN Histone H2A type 1-D
TBIP-388	[150-2]	0	Q16777	3	30.2	3.53	2.50E-06	13988.5	H2A2C_HUMAN Histone H2A type 2-C
TBIP-388	[150-3]	0	Q6FI13	3	30	3.53	2.50E-06	14095.6	H2A2A_HUMAN Histone H2A type 2-A
TBIP-388	[150-4]	0	Q96KK5	3	30.5	3.53	2.50E-06	13906.4	H2A1H_HUMAN Histone H2A type 1-H
TBIP-388	[150-5]	0	Q99878	3	30.5	3.53	2.50E-06	13936.4	H2A1J_HUMAN Histone H2A type 1-J
TBIP-388	[150-6]	0	Q9BTM1	3	30.2	3.53	2.50E-06	14019.5	H2AJ_HUMAN Histone H2A.J
TBIP-388	[150-7]	0	P04908	2	21.5	3.53	2.50E-06	14135.6	H2A1B_HUMAN Histone H2A type 1-B/E
TBIP-388	[150-8]	0	Q7L7L0	2	21.5	3.53	2.50E-06	14121.6	H2A3_HUMAN Histone H2A type 3
TBIP-388	[150-9]	0	Q93077	2	21.5	3.53	2.50E-06	14105.6	H2A1C_HUMAN Histone H2A type 1-C
TBIP-388	[150-10]	1	P16104	2	27.3	1.66	0.001	15144.7	H2AX_HUMAN Histone H2A.x
TBIP-388	[150-11]	1	Q8IUE6	2	30	1.66	0.001	13995.4	H2A2B_HUMAN Histone H2A type 2-B
TBIP-388	[150-12]	1	Q96QV6	2	29.8	1.66	0.001	14233.6	H2A1A_HUMAN Histone H2A type 1-A
TBIP-388	[152]		P07437	5	26.1	1.93	3.40E-04	49671.3	TBB5_HUMAN Tubulin beta chain
TBIP-388	[152-1]	0	P68371	5	26.1	1.93	3.40E-04	49831.5	TBB4B_HUMAN Tubulin beta-4B chain
TBIP-388	[152-2]	0	P04350	4	21.8	1.93	3.40E-04	49586.2	TBB4A_HUMAN Tubulin beta-4A chain
TBIP-388	[152-3]	0	Q13885	4	18.9	1.72	0.0012	49907.4	TBB2A_HUMAN Tubulin beta-2A chain
TBIP-388	[152-4]	0	Q9BVA1	4	18.9	1.72	0.0012	49953.5	TBB2B_HUMAN Tubulin beta-2B chain
TBIP-388	[156]		Q99536	4	20.1	2.3	2.30E-05	41920.6	VAT1_HUMAN Synaptic vesicle membrane protein VAT-1 homolog
TBIP-388	[158]		P49006	2	14.4	3.95	1.30E-05	19528.9	MRP_HUMAN MARCKS-related protein
TBIP-388	[160]		P10451	4	22.3	2.21	7.80E-04	35423	OSTP_HUMAN Osteopontin
TBIP-388	[164]		P61604	2	25.5	4.51	7.20E-08	10931.8	CH10_HUMAN 10 kDa heat shock protein, mitochondrial
TBIP-388	[165]		P02655	5	52.5	1.72	1.60E-04	11284	APOC2_HUMAN Apolipoprotein C-II
TBIP-388	[168]		P60174	4	22.4	2.02	9.40E-05	30791.3	TPIS_HUMAN Triosephosphate isomerase
TBIP-388	[169]		P80303	4	13.8	2.03	2.50E-04	50196.1	NUCB2_HUMAN Nucleobindin-2
TBIP-388	[174]		Q9H4G4	2	16.9	3.23	2.80E-06	17218.5	GAPR1_HUMAN Golgi-associated plant pathogenesis-related protein 1
TBIP-388	[175-3]	2	P30464	3	10.2	1.66	2.80E-04	40388.4	1B15_HUMAN HLA class I histocompatibility antigen, B-15 alpha chain
TBIP-388	[175-4]	2	P30484	3	10.2	1.66	2.80E-04	40440.5	1B46_HUMAN HLA class I histocompatibility antigen, B-46 alpha chain
TBIP-388	[176]		P51148	4	23.6	1.82	1.50E-04	23482.8	RAB5C_HUMAN Ras-related protein Rab-5C
TBIP-388	[178]		O94905	4	14.5	2.21	8.30E-06	37839.9	ERLN2_HUMAN Erlin-2
TBIP-388	[179]		P55327	3	19.6	2.04	2.00E-04	24327.2	TPD52_HUMAN Tumor protein D52

TBIP-388	[181]		P61019	3	20.3	2.29	2.80E-05	23545.8	RAB2A_HUMAN Ras-related protein Rab-2A
TBIP-388	[184]		Q15365	5	23	1.48	5.30E-04	37498.2	PCBP1_HUMAN Poly(rC)-binding protein 1
TBIP-388	[191]		P62266	3	27.3	2.06	7.20E-05	15807.7	RS23_HUMAN 40S ribosomal protein S23
TBIP-388	[193]		P30050	2	18.2	3.26	5.20E-06	17818.7	RL12_HUMAN 60S ribosomal protein L12
TBIP-388	[197]		Q9NQE9	4	29.1	1.8	3.20E-05	20361.5	HINT3_HUMAN Histidine triad nucleotide-binding protein 3
TBIP-388	[199]		P62917	2	16	2.79	1.70E-05	28024.9	RL8_HUMAN 60S ribosomal protein L8
TBIP-388	[201]		Q96A49	3	13.6	2.14	1.90E-05	39933.7	SYAP1_HUMAN Synapse-associated protein 1
TBIP-388	[204]		P62753	5	28.5	1.1	0.0021	28680.9	RS6_HUMAN 40S ribosomal protein S6
TBIP-388	[207]		O95881	3	39.5	1.78	0.0014	19205.9	TXD12_HUMAN Thioredoxin domain-containing protein 12
TBIP-388	[209]		P48047	2	13.1	2.36	9.10E-05	23277.5	ATPO_HUMAN ATP synthase subunit O, mitochondrial
TBIP-388	[212]		P16401	2	12.4	2.77	1.40E-06	22580.3	H15_HUMAN Histone H1.5
TBIP-388	[215]		P39019	3	20	1.6	0.0012	16060.6	RS19_HUMAN 40S ribosomal protein S19
TBIP-388	[216]		P62888	3	34.8	1.84	1.70E-04	12784.2	RL30_HUMAN 60S ribosomal protein L30
TBIP-388	[217]		P29966	3	11.4	1.93	5.10E-04	31554.9	MARCS_HUMAN Myristoylated alanine-rich C-kinase substrate
TBIP-388	[220]		O43504	3	74.7	1.72	2.90E-04	9614	HBXIP_HUMAN Hepatitis B virus X-interacting protein
TBIP-388	[224]		P13796	3	10	2.04	2.80E-05	70289	PLSL_HUMAN Plastin-2
TBIP-388	[225]		Q13283	3	12.2	1.65	6.40E-04	52164.7	G3BP1_HUMAN Ras GTPase-activating protein-binding protein 1
TBIP-388	[226]		P62241	2	12	2.03	3.20E-04	24205.4	RS8_HUMAN 40S ribosomal protein S8
TBIP-388	[227]		Q13501	2	10.5	2.2	1.80E-04	47687.6	SQSTM_HUMAN Sequestosome-1
TBIP-388	[229]		P62750	4	23.7	1.26	0.0012	17695.2	RL23A_HUMAN 60S ribosomal protein L23a
TBIP-388	[232]		P07339	4	18	1.05	0.0029	44552.6	CATD_HUMAN Cathepsin D
TBIP-388	[235]		Q06830	2	15.1	2.14	6.70E-04	22110.5	PRDX1_HUMAN Peroxiredoxin-1
TBIP-388	[237]		Q12907	2	10.7	2.11	4.00E-05	40229	LMAN2_HUMAN Vesicular integral-membrane protein VIP36
TBIP-388	[238]		P62081	3	25.8	1.42	0.001	22127	RS7_HUMAN 40S ribosomal protein S7
TBIP-388	[240]		P35268	2	30.5	2.21	4.30E-05	14787.1	RL22_HUMAN 60S ribosomal protein L22
TBIP-388	[242]		P26447	3	19.8	1.61	1.90E-04	11728.6	S10A4_HUMAN Protein S100-A4
TBIP-388	[244]		P78537	3	33.3	1.28	6.00E-04	17262.7	BL1S1_HUMAN Biogenesis of lysosome-related organelles complex 1 subunit 1
TBIP-388	[246]		P62328	3	61.4	1.25	0.0028	5052.7	TYB4_HUMAN Thymosin beta-4
TBIP-388	[246-1]	0	A8MW06	2	54.5	0.87	0.0067	5062.7	TMSL3_HUMAN Thymosin beta-4-like protein 3
TBIP-388	[248]		P61586	3	24.4	1.32	3.00E-04	21768.3	RHOA_HUMAN Transforming protein RhoA
TBIP-388	[249]		P35244	2	29.8	1.82	2.00E-04	13568.9	RFA3_HUMAN Replication protein A 14 kDa subunit
TBIP-388	[253]		Q9NRV9	2	16.9	1.59	3.00E-04	21097.2	HEBP1_HUMAN Heme-binding protein 1
TBIP-388	[254]		P46778	2	20.6	1.53	9.50E-04	18565	RL21_HUMAN 60S ribosomal protein L21
TBIP-388	[257]		P46776	3	31.1	1.09	0.0029	16561.5	RL27A_HUMAN 60S ribosomal protein L27a
TBIP-388	[258]		P30040	3	14.2	1.29	0.0012	28993.7	ERP29_HUMAN Endoplasmic reticulum resident protein 29
TBIP-388	[260]		P62273	3	48.2	1.27	6.50E-04	6676.8	RS29_HUMAN 40S ribosomal protein S29
TBIP-388	[261]		P11441	4	30.6	1.29	2.70E-04	17776.6	UBL4A_HUMAN Ubiquitin-like protein 4A
TBIP-388	[262]		P62854	2	18.3	1.84	7.50E-05	13015.5	RS26_HUMAN 40S ribosomal protein S26
TBIP-388	[262-1]	0	Q5JNZ5	2	18.3	1.84	7.50E-05	13002.5	RS26L_HUMAN Putative 40S ribosomal protein S26-like 1
TBIP-388	[263]		Q9NVJ2	3	18.3	1.36	2.20E-04	21539.2	ARL8B_HUMAN ADP-ribosylation factor-like protein 8B
TBIP-388	[266]		P60033	2	16.5	1.67	1.10E-04	25809.7	CD81_HUMAN CD81 antigen
TBIP-388	[269]		Q6ICB0	2	19.6	1.5	0.0016	18262.8	PPDE2_HUMAN PPPDE peptidase domain-containing protein 2
TBIP-388	[273]		P13284	2	14.8	1.57	1.80E-04	27963.9	GILT_HUMAN Gamma-interferon-inducible lysosomal thiol reductase
TBIP-388	[276]		Q13151	2	10.2	1.52	4.00E-04	30840.9	ROA0_HUMAN Heterogeneous nuclear ribonucleoprotein A0
TBIP-388	[281]		P23284	3	16.2	1.35	1.10E-04	23742.7	PPIB_HUMAN Peptidyl-prolyl cis-trans isomerase B

TBIP-388	[287]		P49755	2	12.8	1.5	9.10E-04	24976.2	TMEDA_HUMAN Transmembrane emp24 domain-containing protein 10
TBIP-388	[291]		P61769	2	26.9	1.39	1.90E-04	13714.7	B2MG_HUMAN Beta-2-microglobulin
TBIP-388	[293]		P36222	3	10.4	0.97	8.20E-04	42625.8	CH3L1_HUMAN Chitinase-3-like protein 1
TBIP-388	[295]		P30405	2	27.1	1.25	7.00E-04	22040.4	PPIF_HUMAN Peptidyl-prolyl cis-trans isomerase F, mitochondrial
TBIP-388	[310]		P04792	2	13.2	1.07	0.0029	22782.7	HSPB1_HUMAN Heat shock protein beta-1
TBIP-388	[315]		O75506	2	47.4	1.11	0.0031	8543.7	HSBP1_HUMAN Heat shock factor-binding protein 1
TBIP-388	[318]		P42677	2	25	1.24	9.10E-04	9461.2	RS27_HUMAN 40S ribosomal protein S27
TBIP-388	[318-1]	0	Q71UM5	2	25	1.24	9.10E-04	9477.3	RS27L_HUMAN 40S ribosomal protein S27-like
TBIP-388	[322]		P09497	3	10.9	1.01	8.10E-04	25190.7	CLCB_HUMAN Clathrin light chain B
TBIP-388	[353]		P68431	2	13.2	0.78	0.008	15404.2	H31_HUMAN Histone H3.1
TBIP-388	[353-1]	0	P84243	2	13.2	0.78	0.008	15328	H33_HUMAN Histone H3.3
TBIP-388	[353-2]	0	Q16695	2	13.2	0.78	0.008	15508.4	H31T_HUMAN Histone H3.1t
TBIP-388	[353-3]	0	Q71DI3	2	13.2	0.78	0.008	15388.2	H32_HUMAN Histone H3.2
TBIP-388	[374]		P46779	2	16.1	0.89	6.70E-04	15747.6	RL28_HUMAN 60S ribosomal protein L28
TBIP-388	[383]		Q01469	2	17.8	0.62	0.0076	15164.6	FABP5_HUMAN Fatty acid-binding protein, epidermal
TBIP-388	[394]		P07203	2	15.8	0.69	0.0021	22088.4	GPX1_HUMAN Glutathione peroxidase 1
TBIP-388	[398]		P18621	2	10.3	0.57	0.0043	21397.2	RL17_HUMAN 60S ribosomal protein L17
TBIP-388	[444]		P15153	2	10.9	0.4	0.0062	21429	RAC2_HUMAN Ras-related C3 botulinum toxin substrate 2
TBIP-388	[444-1]	0	P60763	2	10.9	0.4	0.0062	21379.1	RAC3_HUMAN Ras-related C3 botulinum toxin substrate 3
TBIP-388	[444-2]	0	P63000	2	10.9	0.4	0.0062	21450.3	RAC1_HUMAN Ras-related C3 botulinum toxin substrate 1
TBIP-389	[3]		P02545	29	46.5	4.37	4.90E-07	74140.1	LMNA_HUMAN Prelamin-A/C
TBIP-389	[3-1]	11	P20700	12	25.3	2.96	3.30E-05	66408.9	LMNB1_HUMAN Lamin-B1
TBIP-389	[3-2]	5	Q03252	6	10.8	1.58	8.40E-05	67689.4	LMNB2_HUMAN Lamin-B2
TBIP-389	[4]		P11021	23	42.7	4.32	6.80E-08	72333.5	GRP78_HUMAN 78 kDa glucose-regulated protein
TBIP-389	[4-1]	16	P11142	17	34.7	3.37	1.70E-06	70898.7	HSP7C_HUMAN Heat shock cognate 71 kDa protein
TBIP-389	[4-2]	5	P54652	6	11.1	3.11	1.70E-06	70021.5	HSP72_HUMAN Heat shock-related 70 kDa protein 2
TBIP-389	[5]		O75410	21	34.5	5.13	3.90E-09	87795	TACC1_HUMAN Transforming acidic coiled-coil-containing protein 1
TBIP-389	[7]		P23246	22	41.6	3.61	8.80E-07	76150	SFPQ_HUMAN Splicing factor, proline- and glutamine-rich
TBIP-389	[7-1]	15	Q15233	16	49.3	3.7	1.50E-06	54232	NONO_HUMAN Non-POU domain-containing octamer-binding protein
TBIP-389	[9]		P07237	18	40	4.21	8.90E-07	57116.8	PDIA1_HUMAN Protein disulfide-isomerase
TBIP-389	[10]		P60709	15	61.1	4.87	1.70E-08	41737.1	ACTB_HUMAN Actin, cytoplasmic 1
TBIP-389	[10-1]	1	P63261	15	61.1	4.55	5.70E-08	41793.2	ACTG_HUMAN Actin, cytoplasmic 2
TBIP-389	[10-2]	2	P62736	9	28.9	3.2	1.50E-06	42009.4	ACTA_HUMAN Actin, aortic smooth muscle
TBIP-389	[10-3]	2	P63267	9	29	3.2	1.50E-06	41877.3	ACTH_HUMAN Actin, gamma-enteric smooth muscle
TBIP-389	[10-4]	2	P68032	9	28.9	3.2	1.50E-06	42019.4	ACTC_HUMAN Actin, alpha cardiac muscle 1
TBIP-389	[10-5]	2	P68133	9	28.9	3.2	1.50E-06	42051.4	ACTS_HUMAN Actin, alpha skeletal muscle
TBIP-389	[10-7]	1	Q562R1	4	14.1	2.41	1.40E-05	42003.6	ACTBL_HUMAN Beta-actin-like protein 2
TBIP-389	[11]		P27797	13	48.9	5.73	3.90E-10	48141.9	CALR_HUMAN Calreticulin
TBIP-389	[14]		P30101	16	40.8	3.37	6.30E-06	56782.9	PDIA3_HUMAN Protein disulfide-isomerase A3
TBIP-389	[16]		Q01518	12	25.7	4.72	2.90E-08	51901.9	CAP1_HUMAN Adenylyl cyclase-associated protein 1
TBIP-389	[17]		P10809	16	38.4	3.07	2.40E-05	61055.2	CH60_HUMAN 60 kDa heat shock protein, mitochondrial
TBIP-389	[18]		P04264	13	24.5	3.52	9.90E-05	66039.2	K2C1_HUMAN Keratin, type II cytoskeletal 1
TBIP-389	[18-1]	4	P35908	5	10.3	2.71	3.90E-05	65433.4	K22E_HUMAN Keratin, type II cytoskeletal 2 epidermal
TBIP-389	[20]		P49748	17	34.8	2.9	1.40E-05	70390.7	ACADV_HUMAN Very long-chain specific acyl-CoA dehydrogenase, mitochondrial
TBIP-389	[22]		P08670	15	39.7	3.67	5.30E-07	53652.1	VIME_HUMAN Vimentin

TBIP-389	[23]		P11940	14	28.1	3.61	7.10E-07	70671.5	PABP1_HUMAN Polyadenylate-binding protein 1
TBIP-389	[23-1]	4	Q13310	12	25.2	3.61	7.10E-07	70783.5	PABP4_HUMAN Polyadenylate-binding protein 4
TBIP-389	[26]		P50897	11	46.1	4.42	2.30E-08	34193.8	PPT1_HUMAN Palmitoyl-protein thioesterase 1
TBIP-389	[30]		P14314	12	30.7	3.87	1.20E-07	59425.9	GLU2B_HUMAN Glucosidase 2 subunit beta
TBIP-389	[33]		P60660	10	66.9	4.01	6.80E-08	16930.2	MYL6_HUMAN Myosin light polypeptide 6
TBIP-389	[33-1]	0	P14649	2	11.5	2.75	1.90E-05	22764.2	MYL6B_HUMAN Myosin light chain 6B
TBIP-389	[35]		P09382	8	72.6	5.21	6.80E-09	14715.8	LEG1_HUMAN Galectin-1
TBIP-389	[37]		Q96PK6	9	18.2	4.47	4.80E-08	69492.2	RBM14_HUMAN RNA-binding protein 14
TBIP-389	[39]		P67809	7	45.1	4.31	8.40E-06	35924.5	YBOX1_HUMAN Nuclease-sensitive element-binding protein 1
TBIP-389	[42]		Q08379	11	17.7	2.95	4.00E-05	113087.2	GOGA2_HUMAN Golgin subfamily A member 2
TBIP-389	[43]		P62873	10	45.9	3.09	7.90E-06	37377.3	GBB1_HUMAN Guanine nucleotide-binding protein G(I)/G(S)/G(T) subunit beta-1
TBIP-389	[43-1]	2	P62879	6	23.8	2.58	7.90E-06	37331.4	GBB2_HUMAN Guanine nucleotide-binding protein G(I)/G(S)/G(T) subunit beta-2
TBIP-389	[43-2]	2	Q9HAV0	5	17.1	1.95	1.00E-04	37567.5	GBB4_HUMAN Guanine nucleotide-binding protein subunit beta-4
TBIP-389	[45]		P06576	9	32.1	3.19	1.30E-05	56560.4	ATPB_HUMAN ATP synthase subunit beta, mitochondrial
TBIP-389	[49]		O14950	7	51.7	4.45	5.20E-08	19779.3	ML12B_HUMAN Myosin regulatory light chain 12B
TBIP-389	[49-1]	0	P19105	7	52	4.45	5.20E-08	19794.3	ML12A_HUMAN Myosin regulatory light chain 12A
TBIP-389	[49-2]	0	P24844	3	22.7	4.45	5.20E-08	19827.4	MYL9_HUMAN Myosin regulatory light polypeptide 9
TBIP-389	[55]		P31943	7	22.9	4.11	3.60E-07	49229.9	HNRH1_HUMAN Heterogeneous nuclear ribonucleoprotein H
TBIP-389	[58]		O43399	7	48.1	3.65	1.80E-06	22237.9	TPD54_HUMAN Tumor protein D54
TBIP-389	[59]		P06733	7	29.3	4.32	6.80E-08	47169.4	ENOA_HUMAN Alpha-enolase
TBIP-389	[59-1]	1	P13929	3	14.5	4.32	6.80E-08	46932.2	ENOB_HUMAN Beta-enolase
TBIP-389	[62]		P52272	11	18.8	2.88	1.30E-06	77516.4	HNRPM_HUMAN Heterogeneous nuclear ribonucleoprotein M
TBIP-389	[70]		P25705	9	22.6	2.91	5.00E-06	59751.1	ATPA_HUMAN ATP synthase subunit alpha, mitochondrial
TBIP-389	[71]		P38646	6	11.6	3.93	6.50E-07	73681.1	GRP75_HUMAN Stress-70 protein, mitochondrial
TBIP-389	[78]		P10412	7	26.9	3.01	3.00E-06	21865.4	H14_HUMAN Histone H1.4
TBIP-389	[78-1]	1	P16403	6	25.8	2.95	3.00E-06	21364.9	H12_HUMAN Histone H1.2
TBIP-389	[78-2]	0	P16402	5	17.2	2.65	1.80E-05	22350.1	H13_HUMAN Histone H1.3
TBIP-389	[79]		P14625	8	13.9	3.35	7.00E-07	92469.6	ENPL_HUMAN Endoplasmin
TBIP-389	[84]		P09651	4	18	5.38	1.60E-09	38746.9	ROA1_HUMAN Heterogeneous nuclear ribonucleoprotein A1
TBIP-389	[89]		Q9H0U4	6	47.3	3.55	2.50E-07	22171.4	RAB1B_HUMAN Ras-related protein Rab-1B
TBIP-389	[89-1]	3	P62820	7	45.9	2.45	9.00E-06	22678	RAB1A_HUMAN Ras-related protein Rab-1A
TBIP-389	[89-2]	0	Q92928	4	27.4	3.55	2.50E-07	22017.2	RAB1C_HUMAN Putative Ras-related protein Rab-1C
TBIP-389	[89-3]	1	P61026	3	16.5	2.69	1.00E-04	22541.1	RAB10_HUMAN Ras-related protein Rab-10
TBIP-389	[89-4]	0	P59190	2	10.4	1.63	1.00E-04	24390.8	RAB15_HUMAN Ras-related protein Rab-15
TBIP-389	[89-5]	0	P61006	2	10.6	1.63	1.00E-04	23668.4	RAB8A_HUMAN Ras-related protein Rab-8A
TBIP-389	[89-6]	0	Q15286	2	10.9	1.63	1.00E-04	23025.4	RAB35_HUMAN Ras-related protein Rab-35
TBIP-389	[89-7]	0	Q92930	2	10.6	1.63	1.00E-04	23584.3	RAB8B_HUMAN Ras-related protein Rab-8B
TBIP-389	[94]		P13645	9	19.9	2.48	1.10E-05	58827.5	K1C10_HUMAN Keratin, type I cytoskeletal 10
TBIP-389	[96]		P62158	4	46.3	4.27	6.50E-08	16837.7	CALM_HUMAN Calmodulin
TBIP-389	[100]		P22307	6	12.8	3.38	2.70E-06	58994.2	NLTP_HUMAN Non-specific lipid-transfer protein
TBIP-389	[102]		P37802	4	27.1	4.31	2.40E-07	22391.7	TAGL2_HUMAN Transgelin-2
TBIP-389	[103]		Q7Z417	6	17.3	3.16	7.30E-06	76121.7	NUFP2_HUMAN Nuclear fragile X mental retardation-interacting protein 2
TBIP-389	[104]		P47756	7	31.4	2.35	1.20E-04	31350.8	CAPZB_HUMAN F-actin-capping protein subunit beta
TBIP-389	[107]		Q9NW68	7	22.3	2.94	2.50E-06	47163.6	BSDC1_HUMAN BSD domain-containing protein 1
TBIP-389	[111]		P14618	6	20.2	2.62	2.00E-05	57937.4	KPYM_HUMAN Pyruvate kinase isozymes M1/M2

TBIP-389	[119]		Q13283	6	15.5	3.17	1.70E-06	52164.7	G3BP1_HUMAN Ras GTPase-activating protein-binding protein 1
TBIP-389	[119-1]	3	Q9UN86	4	10	1.98	4.20E-05	54121.6	G3BP2_HUMAN Ras GTPase-activating protein-binding protein 2
TBIP-389	[120]		O14773	5	17.8	2.96	2.00E-05	61248.4	TPP1_HUMAN Tripeptidyl-peptidase 1
TBIP-389	[122]		P40926	4	16.9	4.02	9.50E-07	35503.6	MDHM_HUMAN Malate dehydrogenase, mitochondrial
TBIP-389	[123]		P62829	5	40	2.99	1.50E-05	14865.6	RL23_HUMAN 60S ribosomal protein L23
TBIP-389	[124]		O60664	4	13.8	3.64	1.40E-06	47075.4	PLIN3_HUMAN Perilipin-3
TBIP-389	[127]		P61604	3	37.3	5.24	3.60E-09	10931.8	CH10_HUMAN 10 kDa heat shock protein, mitochondrial
TBIP-389	[128]		P16401	4	18.6	4.26	1.60E-08	22580.3	H15_HUMAN Histone H1.5
TBIP-389	[131]		P25398	3	37.9	5.06	5.00E-08	14515.1	RS12_HUMAN 40S ribosomal protein S12
TBIP-389	[136]		P62263	6	41.1	2.14	3.30E-04	16272.9	RS14_HUMAN 40S ribosomal protein S14
TBIP-389	[137]		P68104	6	21.6	2.29	2.40E-05	50141.3	EF1A1_HUMAN Elongation factor 1-alpha 1
TBIP-389	[137-1]	0	Q5VTE0	6	21.6	2.29	2.40E-05	50185.5	EF1A3_HUMAN Putative elongation factor 1-alpha-like 3
TBIP-389	[137-2]	0	Q05639	4	10.4	2.29	2.40E-05	50470.6	EF1A2_HUMAN Elongation factor 1-alpha 2
TBIP-389	[140]		P62937	5	50.9	3.03	1.90E-06	18012.7	PPIA_HUMAN Peptidyl-prolyl cis-trans isomerase A
TBIP-389	[141]		P19338	6	11.4	2.58	4.20E-06	76615	NUCL_HUMAN Nucleolin
TBIP-389	[142]		P30040	5	37.5	2.5	3.60E-05	28993.7	ERP29_HUMAN Endoplasmic reticulum resident protein 29
TBIP-389	[149]		P38159	6	17.4	2.51	9.00E-06	42332.2	RBMX_HUMAN RNA-binding motif protein, X chromosome
TBIP-389	[164]		Q9Y371	5	19.2	2.39	7.50E-05	40796.7	SHLB1_HUMAN Endophilin-B1
TBIP-389	[165]		P06748	5	32.7	2.41	2.50E-05	32575.3	NPM_HUMAN Nucleophosmin
TBIP-389	[173]		O75531	3	42.7	3.41	8.70E-06	10058.7	BAF_HUMAN Barrier-to-autointegration factor
TBIP-389	[176]		P35637	4	16.3	2.24	8.00E-05	53426.2	FUS_HUMAN RNA-binding protein FUS
TBIP-389	[179]		P05107	9	15.1	1.41	1.70E-04	84782.7	ITB2_HUMAN Integrin beta-2
TBIP-389	[183]		P51149	4	23.2	2.57	2.60E-05	23490	RAB7A_HUMAN Ras-related protein Rab-7a
TBIP-389	[187]		P80723	4	41.9	2.6	1.30E-05	22693.6	BASP1_HUMAN Brain acid soluble protein 1
TBIP-389	[188]		P23528	4	39.8	2.36	4.40E-05	18502.7	COF1_HUMAN Cofilin-1
TBIP-389	[190]		Q12800	3	10.2	2.82	3.60E-05	57256.1	TFCP2_HUMAN Alpha-globin transcription factor CP2
TBIP-389	[193]		P49585	3	13.1	3.05	2.10E-06	41731.4	PCY1A_HUMAN Choline-phosphate cytidylyltransferase A
TBIP-389	[196]		P22626	4	17.3	2.24	4.00E-05	37430	ROA2_HUMAN Heterogeneous nuclear ribonucleoproteins A2/B1
TBIP-389	[197]		P07910	3	11.8	3.13	1.20E-05	33670.3	HNRPC_HUMAN Heterogeneous nuclear ribonucleoproteins C1/C2
TBIP-389	[199]		P05387	3	55.7	2.93	3.30E-06	11665	RLA2_HUMAN 60S acidic ribosomal protein P2
TBIP-389	[203]		P62805	4	38.8	2	3.00E-04	11367.4	H4_HUMAN Histone H4
TBIP-389	[205]		Q04837	2	20.3	3.43	8.80E-07	17259.8	SSBP_HUMAN Single-stranded DNA-binding protein, mitochondrial
TBIP-389	[206]		P31949	2	25.7	3.65	1.10E-06	11740.6	S10AB_HUMAN Protein S100-A11
TBIP-389	[207]		P04075	3	12.4	3.17	1.50E-06	39420.4	ALDOA_HUMAN Fructose-bisphosphate aldolase A
TBIP-389	[211]		P31146	5	16.1	2.06	3.00E-05	51026.7	COR1A_HUMAN Coronin-1A
TBIP-389	[215]		Q9NYL9	4	16.2	2.14	1.60E-05	39595.1	TMOD3_HUMAN Tropomodulin-3
TBIP-389	[216]		P17844	4	10.3	2.09	9.30E-05	69148.7	DDX5_HUMAN Probable ATP-dependent RNA helicase DDX5
TBIP-389	[221]		P49006	2	14.4	3.81	1.90E-06	19528.9	MRP_HUMAN MARCKS-related protein
TBIP-389	[227]		P52907	3	15	2.33	7.90E-05	32923	CAZA1_HUMAN F-actin-capping protein subunit alpha-1
TBIP-389	[236]		P61981	3	12.1	2.61	2.90E-05	28302.8	1433G_HUMAN 14-3-3 protein gamma
TBIP-389	[239]		P07339	4	13.6	1.72	1.60E-04	44552.6	CATD_HUMAN Cathepsin D
TBIP-389	[244]		P35527	4	10.1	2.02	3.00E-05	62064.8	K1C9_HUMAN Keratin, type I cytoskeletal 9
TBIP-389	[247]		P07737	4	55	1.68	2.80E-04	15054.4	PROF1_HUMAN Profilin-1
TBIP-389	[250]		P07305	3	18.6	1.94	9.00E-05	20863.1	H10_HUMAN Histone H1.0
TBIP-389	[251]		P15927	2	13	2.96	3.80E-05	29247.1	RFA2_HUMAN Replication protein A 32 kDa subunit

TBIP-389	[255]		P16220	4	15.5	1.64	2.40E-04	36688.4	CREB1_HUMAN Cyclic AMP-responsive element-binding protein 1
TBIP-389	[260]		P39019	4	27.6	1.52	4.20E-04	16060.6	RS19_HUMAN 40S ribosomal protein S19
TBIP-389	[262]		O95881	2	16.9	2.47	1.40E-04	19205.9	TXD12_HUMAN Thioredoxin domain-containing protein 12
TBIP-389	[264]		P02655	4	50.5	1.52	1.80E-04	11284	APOC2_HUMAN Apolipoprotein C-II
TBIP-389	[265]		P62266	3	35.7	2.21	3.60E-05	15807.7	RS23_HUMAN 40S ribosomal protein S23
TBIP-389	[266]		P30048	2	17.6	2.4	2.80E-04	27692.9	PRDX3_HUMAN Thioredoxin-dependent peroxide reductase, mitochondrial
TBIP-389	[267]		P35268	2	30.5	2.49	5.40E-05	14787.1	RL22_HUMAN 60S ribosomal protein L22
TBIP-389	[268]		P10451	2	14.3	2.46	3.80E-04	35423	OSTP_HUMAN Osteopontin
TBIP-389	[274]		Q9H4G4	2	16.9	2.25	9.90E-05	17218.5	GAPR1_HUMAN Golgi-associated plant pathogenesis-related protein 1
TBIP-389	[279]		Q9BS26	4	13.8	1.48	9.40E-04	46971.6	ERP44_HUMAN Endoplasmic reticulum resident protein 44
TBIP-389	[280]		P62491	3	14.8	1.85	4.10E-04	24393.7	RB11A_HUMAN Ras-related protein Rab-11A
TBIP-389	[280-1]	0	Q15907	3	14.7	1.85	4.10E-04	24488.7	RB11B_HUMAN Ras-related protein Rab-11B
TBIP-389	[282]		P07858	2	10.6	2.6	1.60E-05	37822	CATB_HUMAN Cathepsin B
TBIP-389	[283]		O43504	3	70.3	1.72	2.80E-04	9614	HBXIP_HUMAN Hepatitis B virus X-interacting protein
TBIP-389	[287]		P27824	4	10.3	1.36	9.70E-04	67568.9	CALX_HUMAN Calnexin
TBIP-389	[290]		P62328	3	61.4	1.42	0.004	5052.7	TYB4_HUMAN Thymosin beta-4
TBIP-389	[290-1]	0	A8MW06	2	54.5	0.5	0.004	5062.7	TMSL3_HUMAN Thymosin beta-4-like protein 3
TBIP-389	[303]		Q13951	2	23.1	2.02	1.10E-04	21508.3	PEBB_HUMAN Core-binding factor subunit beta
TBIP-389	[304]		P51148	2	13	1.84	1.10E-04	23482.8	RAB5C_HUMAN Ras-related protein Rab-5C
TBIP-389	[305]		P61769	3	37.8	1.71	1.40E-04	13714.7	B2MG_HUMAN Beta-2-microglobulin
TBIP-389	[312]		P62273	3	48.2	1.18	0.0037	6676.8	RS29_HUMAN 40S ribosomal protein S29
TBIP-389	[317]		P84090	2	16.3	2.33	1.10E-05	12259.1	ERH_HUMAN Enhancer of rudimentary homolog
TBIP-389	[325]		P04792	2	13.2	1.71	3.00E-04	22782.7	HSPB1_HUMAN Heat shock protein beta-1
TBIP-389	[339]		Q9H299	2	19.4	1.86	5.90E-05	10437.8	SH3L3_HUMAN SH3 domain-binding glutamic acid-rich-like protein 3
TBIP-389	[350]		Q96C19	3	15.4	1.29	5.30E-04	26697.5	EFHD2_HUMAN EF-hand domain-containing protein D2
TBIP-389	[354]		O94905	3	11.8	1.25	3.70E-04	37839.9	ERLN2_HUMAN Erlin-2
TBIP-389	[361]		P62753	2	14.9	1.34	9.50E-04	28680.9	RS6_HUMAN 40S ribosomal protein S6
TBIP-389	[369]		P62750	2	15.4	1.21	8.10E-04	17695.2	RL23A_HUMAN 60S ribosomal protein L23a
TBIP-389	[391]		P09496	3	12.1	0.84	0.0043	27076.9	CLCA_HUMAN Clathrin light chain A
TBIP-389	[424]		P04908	2	21.5	1.11	0.0011	14135.6	H2A1B_HUMAN Histone H2A type 1-B/E
TBIP-389	[424-1]	0	P0C0S8	2	21.5	1.11	0.0011	14091.6	H2A1_HUMAN Histone H2A type 1
TBIP-389	[424-2]	0	P20671	2	21.5	1.11	0.0011	14107.6	H2A1D_HUMAN Histone H2A type 1-D
TBIP-389	[424-3]	0	Q16777	2	21.7	1.11	0.0011	13988.5	H2A2C_HUMAN Histone H2A type 2-C
TBIP-389	[424-4]	0	Q6FI13	2	21.5	1.11	0.0011	14095.6	H2A2A_HUMAN Histone H2A type 2-A
TBIP-389	[424-5]	0	Q7L7L0	2	21.5	1.11	0.0011	14121.6	H2A3_HUMAN Histone H2A type 3
TBIP-389	[424-6]	0	Q93077	2	21.5	1.11	0.0011	14105.6	H2A1C_HUMAN Histone H2A type 1-C
TBIP-389	[424-7]	0	Q96KK5	2	21.9	1.11	0.0011	13906.4	H2A1H_HUMAN Histone H2A type 1-H
TBIP-389	[424-8]	0	Q99878	2	21.9	1.11	0.0011	13936.4	H2A1J_HUMAN Histone H2A type 1-J
TBIP-389	[424-9]	0	Q9BTM1	2	21.7	1.11	0.0011	14019.5	H2AJ_HUMAN Histone H2A.J
TBIP-389	[424-10]	1	P16104	2	27.3	0.84	0.0054	15144.7	H2AX_HUMAN Histone H2A.x
TBIP-389	[424-11]	1	Q8IUE6	2	30	0.84	0.0054	13995.4	H2A2B_HUMAN Histone H2A type 2-B
TBIP-389	[424-12]	1	Q96QV6	2	29.8	0.84	0.0054	14233.6	H2A1A_HUMAN Histone H2A type 1-A
TBIP-390	[3]		P04264	15	25.2	4.7	2.00E-08	66039.2	K2C1_HUMAN Keratin, type II cytoskeletal 1
TBIP-390	[3-1]	8	P35908	9	18.8	4.3	7.30E-08	65433.4	K22E_HUMAN Keratin, type II cytoskeletal 2 epidermal
TBIP-390	[27]		P13645	9	14.4	3.13	4.10E-06	58827.5	K1C10_HUMAN Keratin, type I cytoskeletal 10

TBIP-391	[1]		P05107	15	20.2	4.54	1.20E-07	84782.7	ITB2_HUMAN Integrin beta-2
TBIP-391	[2]		P35579	21	10.4	3.11	1.40E-06	226534.2	MYH9_HUMAN Myosin-9
TBIP-391	[3]		O60488	14	16.3	3.65	7.60E-07	79188.8	ACSL4_HUMAN Long-chain-fatty-acid--CoA ligase 4
TBIP-391	[4]		Q0VD83	12	14.6	2.46	3.80E-05	114820.9	APOBR_HUMAN Apolipoprotein B receptor
TBIP-391	[6]		P60709	6	14.9	4.04	8.40E-08	41737.1	ACTB_HUMAN Actin, cytoplasmic 1
TBIP-391	[6-1]	0	P63261	6	14.9	4.04	8.40E-08	41793.2	ACTG_HUMAN Actin, cytoplasmic 2
TBIP-391	[7]		P23786	10	17.6	2.74	1.00E-05	73777.7	CPT2_HUMAN Carnitine O-palmitoyltransferase 2, mitochondrial
TBIP-391	[11]		P68371	7	12.8	2.5	5.70E-05	49831.5	TBB4B_HUMAN Tubulin beta-4B chain
TBIP-391	[11-1]	1	P07437	7	12.8	2.43	8.60E-05	49671.3	TBB5_HUMAN Tubulin beta chain
TBIP-391	[11-2]	0	Q13885	6	10.1	2.43	8.60E-05	49907.4	TBB2A_HUMAN Tubulin beta-2A chain
TBIP-391	[11-3]	0	Q9BVA1	6	10.1	2.43	8.60E-05	49953.5	TBB2B_HUMAN Tubulin beta-2B chain
TBIP-391	[13]		P80723	6	57.3	2.68	4.70E-05	22693.6	BASP1_HUMAN Brain acid soluble protein 1
TBIP-391	[18]		Q92520	4	16.7	3.4	8.70E-06	24680.7	FAM3C_HUMAN Protein FAM3C
TBIP-391	[20]		P62269	5	27	2.59	8.10E-05	17718.8	RS18_HUMAN 40S ribosomal protein S18
TBIP-391	[22]		P10412	4	18.7	3.07	1.50E-06	21865.4	H14_HUMAN Histone H1.4
TBIP-391	[22-1]	1	P16403	4	19.2	3.07	1.50E-06	21364.9	H12_HUMAN Histone H1.2
TBIP-391	[22-2]	2	P16401	3	16.4	3.86	1.60E-07	22580.3	H15_HUMAN Histone H1.5
TBIP-391	[22-3]	0	P16402	3	10.9	2.52	4.00E-05	22350.1	H13_HUMAN Histone H1.3
TBIP-391	[22-4]	0	P22492	3	11.6	2.52	4.00E-05	22019.2	H1T_HUMAN Histone H1t
TBIP-391	[22-5]	0	Q02539	3	11.2	2.52	4.00E-05	21842.3	H11_HUMAN Histone H1.1
TBIP-391	[23]		P61006	4	16.9	2.64	5.00E-05	23668.4	RAB8A_HUMAN Ras-related protein Rab-8A
TBIP-391	[24]		Q9UL25	2	11.6	5.04	2.60E-08	24347.8	RAB21_HUMAN Ras-related protein Rab-21
TBIP-391	[26]		O94905	4	13.3	2.47	3.50E-05	37839.9	ERLN2_HUMAN Erlin-2
TBIP-391	[29]		O43615	5	11.7	1.83	5.70E-04	51356.2	TIM44_HUMAN Mitochondrial import inner membrane translocase subunit TIM44
TBIP-391	[41]		P49006	2	14.4	3.58	5.40E-06	19528.9	MRP_HUMAN MARCKS-related protein
TBIP-391	[43]		P02649	4	14.5	2.47	9.60E-06	36154.4	APOE_HUMAN Apolipoprotein E
TBIP-391	[46]		Q9H4G4	2	16.9	3.17	1.10E-05	17218.5	GAPR1_HUMAN Golgi-associated plant pathogenesis-related protein 1
TBIP-391	[47]		P30464	3	11	2.76	1.10E-06	40388.4	1B15_HUMAN HLA class I histocompatibility antigen, B-15 alpha chain
TBIP-391	[47-1]	0	P30466	3	11	2.76	1.10E-06	40275.2	1B18_HUMAN HLA class I histocompatibility antigen, B-18 alpha chain
TBIP-391	[47-2]	0	P30475	3	11	2.76	1.10E-06	40328.3	1B39_HUMAN HLA class I histocompatibility antigen, B-39 alpha chain
TBIP-391	[47-3]	0	P30484	3	11	2.76	1.10E-06	40440.5	1B46_HUMAN HLA class I histocompatibility antigen, B-46 alpha chain
TBIP-391	[47-4]	0	Q29836	3	11	2.76	1.10E-06	40342.3	1B67_HUMAN HLA class I histocompatibility antigen, B-67 alpha chain
TBIP-391	[47-5]	0	Q95365	3	11	2.76	1.10E-06	40416.5	1B38_HUMAN HLA class I histocompatibility antigen, B-38 alpha chain
TBIP-391	[48]		P49755	2	10	3.59	1.40E-06	24976.2	TMEDA_HUMAN Transmembrane emp24 domain-containing protein 10
TBIP-391	[50]		P61586	3	12.4	2.39	2.60E-05	21768.3	RHOA_HUMAN Transforming protein RhoA
TBIP-391	[51]		Q9BV40	4	45	1.48	0.0033	11438.4	VAMP8_HUMAN Vesicle-associated membrane protein 8
TBIP-391	[53]		P51148	3	17.6	2.09	1.10E-04	23482.8	RAB5C_HUMAN Ras-related protein Rab-5C
TBIP-391	[54]		O75396	3	13.5	1.97	1.70E-04	24593.6	SC22B_HUMAN Vesicle-trafficking protein SEC22b
TBIP-391	[56]		P15153	4	22.9	1.82	8.90E-05	21429	RAC2_HUMAN Ras-related C3 botulinum toxin substrate 2
TBIP-391	[56-1]	2	P84095	3	20.9	1.61	5.10E-04	21308.7	RHOG_HUMAN Rho-related GTP-binding protein RhoG
TBIP-391	[56-2]	1	P60953	2	11	2.15	2.90E-05	21258.8	CDC42_HUMAN Cell division control protein 42 homolog
TBIP-391	[56-3]	0	P60763	2	10.9	1.82	8.90E-05	21379.1	RAC3_HUMAN Ras-related C3 botulinum toxin substrate 3
TBIP-391	[56-4]	0	P63000	2	10.9	1.82	8.90E-05	21450.3	RAC1_HUMAN Ras-related C3 botulinum toxin substrate 1
TBIP-391	[61]		P62701	4	11.4	1.78	1.90E-04	29598	RS4X_HUMAN 40S ribosomal protein S4, X isoform
TBIP-391	[64]		Q15363	4	15.4	1.89	7.70E-05	22761.4	TMED2_HUMAN Transmembrane emp24 domain-containing protein 2

TBIP-391	[66]		P30273	3	23.3	2.4	1.00E-05	9667.6	FCERG_HUMAN High affinity immunoglobulin epsilon receptor subunit gamma
TBIP-391	[67]		P54920	2	11.2	2.43	6.80E-04	33233	SNAA_HUMAN Alpha-soluble NSF attachment protein
TBIP-391	[73]		P51572	3	11.4	1.61	6.50E-04	27991.8	BAP31_HUMAN B-cell receptor-associated protein 31
TBIP-391	[77]		P21796	2	11.3	2.24	4.80E-05	30772.8	VDAC1_HUMAN Voltage-dependent anion-selective channel protein 1
TBIP-391	[79]		P05141	4	10.7	1.52	3.60E-04	32852.5	ADT2_HUMAN ADP/ATP translocase 2
TBIP-391	[79-1]	0	P12236	4	10.7	1.52	3.60E-04	32866.6	ADT3_HUMAN ADP/ATP translocase 3
TBIP-391	[82]		P60468	2	28.1	2.16	2.10E-05	9974.5	SC61B_HUMAN Protein transport protein Sec61 subunit beta
TBIP-391	[84]		P09382	3	25.9	1.73	2.50E-04	14715.8	LEG1_HUMAN Galectin-1
TBIP-391	[86]		P62805	2	21.4	2.15	8.50E-05	11367.4	H4_HUMAN Histone H4
TBIP-391	[87]		P62277	2	13.9	2.25	1.40E-04	17222.4	RS13_HUMAN 40S ribosomal protein S13
TBIP-391	[88]		O60814	3	16.7	1.38	6.10E-04	13890.3	H2B1K_HUMAN Histone H2B type 1-K
TBIP-391	[88-1]	0	P57053	3	16.7	1.38	6.10E-04	13944.3	H2BFS_HUMAN Histone H2B type F-S
TBIP-391	[88-2]	0	P58876	3	16.7	1.38	6.10E-04	13936.3	H2B1D_HUMAN Histone H2B type 1-D
TBIP-391	[88-3]	0	P62807	3	16.7	1.38	6.10E-04	13906.3	H2B1C_HUMAN Histone H2B type 1-C/E/F/G/I
TBIP-391	[88-4]	0	Q5QNW6	3	16.7	1.38	6.10E-04	13920.3	H2B2F_HUMAN Histone H2B type 2-F
TBIP-391	[88-5]	0	Q93079	3	16.7	1.38	6.10E-04	13892.2	H2B1H_HUMAN Histone H2B type 1-H
TBIP-391	[88-6]	0	Q99877	3	16.7	1.38	6.10E-04	13922.3	H2B1N_HUMAN Histone H2B type 1-N
TBIP-391	[88-7]	0	Q99879	3	16.7	1.38	6.10E-04	13989.4	H2B1M_HUMAN Histone H2B type 1-M
TBIP-391	[88-8]	0	Q99880	3	16.7	1.38	6.10E-04	13952.3	H2B1L_HUMAN Histone H2B type 1-L
TBIP-391	[89]		P63218	3	30.9	1.56	2.20E-04	7318.5	GBG5_HUMAN Guanine nucleotide-binding protein G(I)/G(S)/G(O) subunit gamma-5
TBIP-391	[93]		P39019	3	20	1.41	0.0022	16060.6	RS19_HUMAN 40S ribosomal protein S19
TBIP-391	[97]		P02655	2	17.8	1.91	2.00E-04	11284	APOC2_HUMAN Apolipoprotein C-II
TBIP-391	[102]		P60660	2	14.6	1.79	3.50E-04	16930.2	MYL6_HUMAN Myosin light polypeptide 6
TBIP-391	[120]		P47756	2	10.5	1.45	5.70E-04	31350.8	CAPZB_HUMAN F-actin-capping protein subunit beta
TBIP-391	[141]		Q9NVJ2	2	10.2	1.33	3.40E-04	21539.2	ARL8B_HUMAN ADP-ribosylation factor-like protein 8B
TBIP-392	[1]		P35579	55	34.9	4.59	6.00E-08	226534.2	MYH9_HUMAN Myosin-9
TBIP-392	[2]		O60488	37	64	5.16	1.30E-07	79188.8	ACSL4_HUMAN Long-chain-fatty-acid--CoA ligase 4
TBIP-392	[4]		P63261	23	69.1	6.09	6.60E-10	41793.2	ACTG_HUMAN Actin, cytoplasmic 2
TBIP-392	[4-1]	1	P60709	23	69.1	5.94	8.80E-10	41737.1	ACTB_HUMAN Actin, cytoplasmic 1
TBIP-392	[4-2]	3	P62736	14	35.8	4.17	4.90E-08	42009.4	ACTA_HUMAN Actin, aortic smooth muscle
TBIP-392	[4-3]	3	P63267	14	35.9	4.17	4.90E-08	41877.3	ACTH_HUMAN Actin, gamma-enteric smooth muscle
TBIP-392	[4-4]	3	P68032	14	35.8	4.17	4.90E-08	42019.4	ACTC_HUMAN Actin, alpha cardiac muscle 1
TBIP-392	[4-5]	3	P68133	14	35.8	4.17	4.90E-08	42051.4	ACTS_HUMAN Actin, alpha skeletal muscle
TBIP-392	[4-7]	2	Q562R1	7	23.7	3.41	6.90E-07	42003.6	ACTBL_HUMAN Beta-actin-like protein 2
TBIP-392	[5]		P05107	28	44.6	4.88	1.80E-09	84782.7	ITB2_HUMAN Integrin beta-2
TBIP-392	[6]		O60664	23	72.1	4.04	6.90E-07	47075.4	PLIN3_HUMAN Perilipin-3
TBIP-392	[8]		Q0VD83	19	28	4.86	1.20E-07	114820.9	APOBR_HUMAN Apolipoprotein B receptor
TBIP-392	[9]		P68363	15	49.4	5.33	2.60E-08	50152.1	TBA1B_HUMAN Tubulin alpha-1B chain
TBIP-392	[9-1]	2	Q71U36	15	49.4	5.33	2.60E-08	50136.1	TBA1A_HUMAN Tubulin alpha-1A chain
TBIP-392	[9-2]	2	Q13748	13	44.2	5.33	2.60E-08	49960	TBA3C_HUMAN Tubulin alpha-3C/D chain
TBIP-392	[9-3]	0	P68366	11	37.7	5.33	2.60E-08	49924.9	TBA4A_HUMAN Tubulin alpha-4A chain
TBIP-392	[9-4]	2	Q6PEY2	10	37.1	5.33	2.60E-08	49859	TBA3E_HUMAN Tubulin alpha-3E chain
TBIP-392	[9-5]	1	Q9BQE3	13	40.5	4.09	9.20E-08	49895.8	TBA1C_HUMAN Tubulin alpha-1C chain
TBIP-392	[9-6]	1	Q9NY65	9	28.7	5.33	2.60E-08	50094	TBA8_HUMAN Tubulin alpha-8 chain
TBIP-392	[10]		P23786	22	46.8	3.08	5.20E-06	73777.7	CPT2_HUMAN Carnitine O-palmitoyltransferase 2, mitochondrial

TBIP-392	[11]		P07437	21	68.7	3.41	9.30E-07	49671.3	TBB5_HUMAN Tubulin beta chain
TBIP-392	[11-1]	5	P68371	21	65.4	3.33	1.50E-06	49831.5	TBB4B_HUMAN Tubulin beta-4B chain
TBIP-392	[11-2]	4	P04350	16	54.1	3.08	7.10E-06	49586.2	TBB4A_HUMAN Tubulin beta-4A chain
TBIP-392	[11-3]	3	Q13885	17	50.8	3.23	9.30E-07	49907.4	TBB2A_HUMAN Tubulin beta-2A chain
TBIP-392	[11-4]	3	Q9BVA1	17	50.8	3.23	9.30E-07	49953.5	TBB2B_HUMAN Tubulin beta-2B chain
TBIP-392	[11-5]	1	Q13509	10	24.7	3.41	9.30E-07	50433.2	TBB3_HUMAN Tubulin beta-3 chain
TBIP-392	[11-6]	2	Q3ZCM7	7	25.5	2.96	1.10E-05	49776.5	TBB8_HUMAN Tubulin beta-8 chain
TBIP-392	[11-7]	5	Q9BUF5	8	21.3	2.02	7.20E-05	49857.6	TBB6_HUMAN Tubulin beta-6 chain
TBIP-392	[11-8]	1	A6NNZ2	6	22.1	1.71	2.70E-04	49573.1	TBB8B_HUMAN Tubulin beta-8 chain B
TBIP-392	[11-9]	1	A6NKZ8	4	15.3	1.71	2.70E-04	41775.5	YI016_HUMAN Putative tubulin beta chain-like protein ENSP00000290377
TBIP-392	[13]		Q12965	12	14	5.09	2.40E-08	127063	MYO1E_HUMAN Unconventional myosin-Ie
TBIP-392	[13-1]	7	O00160	10	10.2	4.91	7.00E-08	124845.4	MYO1F_HUMAN Unconventional myosin-If
TBIP-392	[14]		Q99541	14	44.4	3.98	2.00E-06	48075.8	PLIN2_HUMAN Perilipin-2
TBIP-392	[18]		Q00610	20	17.1	2.52	3.60E-05	191616.3	CLH1_HUMAN Clathrin heavy chain 1
TBIP-392	[19]		P11021	12	22.9	3.89	8.10E-07	72333.5	GRP78_HUMAN 78 kDa glucose-regulated protein
TBIP-392	[21]		P14625	14	22.5	2.9	7.40E-05	92469.6	ENPL_HUMAN Endoplasmin
TBIP-392	[21-1]	7	P08238	8	15.1	2.56	1.60E-05	83264.9	HS90B_HUMAN Heat shock protein HSP 90-beta
TBIP-392	[23]		Q01518	8	20.6	5.34	1.70E-08	51901.9	CAP1_HUMAN Adenylyl cyclase-associated protein 1
TBIP-392	[25]		Q99536	9	31.8	3.8	4.50E-06	41920.6	VAT1_HUMAN Synaptic vesicle membrane protein VAT-1 homolog
TBIP-392	[28]		P49748	15	33.9	2.35	8.70E-05	70390.7	ACADV_HUMAN Very long-chain specific acyl-CoA dehydrogenase, mitochondrial
TBIP-392	[29]		P09874	11	14	3.73	2.60E-07	113084.8	PARP1_HUMAN Poly [ADP-ribose] polymerase 1
TBIP-392	[35]		O60814	7	28.6	4.31	6.40E-07	13890.3	H2B1K_HUMAN Histone H2B type 1-K
TBIP-392	[35-1]	0	P57053	7	28.6	4.31	6.40E-07	13944.3	H2BFS_HUMAN Histone H2B type F-S
TBIP-392	[35-2]	0	P58876	7	28.6	4.31	6.40E-07	13936.3	H2B1D_HUMAN Histone H2B type 1-D
TBIP-392	[35-3]	0	P62807	7	28.6	4.31	6.40E-07	13906.3	H2B1C_HUMAN Histone H2B type 1-C/E/F/G/I
TBIP-392	[35-4]	0	Q5QNW6	7	28.6	4.31	6.40E-07	13920.3	H2B2F_HUMAN Histone H2B type 2-F
TBIP-392	[35-5]	0	Q93079	7	28.6	4.31	6.40E-07	13892.2	H2B1H_HUMAN Histone H2B type 1-H
TBIP-392	[35-6]	0	Q99877	7	28.6	4.31	6.40E-07	13922.3	H2B1N_HUMAN Histone H2B type 1-N
TBIP-392	[35-7]	0	Q99879	7	28.6	4.31	6.40E-07	13989.4	H2B1M_HUMAN Histone H2B type 1-M
TBIP-392	[35-8]	0	Q99880	7	28.6	4.31	6.40E-07	13952.3	H2B1L_HUMAN Histone H2B type 1-L
TBIP-392	[35-9]	1	P06899	6	27.8	4.31	6.40E-07	13904.3	H2B1J_HUMAN Histone H2B type 1-J
TBIP-392	[35-10]	1	P23527	6	27.8	4.31	6.40E-07	13906.3	H2B1O_HUMAN Histone H2B type 1-O
TBIP-392	[35-11]	1	P33778	6	27.8	4.31	6.40E-07	13950.3	H2B1B_HUMAN Histone H2B type 1-B
TBIP-392	[35-12]	1	Q16778	6	27.8	4.31	6.40E-07	13920.3	H2B2E_HUMAN Histone H2B type 2-E
TBIP-392	[35-13]	1	Q8N257	6	27.8	4.31	6.40E-07	13908.2	H2B3B_HUMAN Histone H2B type 3-B
TBIP-392	[36]		P16401	8	30.1	3.68	8.10E-07	22580.3	H15_HUMAN Histone H1.5
TBIP-392	[36-1]	8	P10412	9	31.1	2.59	1.10E-05	21865.4	H14_HUMAN Histone H1.4
TBIP-392	[36-2]	8	P16403	9	35.2	2.35	1.30E-05	21364.9	H12_HUMAN Histone H1.2
TBIP-392	[36-3]	6	P16402	7	21.3	2.19	3.40E-05	22350.1	H13_HUMAN Histone H1.3
TBIP-392	[36-4]	3	P22492	4	12.1	2.19	3.40E-05	22019.2	H1T_HUMAN Histone H1t
TBIP-392	[36-5]	3	Q02539	4	11.6	2.19	3.40E-05	21842.3	H11_HUMAN Histone H1.1
TBIP-392	[37]		Q14697	11	13.8	3.15	2.50E-06	106874.9	GANAB_HUMAN Neutral alpha-glucosidase AB
TBIP-392	[39]		Q15084	6	18.6	4.12	8.50E-07	48121.7	PDIA6_HUMAN Protein disulfide-isomerase A6
TBIP-392	[43]		P50897	9	35.9	3.27	7.10E-07	34193.8	PPT1_HUMAN Palmitoyl-protein thioesterase 1
TBIP-392	[44]		O43615	9	22.6	3.18	1.60E-06	51356.2	TIM44_HUMAN Mitochondrial import inner membrane translocase subunit TIM44

TBIP-392	[46]		P51659	7	13.7	3.71	8.60E-07	79687	DHB4_HUMAN Peroxisomal multifunctional enzyme type 2
TBIP-392	[49]		P62820	6	36.6	3.73	8.10E-07	22678	RAB1A_HUMAN Ras-related protein Rab-1A
TBIP-392	[49-1]	4	Q9H0U4	8	43.8	3	1.60E-06	22171.4	RAB1B_HUMAN Ras-related protein Rab-1B
TBIP-392	[49-2]	5	P61006	7	34.3	2.84	9.80E-06	23668.4	RAB8A_HUMAN Ras-related protein Rab-8A
TBIP-392	[49-3]	2	Q92928	6	31.3	3	1.60E-06	22017.2	RAB1C_HUMAN Putative Ras-related protein Rab-1C
TBIP-392	[49-4]	5	P61106	6	37.7	2.63	1.10E-04	23897.2	RAB14_HUMAN Ras-related protein Rab-14
TBIP-392	[49-5]	4	P51153	5	27.6	2.61	1.70E-05	22774.3	RAB13_HUMAN Ras-related protein Rab-13
TBIP-392	[49-6]	1	P61026	3	16.5	3	1.30E-05	22541.1	RAB10_HUMAN Ras-related protein Rab-10
TBIP-392	[49-7]	2	Q92930	4	20.3	2.32	9.50E-05	23584.3	RAB8B_HUMAN Ras-related protein Rab-8B
TBIP-392	[49-8]	0	P59190	2	10.4	2.32	9.50E-05	24390.8	RAB15_HUMAN Ras-related protein Rab-15
TBIP-392	[49-9]	0	Q15286	2	10.9	2.32	9.50E-05	23025.4	RAB35_HUMAN Ras-related protein Rab-35
TBIP-392	[49-10]	1	P20340	2	12	2.12	1.60E-04	23593	RAB6A_HUMAN Ras-related protein Rab-6A
TBIP-392	[54]		P23396	8	43.2	3.17	2.00E-06	26688.6	RS3_HUMAN 40S ribosomal protein S3
TBIP-392	[55]		O94905	7	26.8	3	2.50E-05	37839.9	ERLN2_HUMAN Erlin-2
TBIP-392	[58]		P62269	7	34.9	2.87	1.40E-05	17718.8	RS18_HUMAN 40S ribosomal protein S18
TBIP-392	[59]		P61224	8	47.8	2.65	2.60E-05	20825	RAP1B_HUMAN Ras-related protein Rap-1b
TBIP-392	[59-1]	1	P62834	6	33.7	2.65	2.60E-05	20987.4	RAP1A_HUMAN Ras-related protein Rap-1A
TBIP-392	[59-2]	0	A6NIZ1	5	27.2	2.48	2.60E-05	20925.1	RP1BL_HUMAN Ras-related protein Rap-1b-like protein
TBIP-392	[67]		P60660	7	66.9	3.31	1.70E-06	16930.2	MYL6_HUMAN Myosin light polypeptide 6
TBIP-392	[67-1]	0	P14649	2	11.5	3.31	1.70E-06	22764.2	MYL6B_HUMAN Myosin light chain 6B
TBIP-392	[68]		P30101	6	14.7	3.07	5.40E-06	56782.9	PDIA3_HUMAN Protein disulfide-isomerase A3
TBIP-392	[74]		P04843	8	18.9	2.49	2.40E-05	68570	RPN1_HUMAN Dolichyl-diphosphooligosaccharide--protein glycosyltransferase subunit 1
TBIP-392	[78]		P07237	4	10.2	4.49	2.80E-07	57116.8	PDIA1_HUMAN Protein disulfide-isomerase
TBIP-392	[81]		P62829	4	34.3	4.23	3.40E-08	14865.6	RL23_HUMAN 60S ribosomal protein L23
TBIP-392	[83]		P51149	5	27.1	3.51	5.50E-06	23490	RAB7A_HUMAN Ras-related protein Rab-7a
TBIP-392	[84]		P62805	7	55.3	2.15	3.80E-04	11367.4	H4_HUMAN Histone H4
TBIP-392	[88]		P09382	5	48.9	3	2.10E-05	14715.8	LEG1_HUMAN Galectin-1
TBIP-392	[95]		P23284	5	26.4	3.48	3.60E-07	23742.7	PPIB_HUMAN Peptidyl-prolyl cis-trans isomerase B
TBIP-392	[97]		P61019	6	33.5	2.84	8.60E-06	23545.8	RAB2A_HUMAN Ras-related protein Rab-2A
TBIP-392	[97-1]	0	Q8WUD1	2	11.6	2.17	8.40E-05	24214.6	RAB2B_HUMAN Ras-related protein Rab-2B
TBIP-392	[100]		P54920	6	27.8	2.33	2.90E-04	33233	SNAA_HUMAN Alpha-soluble NSF attachment protein
TBIP-392	[100-1]	0	Q9H115	2	11.4	1.62	2.90E-04	33557.3	SNAB_HUMAN Beta-soluble NSF attachment protein
TBIP-392	[102]		P61586	5	26.4	3.05	5.80E-06	21768.3	RHOA_HUMAN Transforming protein RhoA
TBIP-392	[102-1]	0	P08134	3	14	2.4	9.70E-05	22006.6	RHOC_HUMAN Rho-related GTP-binding protein RhoC
TBIP-392	[103]		P51148	5	30.1	2.57	8.70E-05	23482.8	RAB5C_HUMAN Ras-related protein Rab-5C
TBIP-392	[104]		P04899	9	33.8	1.68	1.80E-04	40451.3	GNAI2_HUMAN Guanine nucleotide-binding protein G(i) subunit alpha-2
TBIP-392	[104-1]	1	P08754	5	15.3	1.45	1.80E-04	40532.6	GNAI3_HUMAN Guanine nucleotide-binding protein G(k) subunit alpha
TBIP-392	[104-2]	0	P63096	4	12.4	1.45	1.80E-04	40361.5	GNAI1_HUMAN Guanine nucleotide-binding protein G(i) subunit alpha-1
TBIP-392	[108]		P33121	6	10.3	2.63	2.80E-05	77944.1	ACSL1_HUMAN Long-chain-fatty-acid--CoA ligase 1
TBIP-392	[109]		P0C0S8	4	35.4	3.6	5.70E-06	14091.6	H2A1_HUMAN Histone H2A type 1
TBIP-392	[109-1]	0	P20671	4	35.4	3.6	5.70E-06	14107.6	H2A1D_HUMAN Histone H2A type 1-D
TBIP-392	[109-2]	0	Q16777	4	35.7	3.6	5.70E-06	13988.5	H2A2C_HUMAN Histone H2A type 2-C
TBIP-392	[109-3]	0	Q6FI13	4	35.4	3.6	5.70E-06	14095.6	H2A2A_HUMAN Histone H2A type 2-A
TBIP-392	[109-4]	0	Q96KK5	4	35.9	3.6	5.70E-06	13906.4	H2A1H_HUMAN Histone H2A type 1-H
TBIP-392	[109-5]	0	Q99878	4	35.9	3.6	5.70E-06	13936.4	H2A1J_HUMAN Histone H2A type 1-J

TBIP-392	[109-6]	0	Q9BTM1	4	35.7	3.6	5.70E-06	14019.5	H2AJ_HUMAN Histone H2A.J
TBIP-392	[109-7]	0	P04908	3	32.3	3.6	5.70E-06	14135.6	H2A1B_HUMAN Histone H2A type 1-B/E
TBIP-392	[109-8]	0	Q7L7L0	3	32.3	3.6	5.70E-06	14121.6	H2A3_HUMAN Histone H2A type 3
TBIP-392	[109-9]	0	Q93077	3	32.3	3.6	5.70E-06	14105.6	H2A1C_HUMAN Histone H2A type 1-C
TBIP-392	[109-10]	1	P16104	3	32.2	1.37	0.0015	15144.7	H2AX_HUMAN Histone H2A.x
TBIP-392	[109-11]	1	Q96QV6	3	35.1	1.37	0.0015	14233.6	H2A1A_HUMAN Histone H2A type 1-A
TBIP-392	[109-12]	1	Q8IUE6	2	30	1.26	0.0015	13995.4	H2A2B_HUMAN Histone H2A type 2-B
TBIP-392	[111]		O00182	5	17.2	2.74	2.60E-06	39518.5	LEG9_HUMAN Galectin-9
TBIP-392	[111-1]	1	Q3B8N2	5	17.1	2.74	2.60E-06	39660.7	LEG9B_HUMAN Galectin-9B
TBIP-392	[111-2]	1	Q6DKI2	5	17.1	2.74	2.60E-06	39607.8	LEG9C_HUMAN Galectin-9C
TBIP-392	[114]		P35613	5	18.4	2.19	6.70E-04	42200.7	BASI_HUMAN Basigin
TBIP-392	[116]		Q12907	5	23.3	2.99	1.20E-05	40229	LMAN2_HUMAN Vesicular integral-membrane protein VIP36
TBIP-392	[121]		P80723	4	38.8	2.83	1.70E-05	22693.6	BASP1_HUMAN Brain acid soluble protein 1
TBIP-392	[123]		P62249	8	52.7	1.42	0.002	16445.5	RS16_HUMAN 40S ribosomal protein S16
TBIP-392	[133]		P30464	4	13	2.48	1.10E-05	40388.4	1B15_HUMAN HLA class I histocompatibility antigen, B-15 alpha chain
TBIP-392	[133-1]	0	P30484	4	13	2.48	1.10E-05	40440.5	1B46_HUMAN HLA class I histocompatibility antigen, B-46 alpha chain
TBIP-392	[133-2]	3	P01892	4	14	2.52	8.80E-06	40922.2	1A02_HUMAN HLA class I histocompatibility antigen, A-2 alpha chain
TBIP-392	[133-3]	3	P10316	4	14	2.52	8.80E-06	40977.2	1A69_HUMAN HLA class I histocompatibility antigen, A-69 alpha chain
TBIP-392	[137]		P39019	7	38.6	1.7	2.50E-04	16060.6	RS19_HUMAN 40S ribosomal protein S19
TBIP-392	[138]		P62701	6	27	1.74	3.10E-04	29598	RS4X_HUMAN 40S ribosomal protein S4, X isoform
TBIP-392	[138-1]	0	P22090	3	12.2	1.61	7.10E-04	29455.9	RS4Y1_HUMAN 40S ribosomal protein S4, Y isoform 1
TBIP-392	[142]		P46459	7	11.2	1.65	2.10E-04	82595.1	NSF_HUMAN Vesicle-fusing ATPase
TBIP-392	[145]		P62879	5	17.1	1.76	8.30E-04	37331.4	GBB2_HUMAN Guanine nucleotide-binding protein G(I)/G(S)/G(T) subunit beta-2
TBIP-392	[145-1]	2	P62873	5	16.5	2.04	2.00E-05	37377.3	GBB1_HUMAN Guanine nucleotide-binding protein G(I)/G(S)/G(T) subunit beta-1
TBIP-392	[145-2]	0	Q9HAV0	4	13.5	1.76	8.30E-04	37567.5	GBB4_HUMAN Guanine nucleotide-binding protein subunit beta-4
TBIP-392	[147]		P05141	3	10.7	3.26	6.70E-06	32852.5	ADT2_HUMAN ADP/ATP translocase 2
TBIP-392	[149]		P47756	5	24.2	2.32	3.00E-05	31350.8	CAPZB_HUMAN F-actin-capping protein subunit beta
TBIP-392	[150]		P46782	4	27.5	2.55	5.40E-05	22876.6	RS5_HUMAN 40S ribosomal protein S5
TBIP-392	[151]		Q9NQE9	4	29.1	2.46	3.90E-05	20361.5	HINT3_HUMAN Histidine triad nucleotide-binding protein 3
TBIP-392	[152]		O75844	5	13.9	1.82	6.10E-04	54813.4	FACE1_HUMAN CAAX prenyl protease 1 homolog
TBIP-392	[153]		P21964	3	15.9	3.19	2.50E-06	30037.3	COMT_HUMAN Catechol O-methyltransferase
TBIP-392	[159]		P49006	2	14.4	3.87	4.60E-07	19528.9	MRP_HUMAN MARCKS-related protein
TBIP-392	[160]		P10809	5	11	1.66	0.0018	61055.2	CH60_HUMAN 60 kDa heat shock protein, mitochondrial
TBIP-392	[161]		P62851	5	40.8	1.97	1.20E-04	13742.2	RS25_HUMAN 40S ribosomal protein S25
TBIP-392	[167]		P62913	3	20.2	3.21	1.20E-06	20252.6	RL11_HUMAN 60S ribosomal protein L11
TBIP-392	[168]		P27824	5	12.7	1.82	1.80E-04	67568.9	CALX_HUMAN Calnexin
TBIP-392	[173]		P13796	6	11.2	1.62	2.20E-04	70289	PLSL_HUMAN Plastin-2
TBIP-392	[181]		Q9H4G4	2	16.9	3.21	4.90E-06	17218.5	GAPR1_HUMAN Golgi-associated plant pathogenesis-related protein 1
TBIP-392	[190]		P07305	4	23.7	1.94	2.90E-05	20863.1	H10_HUMAN Histone H1.0
TBIP-392	[193]		P02655	3	28.7	2.35	5.80E-05	11284	APOC2_HUMAN Apolipoprotein C-II
TBIP-392	[194]		O75396	3	15.3	2.55	3.40E-05	24593.6	SC22B_HUMAN Vesicle-trafficking protein SEC22b
TBIP-392	[195]		P62491	3	14.8	2.13	1.10E-04	24393.7	RB11A_HUMAN Ras-related protein Rab-11A
TBIP-392	[195-1]	0	Q15907	3	14.7	2.13	1.10E-04	24488.7	RB11B_HUMAN Ras-related protein Rab-11B
TBIP-392	[196]		P62277	3	22.5	2.37	6.70E-05	17222.4	RS13_HUMAN 40S ribosomal protein S13
TBIP-392	[199]		P15153	5	26	1.57	2.10E-04	21429	RAC2_HUMAN Ras-related C3 botulinum toxin substrate 2

TBIP-392	[199-1]	2	P84095	3	26.7	1.17	0.0019	21308.7	RHOG_HUMAN Rho-related GTP-binding protein RhoG
TBIP-392	[199-2]	0	P60763	2	10.9	1.57	2.10E-04	21379.1	RAC3_HUMAN Ras-related C3 botulinum toxin substrate 3
TBIP-392	[199-3]	0	P63000	2	10.9	1.57	2.10E-04	21450.3	RAC1_HUMAN Ras-related C3 botulinum toxin substrate 1
TBIP-392	[199-4]	1	P60953	2	11	1.46	2.00E-04	21258.8	CDC42_HUMAN Cell division control protein 42 homolog
TBIP-392	[205]		P62158	2	20.1	3.18	3.20E-06	16837.7	CALM_HUMAN Calmodulin
TBIP-392	[215]		Q9BVK6	3	16.2	2.16	4.20E-05	27277.6	TMED9_HUMAN Transmembrane emp24 domain-containing protein 9
TBIP-392	[219]		Q14165	3	13	2	1.80E-04	32234.1	MLEC_HUMAN Malectin
TBIP-392	[228]		Q96BM9	4	15.1	1.36	0.0011	21416.1	ARL8A_HUMAN ADP-ribosylation factor-like protein 8A
TBIP-392	[228-1]	0	Q9NVJ2	4	15.1	1.36	0.0011	21539.2	ARL8B_HUMAN ADP-ribosylation factor-like protein 8B
TBIP-392	[229]		Q9UL25	2	11.6	2.55	2.30E-05	24347.8	RAB21_HUMAN Ras-related protein Rab-21
TBIP-392	[232]		P05388	4	14.2	1.47	2.00E-04	34273.8	RLA0_HUMAN 60S acidic ribosomal protein P0
TBIP-392	[232-1]	0	Q8NHW5	4	14.2	1.47	2.00E-04	34364.8	RLA0L_HUMAN 60S acidic ribosomal protein P0-like
TBIP-392	[234]		Q92520	2	11	2.52	4.60E-05	24680.7	FAM3C_HUMAN Protein FAM3C
TBIP-392	[235]		P08670	6	15.7	1.55	6.40E-05	53652.1	VIME_HUMAN Vimentin
TBIP-392	[238]		P0CG47	2	10.9	2.61	2.00E-05	25761.8	UBB_HUMAN Polyubiquitin-B
TBIP-392	[238-2]	0	P62979	2	16	2.61	2.00E-05	17965.1	RS27A_HUMAN Ubiquitin-40S ribosomal protein S27a
TBIP-392	[238-3]	0	P62987	2	19.5	2.61	2.00E-05	14728.5	RL40_HUMAN Ubiquitin-60S ribosomal protein L40
TBIP-392	[254]		P60468	2	28.1	2.69	1.60E-06	9974.5	SC61B_HUMAN Protein transport protein Sec61 subunit beta
TBIP-392	[263]		P42677	2	25	2.31	7.80E-05	9461.2	RS27_HUMAN 40S ribosomal protein S27
TBIP-392	[263-1]	0	Q71UM5	2	25	2.31	7.80E-05	9477.3	RS27L_HUMAN 40S ribosomal protein S27-like
TBIP-392	[286]		P46783	2	14.5	1.73	0.001	18897.9	RS10_HUMAN 40S ribosomal protein S10
TBIP-392	[293]		P51571	2	13.9	1.81	6.30E-05	18998.8	SSRD_HUMAN Translocon-associated protein subunit delta
TBIP-392	[294]		P62273	3	48.2	1.25	0.001	6676.8	RS29_HUMAN 40S ribosomal protein S29
TBIP-392	[310]		Q9BV40	2	23	1.53	0.003	11438.4	VAMP8_HUMAN Vesicle-associated membrane protein 8
TBIP-392	[316]		Q15363	2	10.9	1.47	8.60E-05	22761.4	TMED2_HUMAN Transmembrane emp24 domain-containing protein 2
TBIP-392	[317]		P62241	2	12	1.4	5.70E-04	24205.4	RS8_HUMAN 40S ribosomal protein S8
TBIP-392	[341]		O14950	2	17.4	1.48	3.20E-04	19779.3	ML12B_HUMAN Myosin regulatory light chain 12B
TBIP-392	[341-1]	0	P19105	2	17.5	1.48	3.20E-04	19794.3	ML12A_HUMAN Myosin regulatory light chain 12A
TBIP-392	[349]		P40926	2	10.4	1.1	0.0014	35503.6	MDHM_HUMAN Malate dehydrogenase, mitochondrial
TBIP-392	[350]		P63173	2	31.4	1.51	1.20E-04	8218	RL38_HUMAN 60S ribosomal protein L38
TBIP-392	[430]		Q9H299	2	31.2	0.8	0.002	10437.8	SH3L3_HUMAN SH3 domain-binding glutamic acid-rich-like protein 3